NAVAL POSTGRADUATE SCHOOL
MONTEREY, CALIFORNIA

THESIS

ANNEALING OF DEFECT SITES IN RADIATION DAMAGED INDIUM PHOSPHIDE SOLAR CELLS THROUGH LASER ILLUMINATION

by

Charles T. Chase

December, 1995

Thesis Advisors: **Sherif Michael**
Oscar Biblarz

Approved for public release; distribution is unlimited.

REPORT DOCUMENTATION PAGE

Form Approved OMB No. 0704-0188

1. AGENCY USE ONLY *(Leave blank)*	2. REPORT DATE December 1995	3. REPORT TYPE AND DATES COVERED Master's Thesis

4. TITLE AND SUBTITLE: ANNEALING OF DEFECT SITES IN RADIATION DAMAGED INDIUM PHOSPHIDE SOLAR CELLS THROUGH LASER ILLUMINATION (U)	5. FUNDING NUMBERS
6. AUTHOR(S) Chase, Charles T.	
7. PERFORMING ORGANIZATION NAME(S) AND ADDRESS(ES) Naval Postgraduate School Monterey CA 93943-5000	8. PERFORMING ORGANIZATION REPORT NUMBER
9. SPONSORING/MONITORING AGENCY NAME(S) AND ADDRESS(ES)	10. SPONSORING/MONITORING AGENCY REPORT NUMBER
11. SUPPLEMENTARY NOTES The views expressed in this thesis are those of the author and do not reflect the official policy or position of the Department of Defense or the U.S. Government.	
12a. DISTRIBUTION/AVAILABILITY STATEMENT Approved for public release; distribution is unlimited.	12b. DISTRIBUTION CODE

13. ABSTRACT *(maximum 200 words)* This thesis reports the results of a laser annealing technique used to remove defect sites from radiation damaged indium phosphide diffused junction solar cells. This involves the illumination of damaged solar cells with a continuous wave laser to produce a moderate heating and a large forward-biased current. The InP cells were irradiated with 27 MeV electrons to a given fluence, and tested for degradation. Light from an argon laser was used to illuminate each cell with an irradiance of 2.5 W/cm^2, producing a current density 7 to 10 times larger than under AM0 conditions. Cells were annealed at 48.5°C, 60°C, and 75°C for periods of 15 to 60 minutes, and cooled to 25°C for power recovery determination. Annealing at 48.5°C resulted in a recovery of 17 to 18% of the power lost due to irradiation, and annealing cells at 60°C produced a recovery of 43 to 48%. A single test of the technique at 75°C produced a net recovery of only 21% of the power lost. These results indicate that significant power recovery results from the annealing of defects within InP solar cells. Continuing research should involve the repeating of the test at 75°C, and irradiations with electrons or protons of energies expected in the space environment.

14. SUBJECT TERMS Indium Phosphide, Solar Cells, Annealing, Lasers	15. NUMBER OF PAGES 126
	16. PRICE CODE

17. SECURITY CLASSIFICATION OF REPORT Unclassified	18. SECURITY CLASSIFICATION OF THIS PAGE Unclassified	19. SECURITY CLASSIFICATION OF ABSTRACT Unclassified	20. LIMITATION OF ABSTRACT UL

NSN 7540-01-280-5500

Standard Form 298 (Rev. 2-89)

Prescribed by ANSI Std. 239-18 298-102

Approved for public release; distribution is unlimited.

ANNEALING OF DEFECT SITES IN RADIATION DAMAGED INDIUM PHOSPHIDE SOLAR CELLS THROUGH LASER ILLUMINATION

Charles T. Chase
Lieutentant, United States Navy
B.S., Massachusetts Institute of Technology, 1987

Submitted in partial fulfillment
of the requirements for the degrees of

MASTER OF SCIENCE IN ASTRONAUTICAL ENGINEERING

from the

NAVAL POSTGRADUATE SCHOOL
December 1995

Author: _____
Charles T. Chase

Approved by: _____
Sherif Michael, Thesis Advisor

_____
Oscar Biblarz, Second Reader

_____
Daniel J. Collins, Chairman
Department of Aeronautical and Astronautical Engineering

ABSTRACT

This thesis reports the results of a laser annealing technique used to remove defect sites from radiation damaged indium phosphide diffused junction solar cells. This involves the illumination of damaged solar cells with a continuous wave laser to produce a moderate heating and a large forward-biased current. The InP cells were irradiated with 27 MeV electrons to a given fluence, and tested for degradation. Light from an argon laser was used to illuminate each cell with an irradiance of 2.5 W/cm2, producing a current density 7 to 10 times larger than under AM0 conditions. Cells were annealed at 48.5°C, 60°C, and 75°C for periods of 15 to 60 minutes, and cooled to 25°C for power recovery determination. Annealing at 48.5°C resulted in a recovery of 17 to 18% of the power lost due to irradiation, and annealing cells at 60°C produced a recovery of 43 to 48%. A single test of the technique at 75°C produced a net recovery of only 21% of the power lost. These results indicate that significant power recovery results from the annealing of defects within InP solar cells. Continuing research should involve the repeating of the test at 75°C, and irradiations with electrons or protons of energies expected in the space environment.

TABLE OF CONTENTS

ACKNOWLEDGEMENT

I would like to thank Prof. Sherif Michael for his guidance and support in this research. I thank you for directing my efforts during the research process and financially supporting it.

I give sincere thanks to Rob Walters at the Naval Research Labs, who willingly gave countless hours of his own research time to teach me and answer all of my questions about radiation effects and DLTS. I would also like to acknowledge the assistance and expertise of Phillip Shapiro, also at the NRL, who with Rob Walters provided a thorough analysis of the displacement defects induced in indium phosphide.

Finally, I want to thank my wife, Andrea, for everything she has done for me especially during these past few months of thesis preparation. You supported me when I needed it most and now its time to take that vacation.

I. INTRODUCTION

A. BACKGROUND

Solar cell arrays have been the primary source of electrical power for satellite systems for nearly four decades. Since their first use in a space application on Vanguard I, launched on March 17, 1958, they have been the primary source of power for nearly all communications, navigation, weather, and military surveillance satellites. Solar cells have proven to be reliable, and safe, as well as, being able to provide a high power to weight ratio. In its most simple form, a solar cell is composed of the joining of two types of semiconductor materials (p-type and n-type). The product, a special type of a p-n junction, can directly convert light energy in the form of photons into electricity to be used by the satellite. This general form has changed remarkably little since its inception, yet the efficiency of conversion of sunlight to electric power has dramatically improved. This dramatic improvement is due in large part to the material composition and changes in fabrication techniques. One of the primary problems with the use of solar cells on satellites is the degradation of their properties and output due to exposure to the space environment.

The earliest realization of the effect that subatomic particles had upon solar cells was discovered accidentally in the early days of the space age. Operation "Starfish", a high altitude nuclear explosion conducted on July 9, 1962, at an altitude of 400 km over Johnston Island in the Pacific Ocean, resulted in the trapping of a large number of fission electrons in the Van Allen belts. During this time little was known about the effects of radiation on solar cell output. The effect of this 1.4 megaton nuclear device was the trapping of an estimated 10^{25} electrons in the Van Allen Belts, and the rapid decay of the current produced by the solar arrays of two LEO satellites. These satellites, the Transit 4B and the TRAAC, ceased transmissions due to power failure 24 and 36 days respectively after the detonation. As a result of this and the need for ever increasing output from solar cells, the U.S. Joint Chiefs of Staff established hardening guidelines for

all military satellites. Because of this, solar cell efficiency and the effects of radiation damage to solar cells were to become the subject of intense study. [Ref. 1:p. 215]

Along with the improved efficiencies of solar cells, a marked improvement in a solar cell's ability to withstand the conditions of space exposure has been achieved. This includes, most notably, their resistance to degradation due to exposure to ultraviolet radiation, and subatomic particle irradiation. Subatomic particles, most significantly protons and electrons, cause permanent damage to the crystal which results in the cell's loss in efficiency. Protection from this exposure can be achieved through the shielding of the cell's back surface in some instances. The cell can also be somewhat shielded from proton damage through the application of a transparent coverglass to the front surface. However, ultraviolet radiation has the detrimental effect of darkening this coverglass attached to the cell's surface. The shielding of solar cells has met with moderate success.

The creation of more radiation resistant cells through the utilization of different materials has been equally successful. Recently, a shift from the use of silicon to the more radiation resistant Group III-V semiconductor compounds, such as GaAs and InP, in solar cells has begun. Further, higher beginning of life (BOL) efficiencies are attainable using these Group III-V compounds. Nevertheless, the degradation of solar cells in the space environment is still a significant problem. Because of the degradation of these cells, many satellites are limited in their useful lifetime by their solar array's ability to maintain a minimum required electrical power level in the satellite. As a result, a satellite which requires a given minimum power level throughout its lifetime requires a solar array capable of producing significantly higher power at its beginning of life. When the effect of radiation degradation is taken into account, a satellite system launched into an orbit with a particularly intense radiation environment could require nearly twice the number of solar cells to provide for its end of life minimum power requirements.

Significant changes have been made to improve a solar cell's resistance to radiation damage, including the use of front surface coverglass, and the use of Group III-V compounds for the production of the p-n junction. These techniques have their basis in reducing the degree of damage through preventing exposure to differing types of radiation. While these and other manufacturing techniques are successful in extending

the usable lifetime, a process which could reverse the radiation degradation damage to the cells could further reduce the need for large solar arrays. A process of thermally annealing the damaged solar cells at elevated temperatures was conducted in the laboratory and was found to recover much of the degradation in power conversion efficiency which had been lost due to radiation. The annealing temperature is quite high and will preclude its use while the satellite is in orbit. As a result, annealing methods which can be accomplished with only a moderate degree of heating have been devised. These types of annealing methods, which can be conducted at reduced temperatures, are able to significantly reverse the degradation effects of long duration exposure to subatomic particles. These processes and their success are the basis for this research.

Success of an annealing process, which can be conducted while the satellite is in orbit, would have a tremendous impact upon the design of future solar arrays and satellite systems. The beginning of life power production by the solar array could be maintained for a much greater duration. This eliminates the need for over designing the array to account for the detrimental effects of radiation, and thus reduces the ultimate mass of the solar array and associated hardware. The mission duration of the satellite could be extended and delay the need to launch additional satellites to accomplish a desired mission result. In order to understand the degradation effects of radiation and the annealing techniques to be implemented, an overview of both the space environment and energy conversion within a solar cell is necessary.

The solar cell has been the primary form of electrical power generation for nearly all long term spacecraft. Advantages of using solar cells to provide power include reliability, safety, and high power to weight ratio. Many satellite solar arrays designed for long orbital lifetimes are sized considerably larger than their initial peak power requirement because of losses in solar cell efficiency due to radiation damage. As a result, all solar arrays are designed around the power required by the system at its end of life (EOL). The flux of protons and electrons outside the Earth's atmosphere is dependent upon the orbital altitude and position within the Earth's solar magnetic field. The rate of damage depends on the satellite's orbit, the degree of shielding on the array, and the type of cells used in its construction. The degradation in output of solar cells results from

defects due to the total fluence of subatomic particles upon the solar array. All of these parameters are critical design factors when deploying a satellite, but the use of a means by which radiation induced defects can be removed is not generally even considered. Additionally, returning the efficiency to a damaged solar array could return the power to an otherwise functional satellite, and save a vast amount of money. If one of these techniques could be carried out on a satellite in orbit, a tremendous savings could be achieved. Several methods of returning some of the efficiency to solar cells are currently available and proven, but only in the laboratory. If a technique such as annealing of solar cells were utilized, the mass and volume of the solar array and its hardware required could be significantly reduced.

II. PHOTOVOLTAICS

A. INTRODUCTION

When sunlight strikes a solar cell, the incident energy is converted into electricity and also other forms of energy, primarily heat, without the formation of any material byproducts. The energy conversion process is based upon competing processes which must be carefully controlled to attain the highest efficiency. Almost all solar cells regardless of chemical composition utilize the same basic processes for producing electricity. A caveat to this is the difference between single junction and tandem junction solar cells. This discussion will be limited to the description of the more common single junction cells. Among the many parameters which influence the production of electricity are cell's temperature, the angle of incident light, and the reflectivity of the cell's surface. In addition to these parameters, the degree of radiation degradation, or disorder of the semiconductor crystal lattice, plays a large role in determining the output of the cell. It is this factor which is of primary concern to this research. In order to understand the reasons that all of these parameters affect solar cell output, it is necessary to have a basic understanding of semiconductor physics.

B. SEMICONDUCTOR THEORY

Semiconductor materials, composed of either pure elements such as silicon, or compounds, such as GaAs or InP, all have similar properties based upon their chemical binding mechanisms and crystalline structure. Both the number and type of chemical bonds within a semiconductor are determined by the arrangement of electrons in the outermost shell, or valence shell, of the constituent atoms. There are eight possible electron states in the valence shell of these atoms. To become fully stable, an atom requires that its eight valence shell positions be completely filled. This can be accomplished by the "sharing" of electrons with another atom, and is referred to as a covalent bond. The bond effectively has two electrons, one from each atom. The shell can also be filled by the charging of an atom through its "giving up" of electrons, and the

subsequent electrostatic attraction to atoms with differing electric charges. This is called an ionic bond. Again, the bond effectively is composed of two electrons, both, however, from one atom. While covalent bond energies are typically on the order of a few electron volts per atom, ionic bonds are somewhat larger, and more difficult to break. The number and type of these bonds determines the strength of the binding to other atoms in the crystal.

The type of bonds exhibited in a semiconductor depends on the group, or column in the periodic table, to which its constituent atoms belong. Silicon, a common Group-IV semiconductor, has four electrons in its valence shell. It therefore requires four additional electrons, supplied by four covalent bonds with neighboring atoms, to complete its valence shell. Covalent bonds are typically found in semiconductors which are composed of a single type of element, or in semiconductors in which the elements exhibit nearly identical electronegativities. This is the tendency of an atom to attract and hold onto electrons. GaAs and InP, Group III-V semiconductors, are composed of atoms with differing electronegativities, and thus each exhibits a degree of ionic nature in their covalent bonds. Semiconductors which have ionic bonds in their crystal structure have stronger bonds and require more energy to break an electron free. As will be described later, semiconductors with ionic bonds, have higher band gap energies, and require higher energy photons to produce output current.

1. Crystalline Lattice

Crystal structures are described by a repeated orderly arrangement of atoms in an array referred to as the crystalline lattice. All semiconductors can be described by a repeated unit cell with the lattice atoms held in position by their associated covalent or ionic chemical bonds. The lattice typical of all semiconductors, known as the Diamond or Zinc-Blende structure, is based upon the fact that each atom in the structure is bound to its four closest neighbors, as shown in Figure 2.1. As described above, silicon requires that four covalent bonds share electrons with each atom to produce a stable, completely filled valence shell. Likewise, the atoms of the Group III-V semiconductors, produced by combining two atoms, one each from Group III and Group V, require filled valence shells. This is accomplished in a similar fashion, however, in this case each atom is

surrounded by four Group V phosphorous atoms. The indium atom has only three electrons in its valence shell, and requires five additional electrons to fill the shell. It accomplishes this by ionically bonding with one of these phosphorous atoms, and forming covalent bonds with three of the four others. In this process an electron is transferred from one of the phosphorous atoms to the indium atoms, creating a negatively charged indium atom, and a positively charged phosphorous atom to which it is ionically bound. The three remaining phosphorous atoms are themselves charged by transferring one electron each to the other indium atoms with which they are neighbors. The four bonds are, in reality, equivalent and all exhibit a degree of ionic bond behavior. In essence, the system can be described as having a single negative charge on the "central" indium atom and a small negative charge on each of the surrounding phosphorous atoms. The net result is an overall neutral unit cell with bonds that are somewhat stronger than ordinary covalent bonds, yet exhibit the same lattice structure. [Ref. 2:p. II-3]

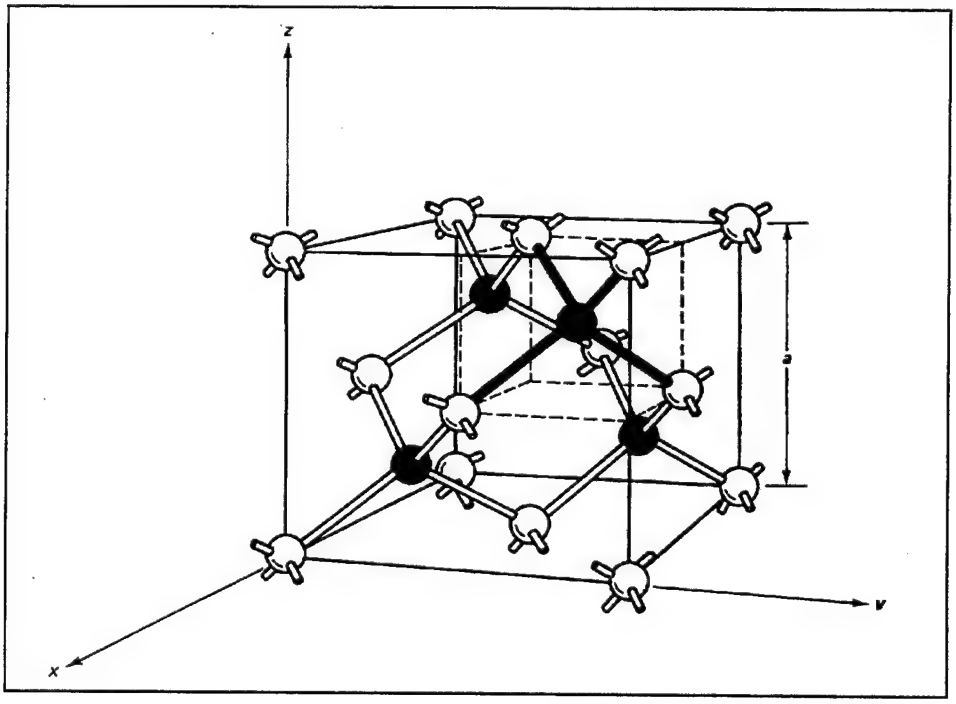

Figure 2. 1 Diamond or Zinc-Blende Crystal Structure.

2. Energy Band Gap

The lattice structure has particular significance to the physical properties of semiconductors because its uniformity or deviations from this uniformity determines the conductivity of the crystal. For every crystal there is an associated energy which, if added to an electron, will allow the transition of this electron from the valence shell to the conduction band. This action essentially frees the electron from an individual atom. Electrons which reside in the conduction band are able to move freely about the material, and thus conduct electricity. Energy addition less than this required energy will not permit this transition, and will result in only the addition of heat to the crystal. This energy difference between the valence band and the conduction band is known as the band gap energy, or band gap, E_g. This description is a somewhat simplified description of the actual band gap of disallowed energy states. In actuality the band gap energy is not a uniquely specific energy, but has a small range of energies. While the conduction band is a continuum of energy states to which excited electrons may enter, there is a finite number of energy levels of the valence band. Each of these may spread slightly depending on allowed vibrational energy states. These vibrational energy states are temperature dependent allowing a spreading of the electron's energy states with increasing temperature. The band gap energy for semiconductors thus depends on temperature, and for Si, GaAs, and InP at 300K their values are 1.12, 1.42, and 1.35 eV, respectively.

3. Conductivity by Thermal Electron-Hole Pair Production

Conductivity in semiconductors has a very strong temperature dependence, and, unlike in metals, the conductivity of semiconductors increases with increasing temperature. The energy necessary to raise an electron from the valence to the conduction band can be added in a variety of forms, including the addition of thermal energy. At any temperature above absolute zero, some finite number of bonds within a semiconductor crystal is broken by thermal ionization. As a result, some electrons are free to conduct. In addition to the electron being freed, a positive charge is left behind at the site of the broken bond. An electron from a neighboring bond may fill the hole that was created, but this in turn produces a hole at the site of that electron's origin. Thus,

"virtual" positive charge carrier, called a "hole", has a mobility like that of the electron which was initially displaced by thermal ionization. The direction of flow of this hole is in the direction opposite to the electrons. These electrons and their positively charged holes will move randomly throughout the semiconductor until they come upon one another and recombine. The recombination rate is proportional to the number of free holes and electrons which, in turn, depends on the ionization rate. The ionization rate, as indicated above, depends on temperature. When at thermal equilibrium, the ionization rate is equal to the recombination rate, and a set number of free charge carriers is always present. This concentration of charge carriers in a pure semiconductor is called the intrinsic carrier concentration. While this carrier concentration was shown to be highly dependent upon temperature, a more common means of changing the carrier concentration is to infuse the semiconductor with dopant atoms.

4. Semiconductor Dopants

The conductivity of the semiconductor can be greatly enhanced by doping the crystal lattice with a relatively small number of atoms with a different number valence electrons. The addition of dopant atoms to a semiconductor reduces the size of the forbidden energy band gap making it easier to ionize a given atom within the lattice. This occurs because the dopant atoms change the localized crystal structure of the semiconductor. The changed crystal structure, in effect, adds additional allowed electron energy states to the forbidden energy band gap. This permits smaller quantities of energy to excite an electron from the valence to the conduction band, enhancing its conductivity. The added dopants provide additional energy levels based upon the number of atoms in their valence shell. As indicated in Figure 2.2, n-type dopants, or donors, add electrons to the conduction band. The ionized dopant just below the conduction band, which is now positively charged, can accept an electron in transition from the valence band. Likewise, acceptors add holes to the valence band and their ionized form remains in an energy level just above the valence band.

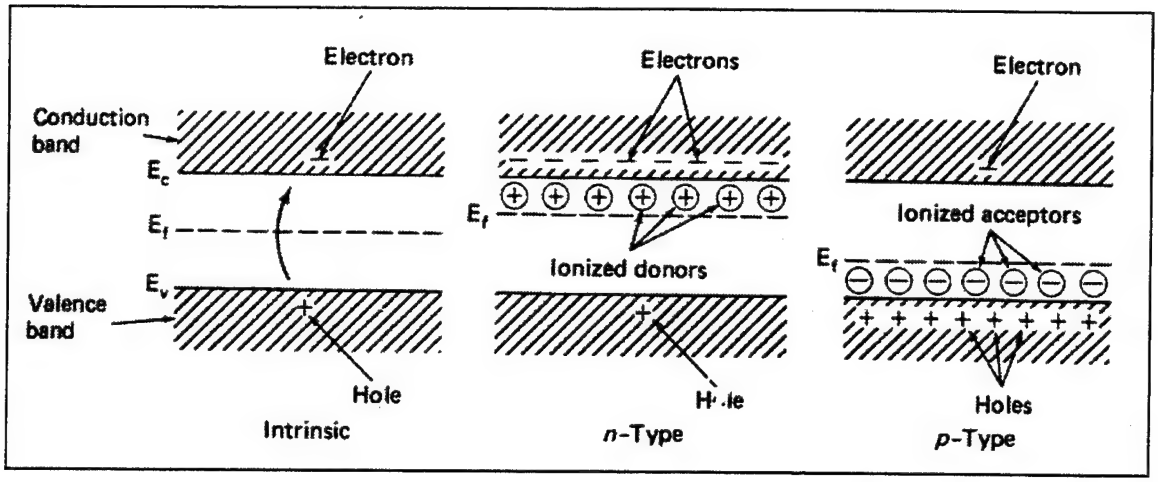

Figure 2. 2 Energy Band Gap Reduction Due to Dopants. [Ref. 1:p. 15]

Dopants add energy levels to a crystal's band gap, but more importantly, as alluded to above, the doping of the crystal directly adds charge carriers in the form of extra unbound electrons or holes. Dopant atoms infused into the semiconductor during manufacturing will take the place of a small number of normally bound semiconductor atoms. A dopant which takes the place of an atom that has more electrons in its valence shell than the original atom is called a donor. This is because it donates excess electrons to the material to fill empty valence shells of other atoms. Likewise, if the dopant has fewer electrons, then it is referred to as an acceptor, and accepts excess electrons from the other atoms in the material. The accepting and donating of electrons has no effect on the charge of the semiconductor. The dopant atoms and the semiconductor atoms are electrically neutral. The donation is simply the filling of a valence shell which stabilizes the atom. For instance, if a silicon atom is replaced with a neutral phosphorus atom, which has five valence electrons, then four of the electrons will be convalently bound to the four neighboring silicon atoms. It also results in setting one electron free within the crystal, but in doing so, there is a positive charge left on the dopant atom. Group V donor dopants, like phosphorous, add electrons to the material which are free to move in the conduction band and this results in an n-type semiconductor. Group III dopant atoms such as boron, add holes to the valence band, by a similar process. Because of the increase in the number of charge carriers, both dopant types increase semiconductor conductivity, and yet add no overall electrical charge to the material.

The concentration of a type of free charge carrier in a semiconductor varies depending upon the doping level, and concentration of the charge carriers of the opposite sign. The charge carrier which is more populous is referred to as the majority charge carrier, and the other is the minority charge carrier. For example, in an n-type material the majority carriers are electrons while the minority carriers are holes. Under equilibrium conditions a relation exists between the concentration of majority and minority charge carriers. Their product is a constant equal to the square of the intrinsic carrier concentration ($n_i^2=n*p$), that is the concentration of carriers without dopants. Also, the concentration of majority carriers at thermal equilibrium equals the concentration of dopant atoms ($n_{n0}=N_D$). The minority carriers, or holes in the case of n-type semiconductors, are primarily generated by thermal ionization, and the concentration of minority carriers is therefore a function of temperature. If the intrinsic concentration is known, however, the minority carrier concentration can be easily determined ($p_{n0}=n_i^2/N_D$). Identical processes occur in p-type semiconductors in which case the majority carriers are holes, and minority carriers are electrons.

5. P-N Junctions

All solar cells are based upon the merging of these two different types of semiconductor materials together, and are referred to as a p-n junctions. When these two materials are brought together, there are fixed positive charges in the n-type donor due to dopant atoms which have lost their electrons. These can be thought to repel the free holes in the p-type material across the junction. Likewise, there exist fixed negative charges in the p-type material which are produced by dopant atoms that have accepted an extra electron. These are thus negatively charged, and electrically repel the electrons in the n-type material. What is left is a thin region at the interface which is void of freely moving charges, as depicted in Figure 2.3. This "space-charge" or "depletion" region has only fixed charges of opposite signs on opposing sides of the junction. This results in a significant electrical potential buildup. If a free charge carrier arrives in the vicinity it will be influenced by the electrical potential across this region. How and which free charges are produced and driven across this junction is the topic of the next section.

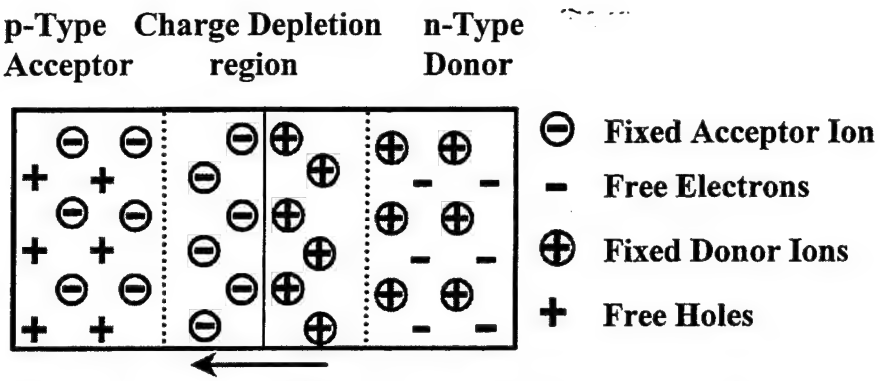

Figure 2. 1 Charge Depletion Region in a P-N Junction.

C. PHOTOVOLTAIC EFFECT

A p-n junction, the joining of a p-type and an n-type semiconductor, is the basis for photovoltaic cells, as well as, many other types of semiconductor electronics. It is well known that photons of light are responsible for the production of current in solar cells. Light incident upon any medium will either be absorbed, reflected, or transmitted. If the photon is absorbed by a solar cell, it will transfer some or all of its energy to the medium, before being reemitted by the cell. The energy imparted may be small in the case of long wavelength photons and result simply in a small amount of heating of the cell. If the energy transferred by the photon is large enough, greater than, or equal to the energy band gap, it will excite an electron from its valence shell into the conduction band of the material. This produces, as in the case of thermal excitation, an electron-hole pair. This free electron and hole will randomly move throughout the cell, and if nothing happens this electron-hole pair will recombine giving up their energy in the form of a photon, a phonon, or heat. In order to produce current, the charge carriers must be forced to flow uniformly in opposite directions, based upon their charge.

1. Drift and Diffusion Current

The current produced by a photovoltaic cell depends on two competing currents; the diffusion current and the drift current. In a solar junction two competing mechanisms drive electrons and holes through the semiconductor. The first, diffusion, is due to random thermal motion of the charges. This random motion of the charges results in no useful current flow, instead it forces the recombination of the charge carriers. The second mechanism which drives electric current is carrier drift. The carrier drift current is the

result of the electric field across or within the junction of the semiconductor. Electrons and holes which come into the vicinity of the cell's junction may be influenced by the electric field, and forced to the opposite side, producing a current, as shown in Figure 2.4. A more complete description will follow.

The diffusion current, introduced above, depends on the random motion of electrons and holes within the semiconductor. The relative concentration of these charge carriers across the region of contact between these semiconductors, the depletion region, drives their flow. Since the concentration of electrons in the n-type material is much greater than the concentration of electrons in the p-type material, the flow of electrons is from the n-type to the p-type side. Conversely, the concentration of holes is high in the p-type and low in the n-type material. As a result, holes flow from p-type to n-type utilizing the standard convention of current flow definition as the direction of flow of positive charges. These two current components, the flow of holes and the flow of electrons, add and are called the diffusion current. The flow of diffusion current is from the p-type to n-type semiconductor.

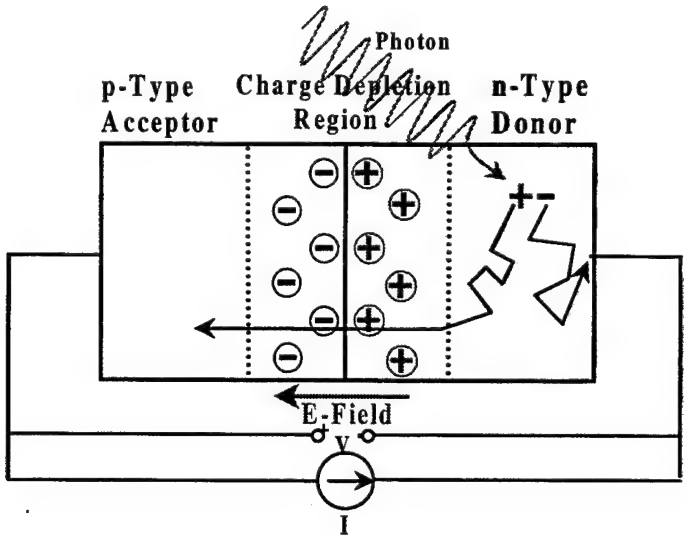

Figure 2. 4 Drift Current Due to Charge Separation by the Depletion Region.

In the case of a solar cell under open circuit conditions, holes that diffuse from the p-type region across the junction are quickly recombined with free electrons in the n-type material. This recombination of holes and electrons uses up some of the electrons which had previously been neutralizing bound positive charges in the n-type material. This

action takes place very quickly upon hole diffusion across the junction and as a result, the only bound positive charges which are uncovered are within a few microns of entry within the n-type material. A similar process occurs when electrons diffuse across the junction in the opposite direction. This thin region of reduced free to move charge is called the depletion region, or space charge region. The bound charges which are uncovered along the junction create an electric field which is in the direction from the n-type to the p-type semiconductor. The electric field opposes the further diffusion of holes across the junction to the n-region and electrons to the p-region. Thus, the potential across the depletion region acts as a barrier to diffusion current composed of free majority charge carriers.

The drift current is a current composed of free minority charge carriers (electrons for p-type, and holes for n-type). For most semiconductors, these minority carriers are produced in small numbers depending on their thermal generation and recombination rates. These minority carriers move randomly throughout the semiconductor until they recombine or are in close enough proximity to the depletion region to be affected by its electric field. Once near, the minority carriers are accelerated across the depletion region. The drift current unlike the diffusion current is independent of the potential across the depletion region. This motion of electrons from the p-type and holes from the n-type semiconductor results in a drift current that opposes the diffusion current and under open circuit conditions they are equal in magnitude. Ultimately, it is the drift current composed of minority charge carriers which opposes the diffusion current and produces useful output from a solar cell. It is the concentration of minority charge carriers and their acceleration across the junction which is of primary concern for the production of power.

The drift current produced in a solar cell depends on several factors including the charge density, the charge magnitude, the mobility of the charge carrier, and also the electric field applied by the junction. [Ref. 3:p. 1-10] The drift current is usually expressed in terms of a current density, and is found by summing the drift current densities for both types of charge carriers. As mentioned earlier, the standard convention defines the flow of the current as the direction of flow of positive charges. The total

current density is simply the sum of the product of these four terms for both the electron and hole components. In the following equations, J is the current density in amperes/cm^3, q is the charge in coulombs, p or n is the charge carrier concentration in cm^3, μ is the charge carrier's mobility in cm^2/V*sec, and E is the electric field of the junction in V/cm. Note that the equation for conductivity (σ) of the solar cell, in terms of carrier mobility and charge density, is easily obtained from the last equation.

$$\bar{J}_{p\_drift} = qp\mu_p\bar{E} \qquad \bar{J}_{n\_drift} = qn\mu_n\bar{E}$$
$$\bar{J}_{Drift} = (qp\mu_p + qn\mu_n)\bar{E} = \sigma\bar{E} \tag{2.1}$$

As described earlier, the diffusion current is dependent on temperature, but it is usually defined in terms of the gradient of the concentration charge carriers that is developed on either side of the junction. This gradient is also temperature dependent because the concentration of charge carriers is dependent upon the temperature. The diffusion current is analogous to the flow of heat due to a thermal gradient. If a high concentration exists in one part of the cell, the charge carriers will tend to diffuse to the area of lower concentration. In these equations, D, the diffusion constant is in units of cm^2/sec, and (dp/dx) or (dn/dx) is the 1-D gradient of the charge carrier concentration. In this case, the flow of holes was designated to be negative in order to indicate a flow opposing the drift current flow.

$$\bar{J}_{p\_diffusion} = -qD_p\frac{dp}{dx} \qquad \bar{J}_{n\_diffusion} = qD_n\frac{dn}{dx}$$
$$\bar{J}_{Diffusion} = -qD_p\frac{dp}{dx} + qD_n\frac{dn}{dx} \tag{2.2}$$

The diffusion constant, D, is important because with it one can determine the diffusion length, or distance that a minority charge carrier travels before encountering a majority charge carrier and recombining with it. The diffusion coefficient can be related to the charge carrier mobility, a known value, through the following logic. The diffusion constant is equal to one third of the product of the mean free path and the mean thermal

velocity ($D_n=\lambda_n v_n/3$). The definition of mean free path, λ_n, is the distance between collisions based on the mean thermal velocity of the material ($\lambda_n= v_n\tau$). From the kinetic theory of gases, the kinetic energy is related to temperature by, $1/2mv_n^2=3/2kT$, for a particle undergoing motion with three degrees of freedom. Assuming that the mean of the square of the thermal velocity is approximately the square of the mean thermal velocity ($v_n^2\cong(v_n)^2$), then the diffusion constant can be defined in terms of minority carrier lifetime ($D_n=v_n^2\tau/3$). There also is a direct relationship between the carrier mobility and minority carrier lifetime ($\tau=\mu m/e$). Substituting the value of velocity from the kinetic theory of gases and the minority carrier lifetime gives the following relationship between diffusion constant and mobility. The value of Boltzmann's constant, k, is $8.62*10^{-5}$ eV/K, and for kT/e at room temperature is 0.02586V.

$$D_n=\frac{\lambda_n\bar{v}_n}{3} \qquad \lambda_n=\bar{v}_n\tau \qquad \tfrac{1}{2}m\bar{v}_n^{\,2}=\tfrac{3}{2}kT \qquad \mu=\frac{e\tau}{m}$$

$$D_n=\frac{\bar{v}_n^{\,2}\tau}{3}=\frac{kT\tau}{m}=\frac{kT\mu_n}{e} \tag{2.3}$$

The time which it takes for recombination to occur, known as the minority carrier lifetime, is an important measure of the solar cell's output capability, and is a function of three factors. The minority carrier lifetime is inversely proportional to the product of the capture cross section of the minority charge carrier, the thermal velocity of the carrier, and the density of recombination centers. The diffusion length, L, is the square root of the product of the diffusion constant, and this minority carrier lifetime, τ. The creation of additional recombination centers resulting from high energy radiation shortens carrier lifetime and reduces cell performance. The effect of radiation on cell performance is the topic of a following chapter.

$$\tau\propto\frac{1}{\sigma V_{th}N_r}$$
$$L=\sqrt{D\tau} \tag{2.4}$$

Finally, all of the preceding calculations lead to equations which can be used to determine the total current production of a cell. The total current density is the sum of the drift and diffusion current densities, and at equilibrium under open circuit conditions will equal zero.

$$J_{Total} = q(-p\mu_n E + D_n \frac{dn}{dx}) + q(p\mu_p E - D_p \frac{dp}{dx}) \qquad (2.5)$$

This equation is correct, however, it is an oversimplification of the actual current output of a cell. There are two other factors which are normally present which influence the total output of a cell. They are the recombination and shunt current. For normal operation these can be neglected, however, they are important when the solar cell is irradiated, and lattice defects are introduced.

The following table provides electrical properties for InP semiconductor material which indicate that the mobilities for electrons and holes are not equivalent.

Density	4.787 g/cm^3
Band Gap	1.34 eV @ 300K
Electron Affinity	4.38 eV
Temperature Dependence of Band Gap	-4.6*10^{-4} eV/K
Electron Mobility (μ_n)	3000-5000 cm^2/V*sec @ 300K
Hole Mobility (μ_p)	80-150 cm^2/V*sec @ 300K
Diffusion Constant (D_n)	78-129 cm^2/sec @ 300K
Diffusion Constant (D_p)	2.1-3.9 cm^2/sec @ 300K
Electron Diffusion Length	1 μm @ 300K
Hole Diffusion Length	1.6 μm @ 300K
Intrinsic Carrier Concentration	6*10^6 - 2*10^7 cm^{-3}

Table 2. 1 Indium Phosphide Material Properties. [Ref. 4:p. 24] & [Ref. 5:p. 2]

D. SOLAR CELL MATERIALS

The concentration of minority charge carriers in photovoltaic cells depends on the thermal production rate, the recombination rate, and most importantly on their production

rate due to incident photons. Photons with sufficient energy are able to excite the covalent bonds between atoms within either the p-type or the n-type material enough to break them, releasing free electrons and allowing movement of holes. These electron-hole pairs add to the minority charge carrier concentration in the respective sides of the cell. As a result of the electric potential across the junction, they flow and produce current. Since the number of minority charge carriers is dependent on the breaking of covalent bonds in the material, it is directly dependent on their energy and thus the material's band gap energy. It seems that to ensure the greatest production of minority charge carriers one would want to utilize materials with very low band gap energies.

As photons of light are absorbed by a solar cell, three different things can occur. First, the energy could be too low to produce an electron-hole pair. Second, the energy could be precisely enough to produce an electron-hole pair. Finally, it could be more than enough, producing the electron-hole pair, and generating heat within the cell equal to the energy in excess of the band gap energy. If a material with a very low energy band gap were used, much of the energy would be wasted in the form of excess heat generated within the cell. If the material's band gap were too large, the production rate of minority charge carriers could be prohibitively low. The optimum band gap would be that which is somewhat lower than the energy of the maximum intensity of the solar spectrum. This ensures that a majority of the energy incident upon the cell produces electron-hole pairs, and also ensures a lesser degree of heating.

1. Solar Spectrum

The power of the sun in the vicinity of the Earth, but outside the Earth's atmosphere, is called Air Mass Zero, or AM0. This value of solar power incident upon an array in this region fluctuates slightly with the seasonal variations of the Earth's distance from the sun. This distance changes very little throughout the year, and for most solar cell analysis is an accepted constant value of 135.3 ± 2.1 mW/cm^2. [Ref. 6:p.2-1] The energy density of this solar spectrum, which varies with wavelength as a black body with a temperature of 5800 K, is depicted in Figure 2.5.

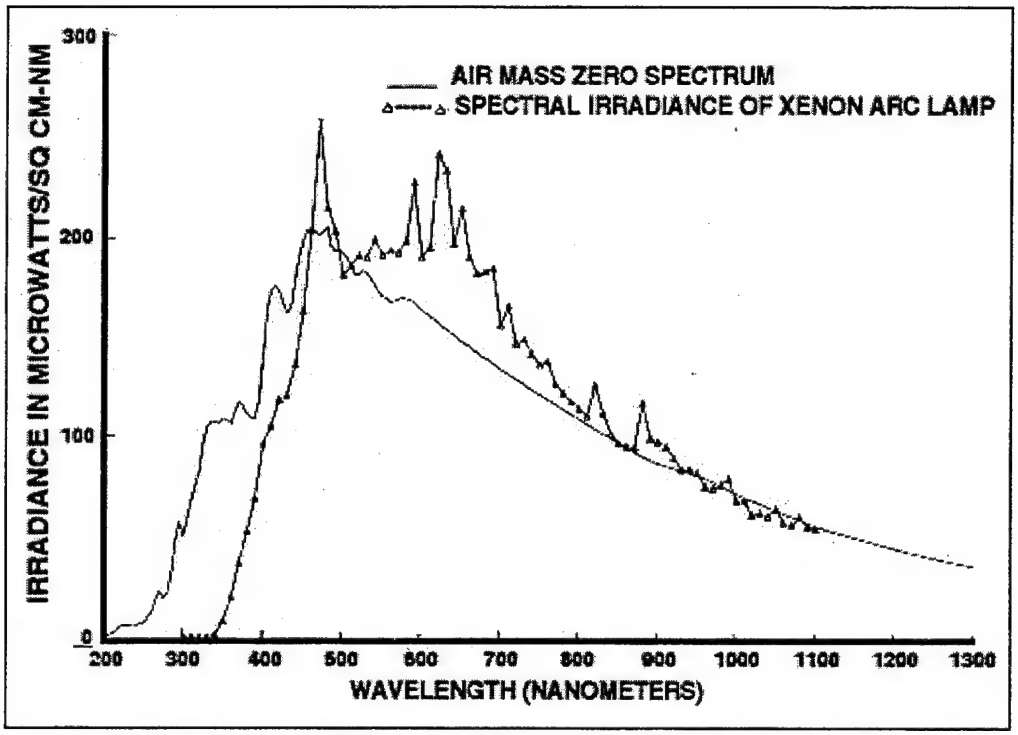

Figure 2. 1 Irradiance of Typical Xenon Arc Lamp Solar Simulator. [Ref. 6:p. 2-6]

The maximum intensity of the solar spectrum is in the range of 450-500 nm (2.76-2.48 eV), and the intensity drops off gradually with decreasing energy. A semiconductor material whose energy band gap is significantly less than this energy would most efficiently utilize these photons. The material which would produce the highest efficiency, based on the energy band gap criteria, is also dependent upon temperature. The optimum band gap energy for producing the highest theoretical output efficiency is depicted in Figure 2.6.

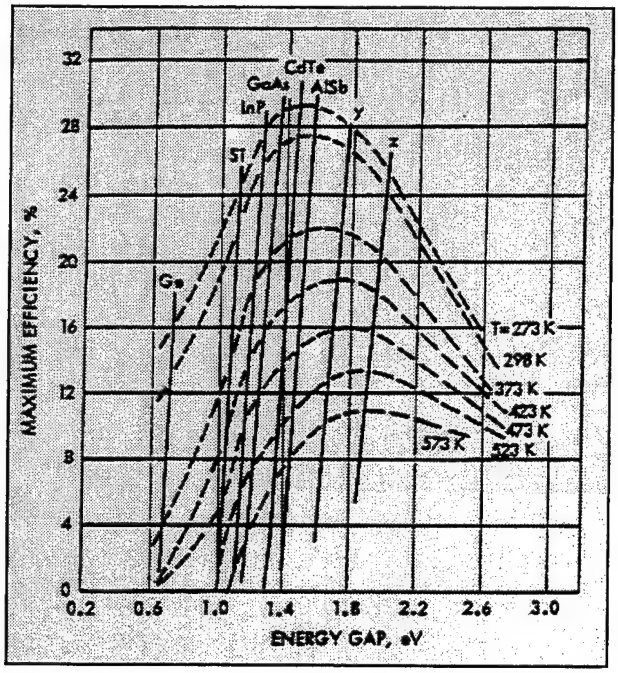

Figure 2. 6 Temperature Dependent Efficiency for Solar Cells. [Ref. 6:p. 1-32]

2. Solar Cell Output Parameters

There are several parameters which characterize the output of a solar cell, the most basic of which are the open circuit voltage (V_{oc}), the short circuit current (I_{sc}), and the fill factor (FF). These are obtained by producing a current verses voltage (I-V) plot of the cell's output under AM0 conditions. From these, almost all other parameters can be determined. The I-V plot, or characteristic, is obtained by reverse biasing the cell during its operation. A range of bias voltages is applied which has the effect of loading the circuit which the cell is driving. The theoretical maximum power of a solar cell is the product of the open circuit voltage and the short circuit current ($P_T=V_{oc}*I_{sc}$). These are the largest voltage and largest current which the cell can produce, and they occur under maximum and minimum cell bias conditions, respectively. When the current is short circuited, the voltage is necessarily zero, and when open circuited, there is no current flow. The cell is never operated at either of these points because at these two points the power produced, the product of voltage and current, is zero. There is, however, a maximum power point in the I-V characteristic which occurs at the knee of the I-V curve in Figure 2.7.

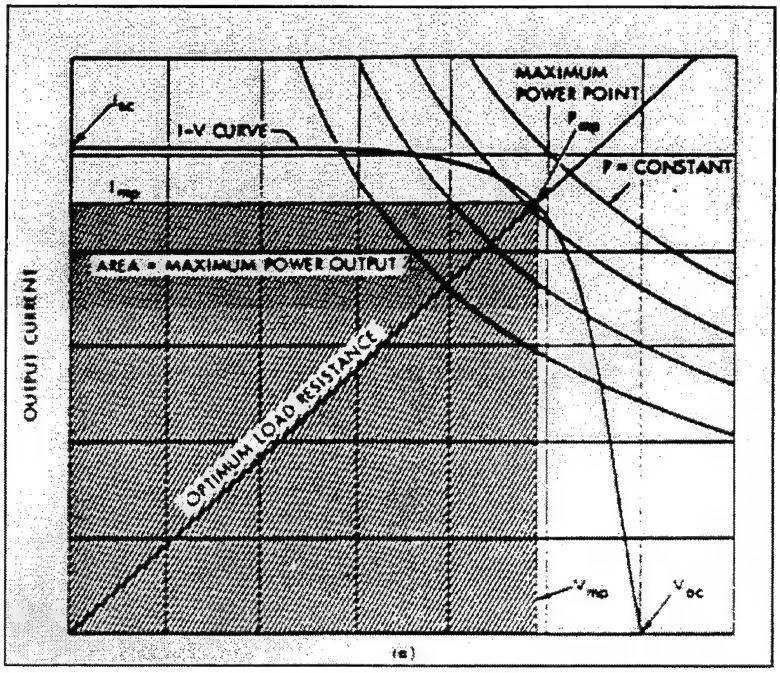

Figure 2. 1 Solar Cell Electrical Output (IV Curve). [Ref. 7:p. 3.2-1]

3. Factors Affecting Efficiency

Due to a multitude of loss factors, the maximum output of the cell, P_m, is less than the theoretical maximum power output. The ratio of this maximum output power to theoretical maximum output power is defined as the fill factor, FF ($FF = P_m/P_T$). This is important to determining the ability of the cell to output based upon losses occurring within the cell. The efficiency of the cell, however, is defined as the ratio of output power, P_m, over the power incident, which, for normal solar incidence, is AM0 ($\eta = P_m/P_{AM0}$). This determines the overall output of the cell based upon all internal and external losses, including reflection of photons from the cell's coverglass.

There are many factors which result in low efficiency of solar cell output. There are losses associated with factors external to the cell including poor incidence angle, reflection by the cell's protective coverglass, and even darkening of the coverglass. Of particular interest are the losses associated with internal factors such as the energy band gap, temperature, recombination or trapping, charge carrier mobility, and overall resistance of the cell. A discussion of the effects which the energy band gap has upon the efficiency of the cell was completed in the previous sections. Further, once a solar cell material and dopant level are chosen, the energy band gap is fixed. The following

discussion will concern primarily those effects which are not fixed, and may influence the overall efficiency.

4. Thermal Effects

The one factor which affects the output of a given solar cell independent of type is the cell's temperature. While terrestrial based solar cells have a relatively constant thermal climate, solar cells on a satellite's solar array can experience extreme heat and cold. As discussed earlier, the conductivity of semiconductors increases with increasing temperature, this is due to the increased thermal production of electron-hole pairs. This is a two fold effect. First, the addition of thermal energy of sufficient quantity produces electron-hole pairs. Additionally, the valence shell electron energy level structure spreads apart when heated, adding vibrational energy states. This increase in energy of the allowed states cuts into the energy band gap, reducing its size. This produces a higher current output because there is a reduced energy band gap, which can now absorb a greater range of photons. Despite this, the short circuit current tends to increase only slightly with temperature.

As the short circuit current increases with increasing temperature, the open circuit voltage tends to decrease with increasing temperature. The ability of the junction to separate charge carriers is seemingly decreased as the temperature increases. This is due to the increased number of charge carriers present. For example, in an n-type material at low temperatures, the number of free electrons is only moderately high, while the number of holes is very low. The junction is able to separate the free charge carriers and maintain a high concentration of free electrons in the n-type material, and holes in the p-type material. As the temperature increases, more electron-hole pairs are produced. At extreme temperatures, the energy of these electron-hole pairs is sufficient to overcome any force which the electrostatic potential of the junction imposes. The result is that random motion of the diffusion current prevails, and when current is flowing, the drift current cannot overcome it fully. The net effect is a loss in the open circuit voltage on the order of 2.3 mV/°C for Si and other semiconductors. [Ref. 3:p. 92] The cell is never operated at the short circuit or open circuit conditions, so these phenomena must be related to the efficiency or maximum power output.

The overall output, or efficiency of the solar cell decreases with increasing temperature, even though the short circuit current increases. The maximum power point, or knee of the I-V curve is most greatly influenced by changes to the open circuit voltage. This is because the change of open circuit voltage with temperature is roughly 10 times the change of short circuit current.

5. Normal Solar Cell Recombination

Another major factor which affects a cell's output efficiency is the phenomenon known as recombination. This is a normal occurrence in operating solar cells in which electron-hole pairs randomly encounter each other and are annihilated, releasing energy. The energy release can be in the form of a photon, a phonon, or heat. A phonon is simply a lattice vibration, or a compression and expansion of the crystal lattice corresponding to an acoustic wave. Recombination occurs most often during the excitation phase, when an electron is first given energy to break a bond and ionize the atom to which it is bound. If the energy is not sufficient, the electron will fall back to the valence band and thus undergo recombination. This direct recombination is a common, but uncontrollable factor. Another form of this mechanism, known as indirect recombination, occurs when a charge carrier is inhibited in its random movement long enough for an opposite charge carrier to encounter and eliminate it. The restraining of a charge carrier, called trapping, occurs because of a defect within the lattice, such as a dopant atom or broken bond, which accepts, or traps the charge carrier. A trapping center is simply an electron state which is induced by a defect within the crystal which lies within the energy band gap. If a small amount of energy is added to an electron, it will be raised to this intermediate semi-stable state. If the charge carrier remains there long enough, it will encounter and be annihilated by a charge carrier of the opposite sign. This phenomenon will be explained further when defect introduction to semiconductors is explained.

III. RADIATION ENVIRONMENT AND EFFECTS

A. SPACE RADIATION ENVIRONMENT

Nearly all long duration satellites in Earth orbit utilize solar cells for their electrical power requirements. The primary cause of degradation of these solar cells and thus a satellite's loss of power is due to the radiation environment in which it resides. Therefore, there is an impetus for engineers designing solar arrays to know as much as possible about this space environment and its adverse effects on solar cells. The radiation environment that solar cells must withstand in orbit varies due to differences in the type of radiation, the energy level, and the density. These factors, in turn, depend on other parameters, both spatial and temporal in nature. These include altitude, magnetic latitude, and solar activity. Radiation in the space environment includes electrons, protons, neutrons, gamma rays, and alpha particles. For this discussion, gamma rays and alpha particles will be eliminated, as they contribute very little to the degradation of solar cells because of relatively low fluxes. For the case of solar cells being irradiated with neutrons, however, another factor plays a role in discounting the effect it has on the degradation process. In this case, most of the displaced atom defects, which result from neutron bombardment, are inherently unstable at room temperature. As a result of thermal motion, many of these induced defects may anneal out. [Ref. 4:p. 248] Therefore, the principal cause of permanent solar cell radiation damage is due to electrons and protons encountered. Throughout its mission, a spacecraft will continually encounter radiation in the form of protons and electrons. These protons and electrons can be the result of man made events, as in the case of "Operation Starfish" described earlier. They may also be the result of natural occurrence, such as the transiting of an area of increased radiation flux in the Van Allen Belts. They might also be the result of radiation which has been released directly by a solar flare. These solar flares are transient in nature, but simultaneously there exists a more continuous emission of radiation called the solar wind. Furthermore, the same radiation can be trapped by the earth's magnetic field. Depending on the satellite's orbital altitude and inclination, this trapped radiation can become a more

permanent part of the satellite's environment. In either of these cases, the effect can be the same. The regions in space where protons and electrons have been trapped above the earth's atmosphere have been named the Van Allen belts. Solar arrays that are orbiting in this region can have serious degradation in power production.

1. Van Allen Belts

Although a continuous flux of high energy particles comes from galactic sources, the primary source of electrons and protons to which a solar array is exposed is from the sun's emissions. Solar wind is the term used for the continuous release of electrons and positive ions from the sun, while a solar flare is responsible for a much higher intensity emission. Radiation emission from the sun comes in the form of a neutral plasma composed of electrons and positive ions (90% protons and 10% Alpha particles He^{2+}). This plasma has an average density of 6.5 ions/cm^3, and an average velocity of over 400 km/sec. [Ref. 8: P 3-1] The path which this wind takes to arrive at the Earth is curved due to the rotation of the sun, and the magnetic influence which the Sun has on these particles at distances less than 3 solar radii. As a result, the solar wind does not arrive at the Earth precisely from the direction of the Sun. However, the interaction of the solar wind and the arriving radiation from the Sun is described as being from the day side. The plasma which arrives has the effect of compressing the Earth's magnetic field from the direction of its arrival, as depicted in Figure 3.1.

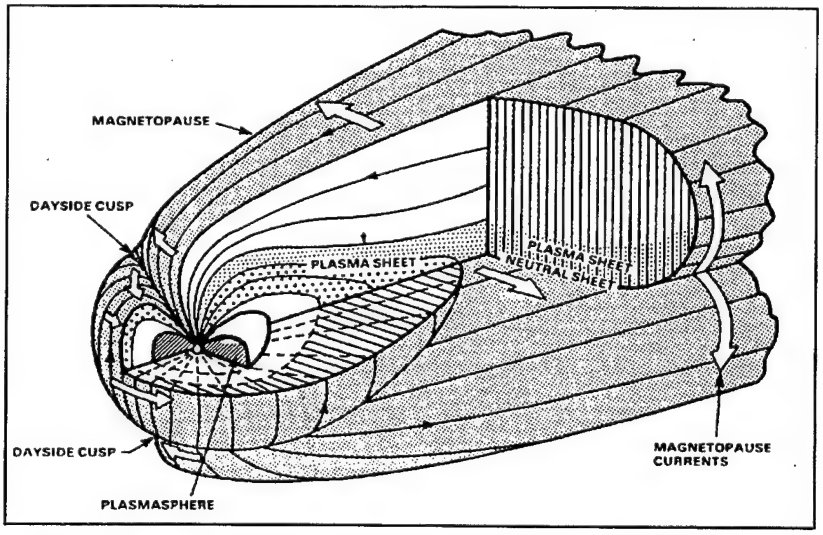

Figure 3. 1 Cross Section of the Earth's Magnetosphere. [Ref. 9:p. 1424]

These particles would quickly transit any region in space if not otherwise influenced. Charged particles arriving from the sun are deflected from their paths and tend to follow the lines of force created by the Earth's magnetic field. The field is thought to be created by the nickel and iron core of the planet, and has an intensity of 0.30 gauss on the Earth's surface at the magnetic equator. [Ref. 1:p. 198] Some of these arriving particles begin to travel in a helical pattern around magnetic field lines eminating from the magnetic poles of the Earth. Some of these may become trapped by the magnetic field depending on their energy. This trapping is due to a mirroring effect which magnetic fields have upon charged particles. When a charged particle arrives and travels in a circular motion about the field lines, it will exhibit some velocity component perpendicular to a magnetic field line. The kinetic energy, $K_{\perp}$, associated with this velocity divided by the strength of the magnetic field, B, is a constant called the magnetic moment, μ. The velocity component of the particle which parallel to the magnetic field line causes the particle to experience a small variation in magnetic field over a distance. As a result, the value of $K_{\perp}$ must change. If the particle senses an increase in field density, that is to say the field lines are growing closer together, the kinetic energy, or velocity, associated with the perpendicular component must increase. Since there is a converging of the field lines in this region, the "perpendicular velocity" actually has a component opposite in direction to the parallel velocity component. [Ref. 8:p. 5-3] At some value of increased magnetic field strength, called the mirror point, the force will completely reverse the direction of the parallel velocity component, as seen in Figure 3.2.

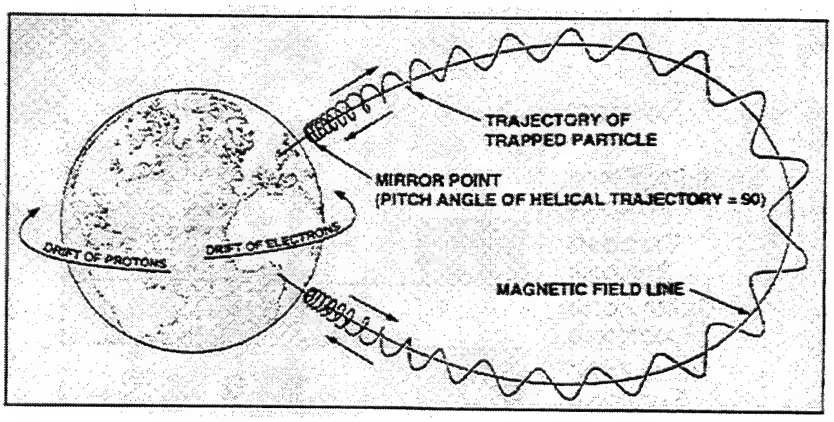

Figure 3. 2 Circulation of Charged Particles in the Van Allen Belts. [Ref. 9:p. 1425]

As stated above, upon reaching the Earth some of the particles below a critical energy level are trapped by the magnetic fields and remain in this region, and are further concentrated into specific toroids, or belts, about the Earth. These belts, called the inner and outer zones, are separated by an area of lower intensity radiation called the slot, as seen in Figure 3.3. [Ref. 9:p. 1425] The inner zone, also called the hard belt, is located between about 1.2 and 2.4 Earth radii and contains electrons with energies between 40 keV and 5 MeV. The intensity of electron radiation in this region, however, is not uniform, with its maximum intensity at about 1.3 to 1.4 Earth radii. This intensity can be as much as three orders of magnitude above the intensity in the slot. The outer zone, or soft belt, is located between 2.8 and 12 Earth radii and electron fluxes in this region can vary to a much greater degree than in the inner zone. It is composed primarily of electrons in the range of 40 keV to 7 MeV from the solar wind, and its flux varies due to intensity changes caused by solar flare activity. The intensity of electron radiation in this zone can vary by several orders of magnitude, during such an event. The outer belt reaches its peak intensity from 4.5 to 5.5 Earth radii depending on solar activity. [Ref. 1:p. 200]

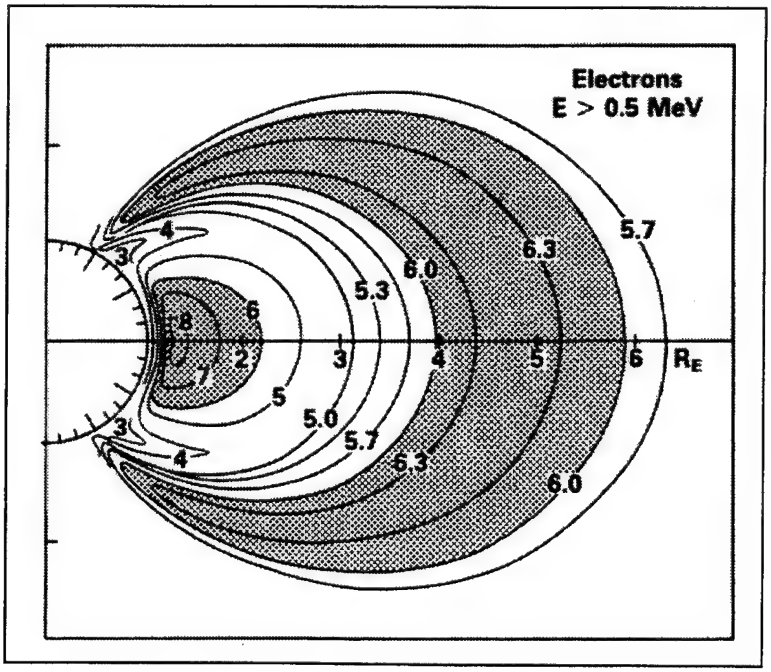

Figure 3. 3 Distribution of Trapped Electrons in the Van Allen Belts. [Ref. 1:p. 200]

As a result of their high intensities, and also due to their relatively large mass, high energy protons contribute the most to total dose effect in low Earth orbits (LEO). Figure 3.4 depicts the distribution of trapped protons. The distribution of the energies of these protons trapped in the Van Allen Belts, however, varies inversely with distance from the earth. High energy protons with energies between 10 MeV to 700 MeV are present in the inner zone, and beyond, to about 3.8 Earth radii. Beyond this point, however, the protons which a satellite might encounter are not trapped by the Van Allen Belts. At the geosynchronous altitude of 5.5 Earth radii, the dose due to trapped protons of greater than 5 MeV is almost negligible. [Ref. 1:p. 201] The much greater mass of protons, compared to electrons, prevents them from turning to follow the curving paths of the Earth's magnetic fields. Protons with energies of 60 MeV and higher are present beyond the 3.8 Earth radii, but are primarily the result of solar flare or solar wind activity.

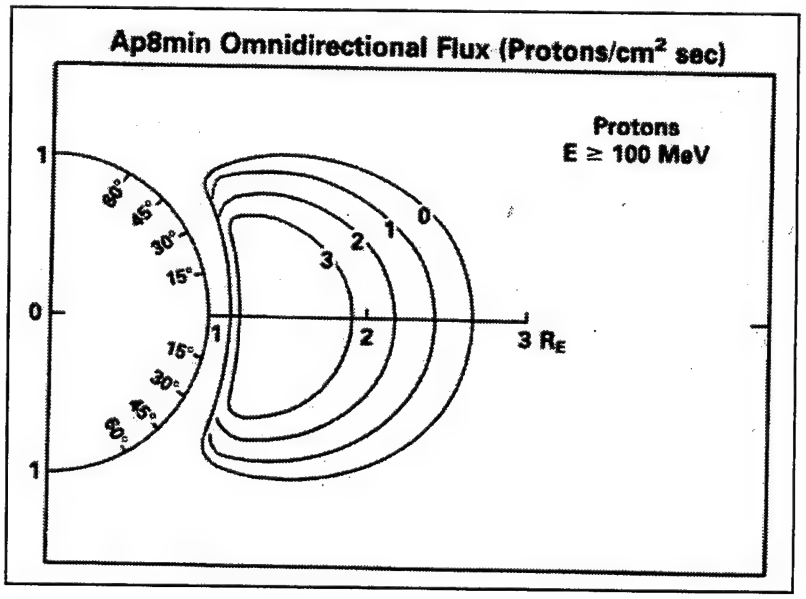

Figure 3. 4 Distribution of Trapped Protons in the Van Allen Belts. [Ref. 1:p. 201]

These radiation belts are not uniformly spherical in nature, but instead follow the lines of the Earth's magnetic field and form a torus-like shape about the earth. They are additionally distorted by the pressure of the solar wind. They are compressed on the side which is exposed to the solar wind (roughly the direction of the sunlit side of the Earth) and are expanded on the opposite side. Further, the intensity of the field varies with magnetic latitude and can be expressed with the following equation, where B_0 ($B_0 = 0.30$

gauss) is the magnetic field on the surface of the Earth at the magnetic equator, λ is the magnetic latitude, and R_E is distance measured in Earth radii.

$$B(R_E, \lambda) = (1 + \sin^2 \lambda)^{1/2} B_0 / R_E \qquad (3.1)$$

Since the exposure which a satellite receives depends on its position in the Van Allen Belts, it also depends on its inclination and altitude. In low Earth orbits (LEO), both protons and electrons play a major role in the degradation of solar cells. Both are present in high concentrations, and high enough energies to cause significant damage. At geosynchronous altitudes, it is electron bombardment which plays the greatest role in solar cell damage, since the concentration of protons at these altitudes is decreased. Protons do, however, cause significant damage to arrays at these altitudes during periods of high radiation flux, such as during solar flares.

B. RADIATION DAMAGE INTERACTIONS

Radiation in the form of trapped protons and electrons can enter the solar cell from all directions including through the coverglass or the substrate. The helical paths of trapped, charged particles in the Van Allen Belts ensure that a uniform distribution of radiation is incident upon the array from all directions. The flux of solar flare protons and electrons will, however, be biased toward the direction of the sun. This is especially true for satellites whose orbit is greater than 3 Earth radii. The damage which radiation causes within a solar cell is quite complex and depends on the size of the particle, its charge, and its energy. For instance, less energetic electrons or protons will damage the surface of the cell and the area nearest the junction, whereas the particles with high energy can penetrate deeper into the cell's substrate. However, some radiation of extremely high energy will pass completely through the cell without being appreciably slowed by it, and thus transfer less energy to the crystal than if stopped. The amount of energy transferred by a particle depends on the mechanism of transfer.

1. Linear Energy Transfer (LET) and Non-Ionizing Energy Loss (NIEL)

There are two primary catagories by which radiation transfers energy into a solid. They are through ionization, in which an electron is removed from an atom, and non-ionization effects. If the transfer mechanism results in the ionization of the target, the rate

of energy transfer is referred to as linear energy transfer (LET), while non-ionizing energy loss (NIEL) refers to the transfer of energy without changing the charge of the target atoms. Most of the kinetic energy of a particle is lost in the through ionization, and only a fraction of a percent is lost through non-ionizing interactions. [Ref. 10:p. IV-1] Both types of energy transfer can affect the output of a solar cell, although the focus of interest in this research is the non-ionizing events. In general, however, the degradation to the cell's performance can be explained by a few types of interactions of the radiation with the atom's electrons and nucleus within the crystal lattice.

When particles collide with the solar cell material they cause several different interactions, of which the dominant interactions are inelastic collisions with bound atomic electrons, and inelastic or elastic collisions with atomic nuclei. Some secondary interactions also occur which are the result of energy transfer effects produced by one of the primary interactions. These indirect energy transfers include the interactions of neutrons, X-rays, and gamma rays which are produced by aforementioned inelastic and elastic collisions. In the case of these dominant interactions, the terms inelastic and elastic refer to the changes in internal energy of the incident particles and the target atoms themselves. If the collision is elastic, the sum of the kinetic energies will not be changed. That is to say, if an energy transfer occurs between the incident particle and the absorber, everything lost by the particle will be gained by the absorber. In the case of an inelastic collision, not all of the energy lost by the incident particle is transferred directly to the target. The result is that some form of energy must be emitted by the process. For example, energy may be released in the form of a photon emission, vibrational quantum called a phonon, or most commonly, heating.

2. Inelastic Collisions with Atomic Electrons

In an inelastic collision with a bound atomic electron, energetic particles such as electrons or protons will "collide", or come close enough to have a coulomb interaction, with an electron and will transfer energy to it. This electron will be raised it to an excited state, or if enough energy is transferred, ionize it by raising it to an unbound state. Since the particle colliding with the target is charged, and the bound electron is also charged, there is an expected coulombic interaction between the two, resulting in a deflection of

the incident particle. In the case of relatively massive protons, bombardment results in only a limited deflection of the incident protons. Incident electrons, however, will be greatly deflected by such an interaction. As a result, incident electrons will take a more tortuous path through the material and will have a greater potential for transferring energy in this manner. Each of these mechanisms results in some linear energy transfer (LET), and an ionization of the atoms within the crystal lattice.

3. Elastic Collisions with Atomic Nuclei

An elastic collision with an atomic nucleus can also result in energy transfer to an atom in the crystal. Protons and electrons which "collide" through Rutherford scattering with the positively charged atomic nucleus are electrostatically repulsed or attracted by the nucleus. In the case of proton bombardment, sufficient energy can be transferred to the nucleus through this coulombic repulsion to displace it from its position in the crystal lattice. Further, this displaced atom could have sufficient energy to displace other atoms in the lattice. Due to the large mass of protons, this interaction may also permanently affect the nucleus of this atom. If a proton is sufficiently energetic, the energy transfer could be large enough to overcome the nuclear binding energy of a neutron within the nucleus and free a neutron, which could cause further damage to the crystal.

Alternatively, electrons will feel a coulombic attraction to the nucleus, and such an electron passing by a nucleus will be tangentially accelerated toward it. The electron may be deviated into an arcing path as it passes by the nucleus, decelerating it, and giving up some of its energy to the nucleus in the process. The energy transferred by the electron may also be enough to displace an atom from its postion in the lattice. An additional elastic interaction is the direct "hard sphere" collision with the atom's nucleus. While this has the potential to displace an atom from the lattice, it is much less likely because of the physical size of the particles and the nucleus. [Ref. 6:pp. 3-1,2] While these interactions can involve coulombic forces, the atom does not change its net charge, and thus the energy lost by the incident radiation is described as non-ionizing energy loss (NIEL).

4. Inelastic Collisions with Atomic Nuclei

Inelastic collsions of protons or electrons with atomic nuclei, like elastic collisions, can also have the effect of adding sufficient energy to an atom within a crystal to displace it from the crystal structure. An energetic proton which undergoes an inelastic collision with an atomic nucleus can drive the nucleus into an excited state. Losses can be in the form of the emission of gamma rays, or the excited and now unstable nucleus can emit highly energetic free nucleons (protons or neutrons). This process of emitting nucleons from the nucleus is known as spallation. These emitted nucleons have a displacement capability similar to the original incident proton, but now with a reduced energy. The resulting lower atomic mass nucleus is displaced from its lattice site due to the recoil of the emitted nucleons. This displaced nucleus can, in turn, cause more displacements if it interacts with other atoms in the lattice. [Ref. 6:pp. 3-2] As described in the elastic collision process, high energy electrons undergoing inelastic colissions with the atom's nucleus will often be deflected due to the charge on the nucleus. As the electron passes by the nucleus, it will have to give up some energy due to its deceleration. In the case of inelastic collisions of high energy electrons with the nucleus of a high atomic number (High Z) material, the result will often be the emission of photons in the X-ray region. The emission of Bremsstrahlung X-rays (German for "braking-radiation") is the result of the transfer of energy due to the braking or slowing down of such an electron during the deflection process. These X-rays may be able to further damage the material through interaction with electrons of other atoms. [Ref. 14:p. 163]

5. Indirectly Ionizing Particle Interactions

Each of the above described interactions can produce some type of indirect ionizing radiation in the form of neutrons, gamma rays, or X-rays. Each of these is uncharged and thus their interactions and energy transfer are unlike those of the charged particles previously described. Each transfers energy without directly ionizing the target material. The energy of each form is transferred from non-ionizing radiation to an ionizing particle. In the case of X-rays, energy can be transferred to orbital electrons which can be ionized and then are able to interact in one of the three primary mechanisms. The more energetic gamma rays are also able to transfer energy through one

of three mechanisms depending upon their energy. For energies less than 500 keV, gamma rays can interact through the photoelectric effect, as X-rays do, and release an orbital electron from its shell.

For energies between 600 keV and 2.5 MeV, a gamma ray is too energetic to transfer all of its energy to an orbital electron. The electron absorbs part of it and the remainder must be released as a lower energy gamma ray. This process, known as the Compton effect, releases a ionized orbital electron and the lower energy photon at angles ranging between 0° and 180°, depending upon the amount of energy transferred to the electron. The probability of Compton scattering depends directly upon the cross section of the target atom which is driven by the atomic number (Z). For the photon energies listed, the cross section is inversely proportional to the photon energy, and decreases moderately for any increase in energy.

A final means by which energy can be transferred from radiation to the material is through the process called pair production. If a photon with energy of at least 1.02 MeV is incident upon the material, there can be a direct transfer of the photon energy (anti-matter) into particles which have mass. The energy of the photon is converted into two particles of equal mass and opposite sign, namely an electron and a positron, or electron pairs. Each of these particles has a mass-energy equivalent to 0.51 MeV or one-half of the required 1.02 MeV incident photon. Any additional energy above the 1.02 MeV will be converted into kinetic energy of the new particles. This takes place more commonly in high Z materials since the probability of this energy transformation depends upon Z^2, or the square of the atomic number. These particles will act in the same way that freed orbital electrons do and have equal potential for damaging the crystal. This pair production is not to be confused with electron-hole pair production which is a normal part of current production in solar cells. This occurs when an electron within a semiconductor is raised from the valence band to the conduction band, leaving a mobile charged hole behind in the crystal lattice. Pair production in the radiation bombardment sense is complete conversion of a photon which has no true mass into two charged particles which have mass.

C. CRYSTAL STRUCTURE DAMAGE TYPES AND EFFECTS

The two primary types of radiation damage to the crystal lattice of a semiconductor are the ionization of atoms by removal of orbital electrons, due to LET, and the displacement of atoms from their original stable positions in the lattice, caused by NIEL. Both forms of damage can result in changes in the electrical output characteristics of the solar cell. Ionization damage caused by incident protons, and electrons (or secondary emissions of protons, electrons, and photons) can have the overall effect of changing the minority and majority carrier concentrations within the solar cell. Displacement damage is produced by the interaction of an energetic proton or electron knocking an atom from its normal lattice position. The resulting void is called a vacancy, and if the displaced atom finds another semi-stable position in the lattice, it is called an interstitial. Pairs of vacancies and interstitials which are in close proximity, as depicted in Figure 3.5, are termed Frenkel pairs. These have the effect of producing site defects which inhibit the mobility of charge carriers, and reduce the minority carrier lifetime of electron-hole pairs produced during normal cell operation. The displaced atoms are meta-stable and "reside" in local energy wells, remaining locally stable, but at an energy higher than that of their original positions in the lattice.

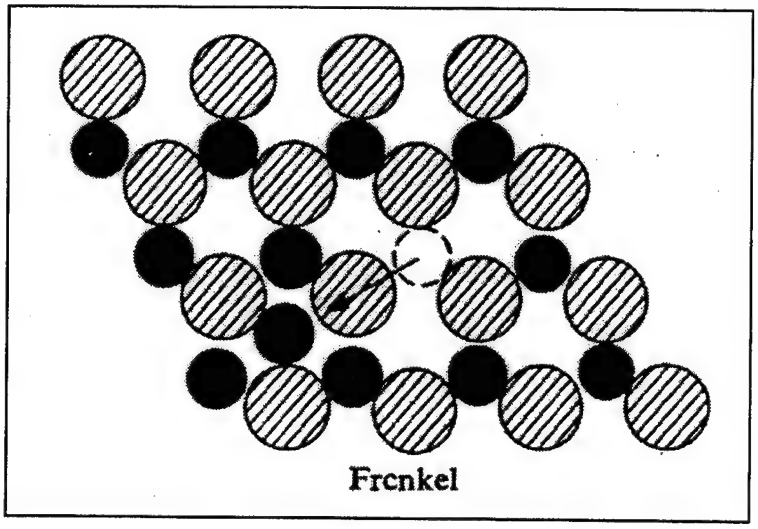

Figure 3. 5 A Representation of Crystal Displacement Damage. Closely Spaced Interstitials and Vacancies are Known as Frenkel pairs. [Ref. 11:p. 181]

1. Ionization Damage

Ionization damage, or the removal of one or more valence shell electrons, by an incident particle produces both ionized atoms and free electrons. This ionization has several effects upon solar cells. This ionization has the effect of darkening the protective coverglass of the solar cell. The coverglass is one of a variety of transparent materials, such as fused silica, bonded to the solar cell to help shield it from protons and electrons causing displacement damage. It has the effect of stopping low energy protons before reaching the semiconductor material and damaging it. The damage which ionizing radiation has upon the coverglass is to produce dark color centers which inhibit the tranmission of light to the cell. This darkening results from the excitation of an orbital electron to the conduction band in the coverglass. Impurities within the coverglass trap the excited electrons changing their absorption spectra, and forming color centers. The coverglass darkens, reducing the transmittance of the coverglass, thereby limiting the illumination of the cell, and its overall efficiency.

A beneficial effect of ionizing radiation is that it has the ability to excite valence band electrons to the conduction band creating electron-hole pairs. This results in the same electron-hole pairs that are generated by visible photon exposure during normal operation. However, because of the transfer mechanism, much more energy, on the order of three times the energy, is required from ionizing radiation to create these electron-hole pairs. [Ref. 6:p. 3-6] As in normal operation, the ionizing radiation has an inelastic interaction with the atomic electron. If the electron is not sufficiently excited, it will not reach the conduction band and will eventually recombine with a hole, transferring its energy back to the cell, often in the form of heat. [Ref. 12:p. II-17] The energy required for pair production from photo-excitation and ionizing radiation are listed in Table 3.1. The table also lists the rate of generation of electron-hole pairs for ionizing radiation for certain solar cell materials.

Material	Eg (eV) Bandgap Energy Photo Excitation @ 300 K	Ep (eV) Ionizing Radiation Electron-hole pair production	Density (g/cm3)	Electron-hole Pair Density generated/rad, g0 (pairs/cm^3)
Si	1.1	3.6	2.328	4×10^{13}
InP	1.34	4.38	4.787	6.8×10^{13}
GaAs	1.42	4.8	5.32	7×10^{13}

Table 3. 1 Electron-hole Pair Generation Rates for Ionizing Radiation in Solar Cell materials. [Ref. 12:p. II-17]

2. Displacement Damage

Displacement fluence is any electromagnetic or particle radiation which has the effect of displacing an atom from its original position in the crystal lattice. Displacements within the crystal structure are typically caused by relatively massive, highly energetic, and fast moving particles, such as protons or neutrons. For man made nuclear reactions, the primary cause of displacement damage is neutrons. However, in the natural space environment protons and electrons are the primary producers of displacement damage. The displaced atoms will take up positions within the crystal which produce stable defects called interstitials and their associated voids called vacancies. [Ref. 1:p. 224] Combinations of these interstitials and vacancies, or combinations of these interstitials and vacancies with dopant atoms, are called defects. These have a negative impact upon the equilibrium charge carrier concentration and the minority carrier lifetime and will affect the cell's output efficiency. They are referred to as recombination or trapping sites due to the fact that they are responsible for trapping a charge carrier and allowing another charge carrier to recombine with it neutralizing both charges. Since these defects are a major cause of solar cell output degradation, their production mechanism and removal of these sites is of primary interest in this research.

D. ELECTRON ENERGY TRANSFER IN INP CRYSTALS

Although a large portion of the energy dissipation by incident electrons is due to their interaction with the atom's orbital electrons (and their subsequent ionization), the permanent degradation of solar cells is due to primarily to displacement effects resulting from NIEL. During electron irradiations, the energy of the particle will determine both

the number and type of interactions that occur. While most solar cell investigations involve 1 MeV electrons, this research utilized electrons with energies in the range of 27 to 30 MeV. A comparison of these two energies will be made for NIEL, as well as, a brief description of the ionizing energy loss will be made.

Both LET and NIEL interactions occur simultaneously and compete for energy of the electron. Therefore the energy required for such a displacement and the mechanism for the energy transfer by NIEL, as well as the energy transferred due to ionizing energy loss inthe form of linear energy transfer (LET) is important to understanding the overall degradation process. A complete analysis of these two mechanisms of these two processes will be described, but the competitive nature of these interactions with each other will not be fully explained.

1. Non-Inonizing Energy Loss (NIEL)

The first step in understanding the processes process is to determine if there is a possibility of sufficient energy transfer to displace an atom in the lattice. During the electron-nucleus interactions, a range of energy may be transferred to the target nucleus dependent upon the proximity of the approach and angle of scattering. The energy required to displace an atom from its lattice site is approximately 12.9 eV for silicon, and 10 eV for GaAs. The displacement threshold energy (T_d) is only 6.7 eV for an In atom, and 8.7 eV for a P atom in indium phosphide [Ref. 13:p. 1379] The maximum energy which could be transferred to the nucleus by the electron with 30 MeV energy is calculated using the equations below. Here the energy, E, of the incident electron (eV) is adjusted for relativistic effects. [Ref. 14:p. 169] The masses of the electron (m) , and of a single atom of In or P (M) are both in kg. [Ref. 5:p. 4] To maintain ease of unit conversion, the value of rest mass or mc^2 is determined in terms of electron volts, and for an electron this value is 0.511 MeV.

$$E_m = 2\left(\frac{m}{M}\right)E\left[2+\frac{E}{mc^2}\right] \tag{3.2}$$

The resulting maximum energies which could be transferred between a 30 MeV electron and either indium or phosphorous atoms are 64 keV and 17 keV, respectively. Since the

displacement energy is only 6.7 or 8.7 eV, this indicates that there exists a possibility of sufficient energy transfer, but gives no idea as to the likelihood of such an occurrence. In fact, using these equations, incident electrons with energies as low as 277 keV can displace indium atoms, while energies of 110 keV can displace phosphorous atoms.

The next step in understanding the displacement process is to determine the probability of interaction or the number of defects induced by a given fluence of electrons. The number of displaced atoms resulting from irradiation is the sum of both the primary knock-on atoms, and the secondaries displaced. The secondaries occur when the primary knock-on atom has energy well above that of the displacement threshold and there is a subsequent energy transfer to other atoms in the lattice. The quantity of primary knock-on atoms (P) displaced is determined by integrating the differential scattering cross-section ($d\sigma/d\Omega$) over all possible collisional angles for which the potential for energy transfer is greater than the displacement threshold energy. Calculating the number of secondaries (S) is more complex, but can be approximated through the Kinchen-Pease model for displacement. [Ref. 5:P. 5] This calculation is similar to that for calculating the number of primary knock-on atoms displaced. The model, however, must take into account the energy of the primary knock-on atom, the displacement energy of potential displaced atoms, and an additional requirement that the primary knock-on have energy equal to twice the displacement threshold. The reason for this requirement can be interpretted as the need for sufficient energy to first displace a secondary atom and then requirement that the primary knock-on atom retain sufficent energy to escape the void left by the displaced secondary atom.

$$P = \int_{\theta(T_d)}^{\pi} \left(\frac{d\sigma}{d\Omega}\right) d\Omega$$

$$S = \frac{1}{2T_d} \int_{\theta(2T_d)}^{\pi} T\left(\frac{d\sigma}{d\Omega}\right) d\Omega \qquad (3.3)$$

The calculation of these integrals is straightforward assuming that the differential scattering cross section ($d\sigma/d\Omega$) for each atom type is known. Calculation of this parameter for phosphorous atoms involves an approximation known as the McKinley-Feshback approximation, while the parameter for indium atoms can be determined through the Curr approximation. The calculation of the cross sections for In and P, and subsequent calculation of the total number of expected displacements was performed by Robert Walters and Phillip Shapiro of the Naval Research Lab. A comparison of displacements due 1 MeV electrons and 30 MeV electrons indicates that the number of primary knock-on atoms displaced changes very little over this range. The number of secondary interactions which result in displacement, however, rapidly increases with increasing energy, as shown in Figure 3.6. This has a significant effect on, not only the number, but the type of defects introduced by the interaction.

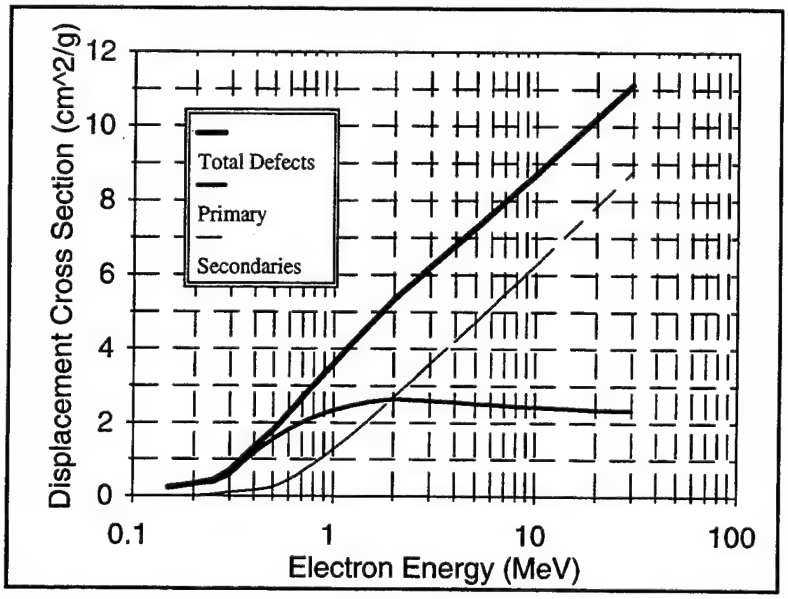

Figure 3. 6 Number of Atomic Displacements vs. Electron Energy for InP.

When radiation displacement damage occurs within a crystal the number of displaced atoms is quite small when compared to the total number of atoms within the crystal. Low energy interactions which produce only primary knock-on displacements, without any secondaries, will have closely spaced vancany and interstitials, called Frenkel pairs. These pairs will have a certain probability of recombining as a result of being activated through energy adddition. As the energy of the incident electron is increased,

more energy is transferred, and secondaries occur. When this happens, the proximity of the interstitial and its original vancany will be significantly increased. As a result, the probability of an interstitial attaining sufficient energy to be returned to its vacancy site is reduced. This fact becomes significant to the annealing process.

The first step is to find the electron stopping power of InP, and apply this to the total cross section for electron-nucleus collisions. From this an estimate of the numbers of displacement can be determined.

2. Stopping Power Calculations (LET)

The next step is to find the LET, otherwise known as, the electron stopping power of InP, and apply this to the total cross section for electron-nucleus collisions. From this an estimate of the energy retained by the electron which is available for displacements could be made. Since the displacement effects are the focus of this investigation the exact calculation of this energy is not significant and only a rough idea of the magnitude of the LET is neccessary.

The expected rate of energy loss of an electron per unit length is called the stopping power (dT/dx) and is expressed in units of MeV/cm. The mass stopping power (dT/ρdx) is determined by dividing the stopping power by the material's density and is expressed in units of MeV cm^2/g. The mass stopping power is usually subdivided into two types of interactions. The collision stopping power is the combined energy losses due to soft and hard collisions, and the radiative stopping power is, in the case of electrons, due to electron-nuclear interactions. The mass collision stopping power of a given energy electron is calculated by the following equation, with the polarization effect (δ) between 3 and 5 for 30 MeV electrons in most materials. [Ref. 14:p. 171]

$$\left(\frac{dT}{\rho dx}\right)_c = k\left[\ln\left(\frac{\tau^2(\tau+2)}{2(I/m_0c^2)^2}\right) + F^-(\tau) - \delta - \frac{2C}{Z}\right] \qquad (3.4)$$

$$\text{where } F^-(\tau) = 1-\beta^2 + \frac{\tau^2/8 - (2\tau+1)\ln 2}{(\tau+1)^2}$$

$$\text{and } \tau = T/m_0c^2$$

The mass radiative stopping power of a given energy electron is calculated with the following equation. Here the stopping power cross section (σ_0) is equal to $1/137(e^2/m_0c^2)^2$ or $5.80\text{x}10^{-28}$ cm^2/atom, and T is in MeV and B_r is roughly 13-14 for 30 MeV electrons. [Ref. 14:p. 171]

$$\left(\frac{dT}{\rho dx}\right)_r = \sigma_0 \frac{N_A Z^2}{A}(T + m_0c^2)\overline{B}_r \tag{3.5}$$

When observing these two equations, the collisional stopping power is proportional to N_AZ/A, and the radiative mass stopping power is proportional to N_AZ^2/A. Their ratio should, therefore, be proportional to atomic number (Z). Also, the equation for radiative stopping power is proportional to T. Assuming small values for m_0c^2, the collisional stopping power can be shown to have a dependence on a function of T. The overall ratio of stopping powers can be approximated by the following formula. [Ref. 15:p. 143]

$$\frac{(dT/\rho dx)_r}{(dT/\rho dx)_c} = \frac{TZ}{n} \tag{3.6}$$

where n is between 700-800 MeV

E. EFFECTS OF LATTICE STRUCTURE DAMAGE

Radiation, in the form of electrons and protons, can create displacement defects called vacancies, interstitials, and defect clusters in a crystalline lattice. The effect of this is the introduction of additional allowed energy states into the energy band gap. These additional energy levels change the electrical properties of p-n junction devices through five mechanisms, four of which are depicted in Figure 3.6 below. They are known as carrier trapping, dopant compensation, electron-hole pair recombination, thermal generation of electron-hole pairs, and tunneling. The first four of these are important to the study of solar cell degradation. [Ref. 16:p. 13] Tunneling is only significant in the case of p-n junctions in which there is an extremely high doping level on both sides of the junction (>10^{18} atoms/cm^3). In the case of the InP solar cells studied here, the dopant levels are much lower than 10^{17} atoms/cm^3.

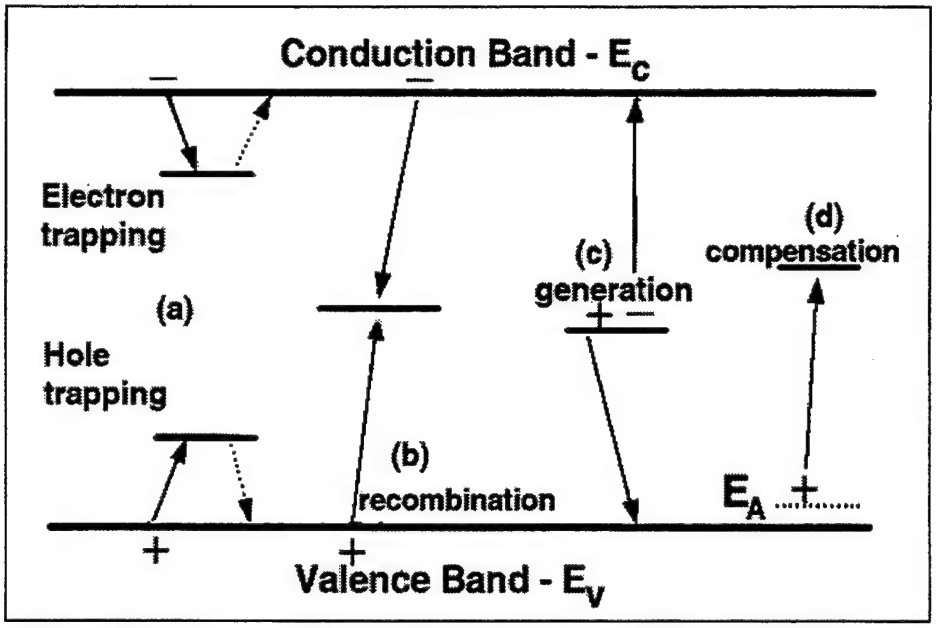

Figure 3. 7 Four of the Primary Mechanisms which alter the Electrical Properties of Semiconductors. a) Electron-hole Trapping, b) Recombination, c) Generation, d) Dopant Compensation. [Ref. 5:p. 14]

1. Trapping

The effect of trapping is the overall reduction in minority charge carriers, due to their restricted movement because of their removal from their original placement in the crystal. A defect has the effect of introducing extra allowed energy bands within the previously disallowed energy band gap. Trapping occurs when a charge carrier such as a free electron falls from the conduction band into one of the newly created energy levels. The defect acts to create a semistable position in the lattice for this extra electron. The electron is now temporarily caught in the energy band gap and cannot act as a charge carrier. An identical mechanism occurs in the case of holes. The distinction is that since a hole is really the absence of an electron, it is "trapped" by a defect of which requires the temporary removal of an electron. The mechanism of trapping is temporary nature, and a trapped electron or hole may be released through the addition of a small amount of energy called the activation energy. A depiction of the two trapping processes is shown in Figure 3.6, above. This small amount of energy addition can be in the form of thermal energy, which can be determined through a technique known as Deep Level Transient Spectroscopy (DLTS). Using this technique, the concentration and activation energy of

these defect sites can be determined. A brief description of this technique will be given in the Chapter IV, as information about the effects of irradiating and annealing processes can be determined from its evaluation.

2. Compensation

Another process, called compensation, can occur if the defect level is near the center of the energy band gap. This is referred to as being "deep" within this region. If the defect site provides a deep site for "trapping" a charge carrier, it may be filled by a charge carrier which comes from a "shallow" area near the edge of the energy band gap. Again, this reaction may proceed or reverse and cause the addition or removal of a small amount of thermal energy. In the case of a p-type semiconductor, a hole from the shallow area of the acceptor region may be transferred to a defect site deep in the energy band gap. This process is the relocation of an electron from a defect site in the center of the energy band gap to fill an acceptor site near the valence band. The effect of such an event is to remove charge carriers from the lattice, and reduce the semiconductor's conductivity.

3. Recombination Current

Defects which trap charge carriers within the energy band gap can also retain these charges for sufficient time periods until charges of the opposite sign are encountered. The result of this extended trapping is the annihilation of the two charges. The charge annihilation which results has two effects. First, there is a reduction in the current flow within the cell. This is because a free electron and its hole have been returned to the valence band of the lattice structure. These charges are no longer able to become influenced by the cell's junction and produce current. The second effect of this recombination is the emission of energy from the recombination site in the form of a photon of light or a lattice vibration, known as a phonon. The production of phonons is particularly important to the annealing process. These changes in the crystal lattice are what diminish the solar cell's photovoltaic output.

4. Generation Current

Recombination of charge carriers occurs due to the changes in the electrical properties at a defect site of a lattice, but the opposite effect, generation, can as well. If

sufficient energy in the form of thermal energy is available at the defect site, an electron-hole pair may be produced. The electron will be energized to the conduction band and leave a hole in the valence band, both of which will add minority charge carriers to the crystal and produce current. Since the recombination and generation processes are essentially equal, but opposite, they are competitive. The net effect on the cell can be reduced to the difference between the rates of the two processes. The net result of these two competitive processes is referred to as the recombination-generation current (I_{rg}).

5. Net Result of Recombination-Generation Current

The processes of recombination and generation depend on a number of properties of the cell and each is coupled to the other by the rates of the other process. The rate of recombination (c_n) depends on the fraction of traps occupied by holes (f_{tp}), the concentration of electrons in the valence band (n), and inversely on the minority carrier lifetime (τ_n). The electron emission, or generation rate, is a function related to the fraction of unoccupied traps (f_t), the density of electrons in the conduction band (n_1), and the minority carrier lifetime (τ). This assumes that in the region of a defect the Fermi energy level of the electron is equal to the Fermi level of the trap. [Ref. 5:p. 17]

$$r_n = \frac{nf_{t_p}}{\tau_n} \qquad g_n = \frac{n_i f_t}{\tau_n} e^{\frac{(E_t - E_i)}{kT}} = \frac{n_1 f_t}{\tau_n} \tag{3.7}$$

Using these two equations of electron emission and capture, the recombination-generation rate can be found by taking their difference. If this results in a positive number, the recombination rate is more prevalent, and if a negative number, then the generation process is dominant. The same holds true for emission and capture of holes. The values of U can be expressed in terms of the concentration of defect site by determining the correlation between it and the minority carrier lifetime (τ). The minority carrier lifetime is inversely proportional to the concentration of the defects (N_t), the average thermal velocity (V_{th}), and the capture cross section of the minority charge carrier (σ).

$$\tau_n = \frac{1}{N_t V_{th_n} \sigma_n} \qquad \tau_p = \frac{1}{N_t V_{th_p} \sigma_p}$$
$$U_n = r_n - g_n \qquad U_p = r_p - g_p \tag{3.8}$$

Under steady state conditions, without an applied external bias, the two values for recombination-generation rates of holes and electrons are necessarily equal. As a result of this, the recombination-generation current depends directly on the concentration of the defects in the crystal. As the number of defects increases, the minority carrier lifetime decreases, and thus, the rate of recombination increases, and the net output current of the cell drops. This result is not readily apparent because if all other variables are constant, the effect of reducing the minority carrier lifetime increases both the recombination, and generation rates, as seen in the equations above. It can be shown that the generation rate is inversely proportional to the concentration of free electrons and holes. This implies that the generation current is negligible outside the depletion region where the charge carrier concentration is highest and recombination dominates. However, the generation current is significant in the depletion region where few charge carriers exist and generation of charges is statistically likely. The effect of the recombination-generation current will be discussed in a following section.

6. Diode Shunt Current

A final current effect which affects solar cells in general, and radiation degraded cells to a greater extent, is the shunt current. The shunt current is an effect that occurs under small applied biases. If a small bias is applied, the depletion region will be increased in size. This increase in junction width is due to the removal of majority charge carriers from opposing sides of the p-n junction. As a result of the increase in width, more defect sites are effectively within the charge depletion region. A current is created much in the same manner as the previously mentioned generation current within the depletion region. This shunt current, which is essentially the creation of charge carriers within the depletion region, has the effect of reducing the ability of the depletion region to separate charge.

7. Total Cell Current (Photo-generated & Dark Current)

The term dark current is given to the combination of current sources which effectively oppose the flow of photogenerated current or drift current in solar cells. The three components of dark current include the diffusion current, which was previously mentioned in the description of solar cells, the recombination-generation current, and the shunt current. Although much of the development has been left out, the drift current and dark current combine to produce the total output of a solar cell. The total current output of a solar cell is given by the equation below, where I_{01} is a part of the diffusion current, I_{02} corresponds to the recombination-generation current, and the final term is the shunt current.

$$I(V) = I_{Drift} - \left(I_{01}(e^{\frac{qV}{kT}} - 1) + I_{02} \frac{(e^{\frac{qV}{kT}} - 1)}{e^{\frac{qV}{kT}} + \cosh\left(\frac{E_t - E_i}{kT}\right)} + \frac{V}{R_{sh}} \right)$$

$$\text{Where: } I_{01} = q\left(\frac{p_n D_p}{L_p} + \frac{n_p D_n}{L_n} \right) \qquad (3.9)$$

$$\text{and: } I_{02} = \frac{qAW}{2} N_t V_{th} \sigma n_i$$

F. DEFECT CHANGES TO SOLAR CELL OUTPUT PARAMETERS

The degradation of the properties of the semiconductor crystal lattice can have severe effects on nearly all solar cell output parameters. The cell parameters which are most affected are short-circuit current, open circuit voltage, and ultimately, the maximum power output, or the efficiency of the cell, as depicted in Figure 3.7. The degree which radiation reduces each of these parameters, and the means by which each accomplished, is described in the following sections.

As described earlier in this chapter, when high energy particles impinge on a semiconductor, there is the potential for displacement of atoms from the crystal lattice. The types of defects which are induced depend on the amount of energy which has been transferred to the primary knock-on atom. Typically, a vacancy and an interstitial are left behind which cause changes in the allowed energy levels. This ultimately affects the way in which electrons and holes are able to move throughout the structure.

1. Short Circuit Current

When an electron-hole pair is created through normal absorption of a photon of sufficient energy, the minority charge carrier diffuses throughout the cell until acted upon by the potential of the junction. When this occurs, the minority carrier is accelerated across this depletion region and becomes a part of the current, I_{sc}, produced by the cell. If this charge carrier is recombined prior to reaching the junction, then it cannot become a part of the current. The production of current is therefore directly tied to the recombination rate and minority carrier lifetime. The introduction of defects due to radiation, therefore, has the primary effect of reducing the current production in the cell.

An interesting phenomenon occurs when the electron-hole pair is actually created within the charge depletion region. An electron-hole pair which is produced within this region is quickly accelerated across the junction and has a very low probability of recombining with another charge carrier. The drift velocity of charge carriers across this junction is several orders of magnitude faster than the diffusion velocity. Since this is so much faster, the radiation degraded minority carrier lifetime which normally stops charge carriers has no effect upon charge carriers created in this region until the lifetime (τ) is severely reduced. As a result, solar cells with very wide depletion regions, such as diffused junction solar cells, or those cells with very low dopant levels, are affected to a much smaller degree by radiation induced defects.

2. Open Circuit Voltage

The radiation induced decrease on the minority carrier lifetime (τ) also has the effect of decreasing the open circuit voltage (V_{oc}). The recombination-generation current was found to be dominated by generation within the depletion region, and as a result, V_{oc} is reduced by this process. This seems counter-intuitive because the creation of electron-hole pairs near the depletion region is the most efficient way of producing current. The creation of charge carriers by this method in the depletion region reduces the electrostatic potential created by the fixed charge carriers in this region. This effectively reduces the open circuit voltage (V_{oc}).

The effect of charge trapping and compensation also have manifestations in the output of the solar cell. Charge trapping reduces the minority charge carrier

concentration, which directly reduces the current output of the cell. The reduction in the charge concentration has the effect of increasing the series resistance within the cell. Compensation has the effect of reducing the concentration of the majority charge carriers, which increases the width of the charge depletion region. This directly increases the recombination-generation current in the depletion region, which results in the dropping of the V_{oc} due to its saturation with charge carriers.

3. Maximum Power Point

The effects which influence the short circuit current and open circuit voltage also affect the maximum power point of the solar cell. For radiation degraded cells, the maximum power point occurs in the region of the I-V curve at which the diffusion current and the recombination current are both significant. As described above, a reduction in minority charge carriers, resulting from the increase in recombination current outside the depletion region, reduces the cell's short circuit current. Just as the decrease in minority carrier concentration affects the short circuit current, it also affects the current at the maximum power point. Likewise, there is a significant drop in the voltage at the maximum power point, due to the drop in electrostatic potential across the depletion region as a result of an increased generation current.

4. Series and Shunt Resistance

Typical radiation effects on solar cells result in an increased series resistance and a decreased shunt resistance. The series and shunt resistance changes due to radiation defects are readily apparent when observed on an IV curve. A normally very high shunt resistance is reduced by radiation defects due to the increase in generation current in the charge depletion region. The reduced shunt resistance will result in a reduction in cell output current proportional to the cell voltage. This causes an overall drop in cell current across the entire IV curve, but no change in V_{oc}. As stated earlier, the loss of minority charge carriers, from a variety of effects, has the effect of increasing the cell's series resistance. The increase in series resistance causes a decrease in the cell voltage proportional to the cell current.

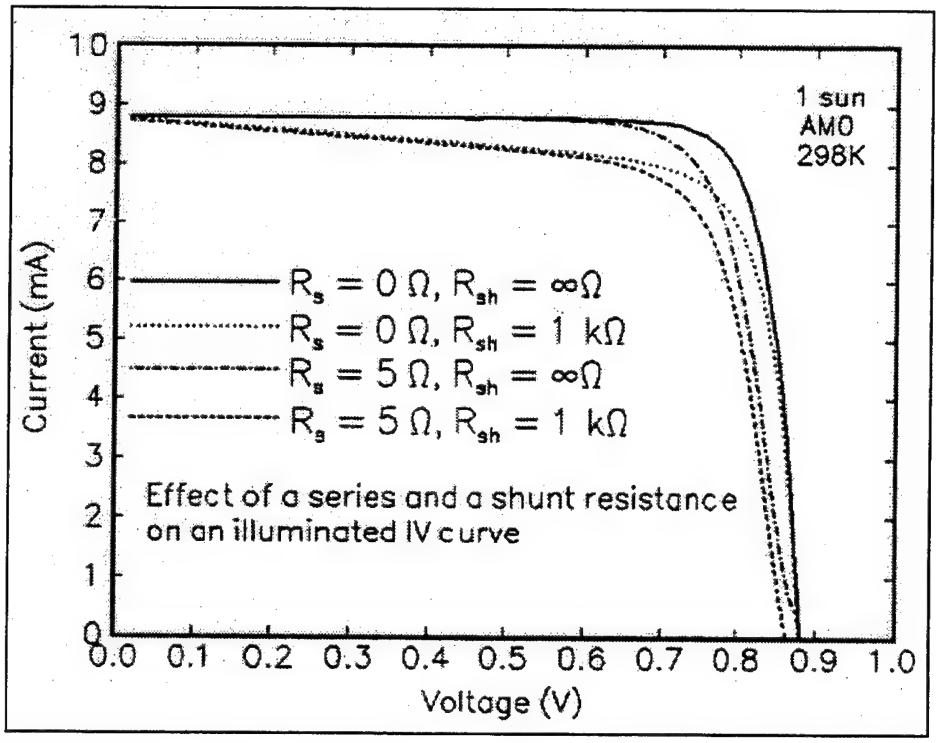

Figure 3. 8 The Effect of Resistance upon the Output of Solar Cells. [Ref. 5:p. 40]

IV. ANNEALING OF RADIATION INDUCED DEFECTS

As described in the previous chapter, the primary cause of degradation in solar cells is the introduction of defects into the semiconductor's crystal lattice. The annealing process is one which reverses the effect which radiation has upon the cell by returning the lattice to its original structure. To accomplish this restructuring, the energy of a displaced atom must be increased to figuratively lift it out of its potential energy well and allow it to return to its original state. Without annealing, all displaced atoms have some probability of moving from their meta-stable defect sites. This can be described by a parameter called mobility. The effect of annealing is to increase the mobility of the site defect, and so its probability moving from the meta-stable defect site to the original site is increased. As will be described, this increase in mobility can be accomplished through one of a variety of means.

A. MEASUREMENT OF RADIATION EFFECTS

The primary effect of radiation defects to a crystal lattice is the reduction in minority carrier diffusion lengths or lifetimes. This, more than any other factor, affects the total electrical output of the cell. The recombination rate has been shown to be inversely proportional to the minority carrier lifetime. The relationship below equates the change in recombination rate of a radiation damaged solar cell to that of an undamaged cell, plus the rate due to fluence levels of proton and electron radiation. As seen below, the relationship between these terms seems straightforward, however, the physical measurement of the minority carrier lifetimes is not practical. [Ref. 6:p. 3-18] The measurement of the diffusion length is possible, but the diffusion length value is not well defined strictly in terms of the total fluence. A direct measurement of the physical properties is ordinarily forgone, and the solar cell's electrical properties are utilized.

$$\frac{1}{\tau} = \frac{1}{\tau_o} + \left(\frac{1}{\tau_e} + \frac{1}{\tau_p} \right) \quad = \frac{1}{\tau_o} + (K_{\tau_e} \times \Phi_e) + (K_{\tau_p} \times \Phi_p) \qquad (4.1)$$

1. Electrical Equivalence for Physical Properties

While the diffusion length and the lifetime of minority charge carriers can be approximated, the relationship between the diffusion length and V_{oc} or I_{sc} is not well defined. For instance, the introduction of defects within the depletion region itself can have a significant effect on the V_{oc}, but relatively little effect on the diffusion length. Alternatively, if similar defects are introduced in the base of the cell, both the diffusion length and electrical properties can be degraded. As a result, direct measurement of the electrical properties gives the most straightforward means of measuring damage to the cell and will be the primary means of measuring damage to the cell in this research. [Ref. 6:p. 3-18]

As noted previously, both I_{sc} and V_{oc} are severely degraded by radiation damage. The effect of radiation can be expressed in terms of the original open circuit voltage, or short circuit current, the total fluence of electrons or protons (Φ), and a parameter (Φ_x) at which degradation is modeled as a linear function of the logarithm of the total fluence. [Ref. 6:p. 3-18]

$$\begin{aligned} I_{sc} &= I_{sc}(0) - C\log\left(1+\frac{\Phi}{\Phi_x}\right) \\ V_{oc} &= V_{oc}(0) - K\log\left(1+\frac{\Phi}{\Phi_x}\right) \end{aligned} \tag{4.2}$$

One property of the solar cell which is not influenced greatly by the fluence level is the fill factor (FF). This applies only to uniform damage to a solar cell, such as when radiation with energies sufficiently high to completely penetrate the cell is encountered. If radiation, such as protons, were to stop within the cell, there would be significant damage to the lattice near the termination of the path. The fill factor retains its value throughout a range of fluence values. As a result, the degradation of the maximum power point can be easily determined by the product of the degraded V_{oc} and I_{sc}. [Ref. 6:p. 3-20]

$$P_{\max} = P_{\max}(0) - H\log\left(1+\frac{\Phi}{\Phi_x}\right) \tag{4.3}$$

2. Damage Equivalence

The types and energies of radiation to which a solar cell may be exposed in space can cover a fairly wide range. As noted in Chapter III, electrons and protons cause the most significant damage. In order to evaluate the damage in different cells due to different energies of to radiation, a baseline has been adopted. This method of equating damage which is due to a variety of different types and energies of radiation to a single type and energy, namely 1 MeV electrons, is known as damage equivalence. [Ref. 6:p. 3-21] For instance, the commonly accepted value for relating damage due to 10 MeV protons to that of an equal fluence level of 1 MeV electrons in silicon is 3000. In this research, a minimum electron energy value of 30 MeV electrons was available. An attempt to determine an electron equivalence for 1 MeV electrons has been made utilizing both calculated values for damage due to 30 MeV electrons and the results of a technique known as DLTS, Deep Level Transient Spectroscopy.

3. DLTS Deep Level Transient Spectroscopy

Deep Level Transient Spectroscopy is a means by which the number and type of defects can be quantified through the measurement of specific electrical properties of the semiconductor. It is well known that lattice damage occurs during radiation of a solar cell, however, the type and number of defects are not adequately known. Deep-levels, or traps near the middle of the energy band gaps, capture and release charges based upon the their position within the band gap and the thermal energy applied to them. The traps can be filled by biasing the semiconductor. This results in the injection of charge carriers into all of the traps of a given type, for instance electron traps. A biasing of the semiconductor in the opposite direction will fill the traps of the opposite type, for instance hole traps. With a continuous current, these traps will effectively remain fully filled. If the current is turned off, the traps will emit the trapped charges at a rate dependent upon the temperature of the material and the type of defect. Measuring the change of capacitance of the semiconductor over time will yield the steady state capacitance and the thermal emission rate of the traps. [Ref. 17:p. 52]

The DLTS technique utilizes the thermal emission rate in a range of temperatures to determine the activation energy, defect density, capture cross section, and characterize

the defect. The process uses what is known as a double box car measurement. The semiconductor is first injected with charge carriers at a given temperature. Next, the fill pulse is removed, and the capacitance is measured at two times, t_1 and t_2, separated by a set time value, called the rate window. The process is repeated for a wide range of temperatures, and a record is made of the difference in the two capacitance measurements at each temperature. A plot is made of the dependence of the capacitance difference with temperature for this rate window. The process is repeated for several rate windows, and from this, the value of the activation energy of the defect can be determined. The height of the capacitance difference measurement is proportional to the defect density within a sample. The exact concentration of the trap can be determined by using this value and the concentrations of the dopants in the sample. [Ref. 17:p. 60] With the aid of Robert Walters of the NRL, the number and type of defects resultant from 30 MeV electrons have been correlated to that resulting from 1 MeV electron irradiation.

B. TYPES OF RADIATION DEFECTS

Energetic photons, such as gamma rays, and subatomic particles, such as electrons, protons, neutrons, and larger ions, can cause the displacement of atoms. Photons can induce displacements through the creation of Compton electrons which then interact with the crystal's atoms. Subatomic particles and larger ions cause these displacements through direct interaction, by either elastic or inelastic collisions. A variety of displacement defects including vacancies, interstitials, and Frenkel or close pairs, which are combinations of vacancies and interstitials, can be produced. In some semiconductors, the vacancies and interstitials are quite mobile and interact with impurities to produce vacancy-oxygen and vacancy-donor pairs. Additionally, multiple defects can be produced through a cascading effect if enough energy is transferred to the primary knock-on atom. The probability of transferring sufficient energy to the primary knock-on atom increases with the mass and energy of the irradiating particle.

C. ANNEALING TECHNIQUES

The annealing of a material is the process by which energy is introduced to a damaged crystal structure to elevate the energy of atoms which have been displaced and are trapped in a meta-stable state. The energized atoms then are able to migrate to a more

stable and orderly energy state in the crystal. This return to a lower energy state, removes defects through the recombination of interstitials and vacancies, and returns the crystal to its original highly structured form.

There are several methods of annealing semiconductors, including thermal annealing and two forms of minority carrier injection annealing. The thermal annealing technique, like that widely used for hardening metals, was the first to be used for reducing the effects of radiation damage in semiconductors. The two types of minority carrier injection annealing are called forward-biased current annealing, and photo-injection annealing. There are advantages and disadvantages to each method depending on the solar cell type and satellite configuration.

1. Thermal Annealing

Thermal annealing has proven successful in annealing out radiation induced defects in solar cells, however, the elevated temperatures required severely limit its applicability to orbiting satellites. Thermal annealing introduces energy directly into a cell by heating it to a desired temperature. When thermal annealing is utilized, the integrity of contacts for electrically connecting the cells of a typical array must be considered. These contacts are typically lead-tin solder, which have a melting temperature of approximately 190°C. This is well below the 300°C needed to anneal silicon cells with fairly low fluences ($1x10^{14}$ e^-/cm^2 and below). Even higher temperatures, in the range of 400° to 500°C, are required for annealing damaged cells with radiation fluences above $3x10^{14}$ e^-/cm^2. GaAs cells typically require approximately 200°C thermal annealing temperatures for 30 minutes or longer, which does not provide a reasonable temperature margin for the solder connections. Further, diffused junction InP cells have been proven to partially anneal at temperatures of 100°C (3 hour annealing time), and almost fully anneal at 227°C (1 hour anneal time). [Ref. 18:p. 2] Even with these reduced temperatures, thermal annealing is not practical for annealing of cells in orbit. The power required to raise the temperature of a cell to these values for an extended period of time is not generally available to a satellite. Of note, is the reduced temperature required for annealing less damaged cells. This emphasizes the importance of periodic annealing for maintaining the efficiency of a cell, prior to complete degradation.

2. Minority Carrier Injection Annealing

A category of annealing which avoids the high temperature of thermal annealing is minority carrier injection annealing. Minority carrier injection annealing is a method that can be subdivided into two categories, namely, current annealing and photo-injection annealing. Both annealing techniques rely on the introduction or the creation of a large quantity of minority charge carriers or current within the solar cell. The primary mechanism for annealing in this technique deals with the trapping and recombination of charge carriers at the radiation induced defect sites. When a large current is passed through the cell, charge carriers continually fill traps and recombine with charge carriers of the opposite sign. When they recombine a small amount of energy is released at that site in the form of a photon or phonon. The phonon causes regions of compression and rarefaction of the crystal lattice as acoustic waves do. These lattice undulations result in the distortion of the energy band structure. [Ref. 4:p. 20] The release of this energy is thought to increase the probability of defect movement and allow a restructuring. This energy release at the site of the defect, in combination with a moderate amount of heating, anneals defects within the cell. The means by which the charge carriers, or current, are introduced is the primary difference between these two methods.

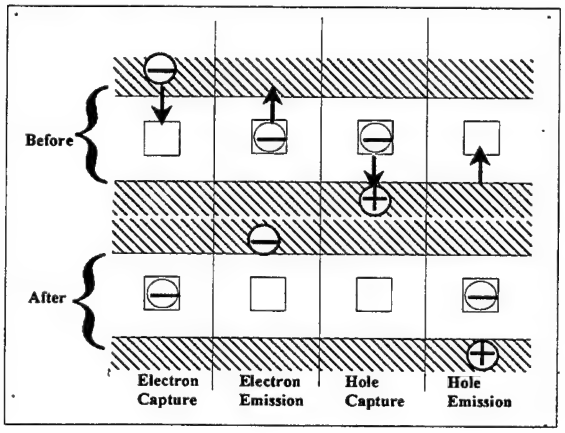

Figure 4. 1 Electron Capture followed by a Hole Capture (Recombination) results in an Energy Release at the Defect Site.

a. Forward-Biased Current Annealing

Forward-biased current annealing is the process in which a significant forward-biased current is applied directly to a degraded cell. The current density applied

can be in the range of about 10 to 50 times the short circuit current, I_{sc}. This causes a dramatic increase in minority carrier concentration and also results in the production of a moderate amount of heat. The procedure for implementing this type of annealing would involve the addition of a small amount of area to an existing array. This additional area would provide current for periodically annealing individual strings of the larger array. The annealing in this manner could be nearly a continuous process of annealing the solar cells prior to significant degradation.

Experimental results involving current injection annealing of GaAs and InP solar cells are excellent. Annealing of GaAs cells with a current density of $0.5A/cm^2$ at a temperature of 90°C (anneal time of 19 hours) was conducted, with the resulting overall regain of approximately 28% of the power lost. Experiments involving diffused junction InP cells with only 0.25 A/cm^2 current density at 90°C (anneal time of 16.5 hours) produced a power recovery of 62% of the lost power. [Ref. 19:p. 37] The application of this type of annealing process should be straightforward and will vastly improve the long term health of the solar array. Although this method of annealing is excellent for future satellite systems, the on-orbit annealing capability must be launched with the satellite. Without the existing additional solar array panel for annealing, and the associated electrical architecture, this annealing procedure is useless.

b. Photo-injection Annealing

An alternative procedure for accomplishing the annealing of an existing array in orbit is photo-injection or laser annealing. This relatively new and unproved technique involves the illumination of solar array panels with a high intensity light source optimized to the cell's peak output. A laser is used to both force the production of a large current and to produce additional heat needed for realigning the crystalline structure of the solar cell. For this process, the temperature increase is actually not as vital as in other forms of annealing, in fact it could be the source of reduced annealing potential. This is due to the fact that the current output of a cell is reduced with increasing temperature.

The key to the laser annealing process is the marked increase in the cell's efficiency to monochromatic light at its peak response. The peak response is associated with the energy band gap of the given cell. Response of a cell to photons with energies

less than the cell's band gap is always zero, and the only effect of such low energy photons is heating of the cell. Excessive heating reduces cell efficiency, and elimination of these low energy photons is therefore beneficial. Additionally, the temperature sensitivity of the cell is directly related to the band gap energy of the material. As the band gap energy increases, the temperature sensitivity will decrease. [Ref. 6:p. 1-31] For silicon the band gap energy is 1.12 eV, and 1.34 eV for InP cells, while for GaAs the band gap is 1.42 eV. [Ref. 16:p. 72] Consequently, silicon cells are quite sensitive to heating, while InP and GaAs cells are much less sensitive to temperature increases, and are better suited to annealing through laser illumination.

Research, using a continuous wave (CW) laser with GaAs solar cells, has indicated a laser annealing response only after extended annealing times. [Ref. 21:p. 57] In this experiment, cells were exposed to 65 MeV electrons to the equivalent dose of $1.5x10^{15}$ e^-/cm^2 fluence of 1 MeV electrons by a linear accelerator. The cell's power was degraded to approximately 80% of its original power, and laser annealing was conducted using a CW argon laser. As in the current injection annealing process for GaAs cells, target annealing parameters of a current density of $0.5A/cm^2$, and a temperature of approximately 90°C was used. The laser used to induce the cell's self-generated current was a CW argon-ion laser which produced an average irradiance of about 2.7 W/cm^2 at wavelengths in the range of 488-514 nm. The peak absorption for GaAs cells is 850 nm, so the theoretical efficiency of the cell at this wavelength is somewhat lower than at its peak. The temperature of the cell was stabilized at 90°C, well below the thermal annealing temperature for GaAs cells, prior to testing to simulate the average temperature of a cell in orbit. The laser was used to both induce the current and simultaneously heat the cell to the target temperature of 90°C. Additional heat was supplied by a resistive heating element. An average annealing time of 20 hours at 90°C was used to prove the concept of annealing GaAs cells by illumination with a CW laser. The lengthy annealing times used in this experiment were due to the fact that proof of concept was required and not a minimization of annealing time. The results were mixed, but an average of about 15% of the cell's lost power was regained.

V. APPLICATION OF LASER ANNEALING TECHNIQUE

A. INTRODUCTION

Because the degradation of a solar array severely limits the overall lifetime of a satellite, it therefore increases the overall cost of a satellite program. The satellite's end of life, EOL, power requirements must be met and thus a larger, more massive, more efficient, and typically more expensive solar array must be designed. The annealing of an existing, in orbit, solar array which extends the satellite's life, has the effect of reducing the overall cost of the satellite program. With a renewed array, a replacement solar array panel, or, for that matter, replacement satellite is not required. Assuming that the laser annealing technique itself affords a degree of recovery in the solar cells, there are still many complex obstacles to be overcome when attempting this process on an existing satellite. The first assumption, for this discussion, is that the laser system is ground-based. This ensures the process is not subject to the problems of transporting and maintaining a space based laser system, but other obstacles are imposed as a result. Among the most significant obstacles is finding a laser system with a wavelength of light that is adequate for both annealing the array and transmission through the Earth's atmosphere. The power and directing capability required by a such a ground-based laser system present even more difficult, but not insurmountable, obstacles.

B. ATMOSPHERIC TRANSMISSION EFFECTS

One primary limit to the intensity required of a ground-based laser to anneal an orbiting solar cell array is the natural tendency of the atmosphere to absorb and scatter light. The scattering and absorption depend on a multitude of factors including the angle with which the laser light must traverse the atmosphere, the size and density of naturally occurring atmospheric molecules (H_20, CO_2, O_3, etc.) and aerosol particles, and variations in the thermal and pressure lapse rates. The value of transmittance (τ) can be approximated by utilizing the appropriate attenuation coefficient (γ) in Beer's law, as seen below. The attenuation coefficient, γ, is the sum of individual coefficients for absorption (α), and scattering (β), for molecular, aerosol and large particle (water droplets)

interactions with photons. For this discussion, it is assumed that each of these coefficients, if encountered at all, is homogeneous along the entire path length. Each of these terms is the product of a concentration (N), and cross section (σ), of a given type, or size of particle. Each of these scattering or absorption coefficients and their associated cross sections will be described in the following sections. Of primary concern to this application are those properties of the atmosphere and those limitations of the technique which cannot be avoided or overcome.

$$\tau = I(z)/I_o = e^{-\gamma z} \quad \text{where:}$$
$$\gamma = \alpha_{molecular} + \beta_{Rayleigh} + (\alpha_{Mie} + \beta_{Mie}) + \beta_{geo} \tag{5.1}$$

1. Energy Band Gap and Absorption Band Limitations

The primary requirement of the laser light utilized is that it has sufficient energy to produce electron-hole pairs within the crystal lattice of the solar cell. Without photons of this energy, namely the band gap energy, the laser annealing technique will succeed only in adding heat to the solar cell. The upper limit of wavelength (i.e., the lower limit of energy) of photons capable of producing current in a given cell is directly related to the band gap energy by the following equation.

$$\lambda_c = 1242/E_g \tag{5.2}$$

In this equation, λ_C is the cutoff wavelength, or highest wavelength (in nm) to which a cell responds by producing current, and E_g is the band gap energy in eV. For silicon the cutoff wavelength is 1127 nm, 926 for InP and for GaAs it is 886 nm. Obviously, light with a shorter wavelength, that is to say, with energies greater than the band gap can be utilized. In fact, while the response curve of solar cells drops off quickly around the upper limit of wavelength, it typically decreases very gradually as the wavelength is decreased, as depicted in Figure 5.1. This sets an upper limit for selection of a laser wavelength for these three types of solar cells at about 850 nm.

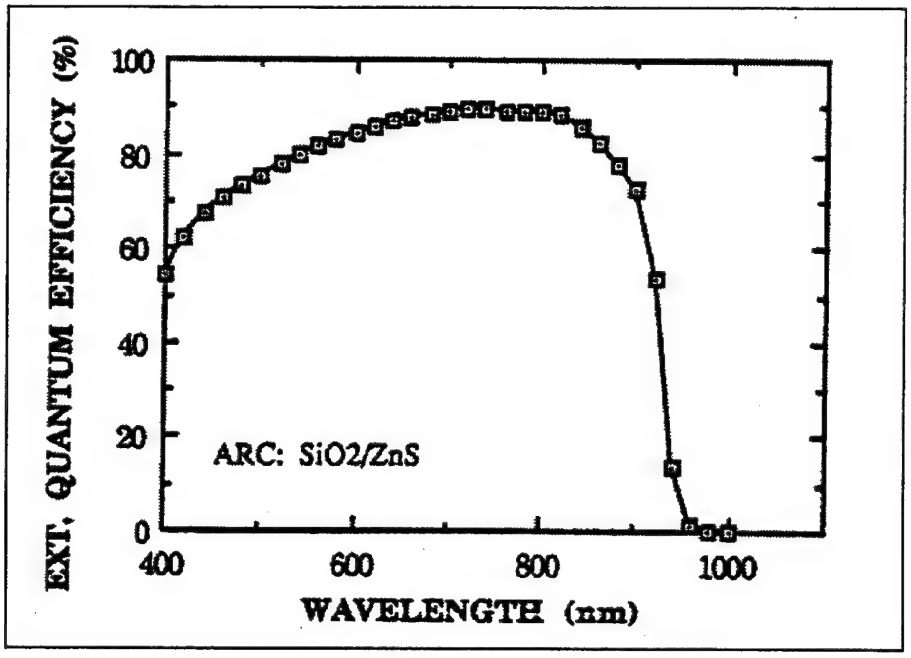

Figure 5. 1 Quantum Efficiency of the Nippon Mining InP Solar Cells used in this Research. [Ref. 33:p. 3]

For the application of laser power from a ground-based source, however, consideration must be given to the response of the cells and also to atmospheric transmittance. There is a unique range of wavelengths which will optimize the output of the cell and speed the photo-injection annealing process. The efficiency of a silicon solar cell exposed to monochromatic light in the wavelength range of 800-1000 nm can be on the order of 40%. The maximum efficiency for InP and GaAs illuminated by light in the range of 800-860 nm is even higher, at approximately 50%. [Ref. 39:p. 1893][Ref. 20:p. 1496] The production of high current density on the order of the $0.5A/cm^2$, as in current injection annealing, is feasible even with a modest intensity of monochromatic light, such as from a laser. Atmospheric considerations, such as absorption by ozone in the atmosphere, put a limit on the lowest wavelength that can be transmitted. As depicted in the following graph, the transmittance of the atmosphere drops significantly in the neighborhood of 350 nm, where the absorption band for atmospheric ozone lies. As shown by Figure 5.2, most of the wavelengths in the range between 450 nm and the upper limit 850 nm permit relatively good transmittance and are the focus of this investigation.

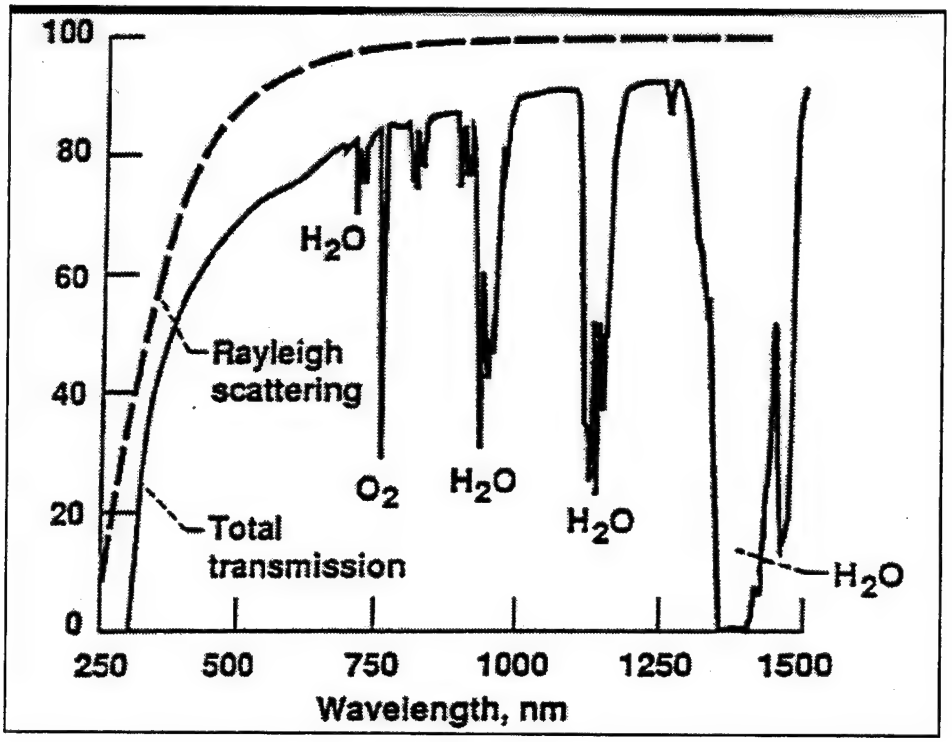

Figure 5. 2 Transmissivity of the Earth's Atmosphere for a Range of Wavelengths. [Ref. 22:p. 15]

Within the above stated range, the molecular atmospheric absorption (α) is relatively low, but the laser intensity to reach a LEO or GEO orbit is so large that this analysis is, obviously, not sufficient. Additionally, this type of qualitative analysis, typically used for determining the transmittance of incoherent light with a broad spectrum of frequencies, is not satisfactory for this application. Within these transmission windows are significant absorption lines which, though quite unlikely, may coincide exactly with the output of a laser, nullifying its output. More importantly, the absorption lines of atmospheric molecules are not strictly lines, but are distributions about the lines. The absorption cross section creating these lines depends upon pressure and temperature and results in a slight spreading of the line width. Since the line widths of a laser are typically very narrow (from 0.001 to 2Å), the spectral absorption regions which need to be investigated must also be very narrow. This ensures that there is not an exact match of absorption line with emission line, and also, considers the role that line spreading has upon the wavelength's transmittance.

2. Mechanisms of Molecular and Aerosol Scattering

Scattering is defined as a process in which there is no loss of energy, but only a directional redistribution of the energy which leads to a significant reduction in beam intensity for large path lengths. The three primary types of scattering of light which occur are called Rayleigh, Mie, and geometric scattering. The degree which each of these will occur depends on the type, concentration, and sizes of the particles, in addition to the wavelength of incident light.

Rayleigh scattering is only significant when the sizes of the particles are very much smaller than the incident light. Rayleigh scattering, also called molecular scattering, is due to the displacement of bound electrons by the electric field of the incident photon. The displacement produces a dipole within an atom or molecule. This dipole oscillates at the same frequency as that of the incident photon, and reradiates the energy. The spatial distribution of the scattering is such that there is a similar degree of forward scattering and backscattering, but there is a somewhat smaller amount of scattering laterally. The degree to which a molecule will scatter energy in this manner depends upon its Rayleigh cross section. This cross section depends on the inverse of wavelength of the light to the 4^{th} power ($\sigma_{s\_Rayleigh} \propto 1/\lambda^4$). Thus, as wavelength increases, the degree of Rayleigh scattering drops off significantly. For our application, the wavelength of light used is relatively fixed at 450 to 850 nm. The sizes of molecules in the atmosphere are typically on the order of a few tenths of a nanometer, and so the concentration of these particles determines the degree of Rayleigh scattering. [Ref. 22:p. 28] The value of molecular, or Rayleigh scattering ($\beta_{Rayleigh}$), is the product of the cross section ($\sigma_{s\_Rayleigh}$), and the concentration of the scattering particles (N_s).

Mie scattering dominates when the radii of the particles and the wavelength of the incident light are nearly equal in size. Aerosol particles and water vapor (such as haze 0.5 μm) in the atmosphere are often only a few tenths of a micrometer. They are approximately the same size as the wavelength in question, and are, thus, responsible for Mie scattering. Mie scattering is characterized by a much higher degree of forward scattering than lateral or backscattering. This degree of forward scattering character also increases with particle size. Particle size is the main factor in determining scattering

character. The Mie theory takes into account a variety of parameters which influence degree of scattering. These include particle shape, dielectric constant, and absorptivity, and are sometimes referred to as aerosol absorption. [Ref. 22:p. 38] Often, these scattering and absorption processes are combined into the total Mie "scattering" or aerosol extinction. The size of the particle is, as indicated, a driving factor. There are other factors, which are in essence absorption factors, used to calculate a multiplicative constant ranging from about 1 to 4, which can significantly increase this loss. This attenuation factor, K, depends on the ratio of particle size, and the wavelength ($\chi=2\pi r/\lambda$). The value of K varies significantly when the value of χ is less than 5. As the size ratio, χ, of the particle increases above 5 times the wavelength, the value of the attenuation factor, K, stabilizes at about 2, as shown in Figure 5.3. [Ref. 22:p. 33] The value of the Mie scattering and absorbing components of the attenuation coefficient is the product of the cross section and the concentration of scattering particles $\alpha_{Mie}+\beta_{Mie}=N_{s\_Mie}\sigma_{Mie}$. The Mie attenuation cross section, σ_{Mie} is the cross sectional area of the particle times K($\sigma_{Mie}=K\pi r^2$). As a result of this factor, K, the attenuation of light in this region, due to Mie scattering, is significantly greater than that of Rayleigh scattering. Although, this graph is strictly for horizontal transmission losses, the attenuation due to Rayleigh scattering in the area of 550 nm is almost insignificant. This is true despite the small concentrations of aerosol particles in the atmosphere.

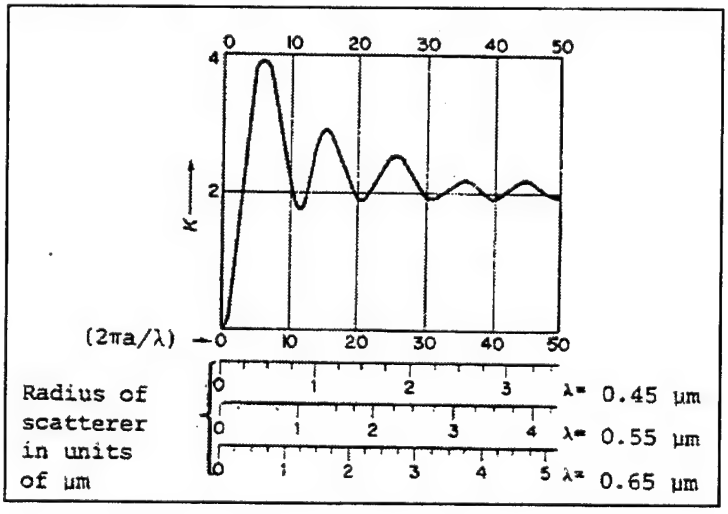

Figure 5. 3 Attenuation Factor (K) for Various Particle Size Ratios. [Ref. 22:p. 33]

It is a daunting task to accurately predict what the actual atmospheric absorption of light of a specific wavelength will be at any given time. This is primarily due to large rapid changes in the lower atmosphere due to weather. As a result, an attempt has been made to correlate a standard meteorological value, namely the visual range at the Earth's surface, to the attenuation of light at a specific wavelength resulting from aerosol extinction. Transmittance at a specific wavelength has been shown to be in close agreement with the equation below. Here, the visual range, V, and path length, z, are in km, and λ is in nm. [Ref. 22:p. 38]

$$\tau = e^{-(\beta_{Mie}+\alpha_{Mie})z} = e^{-\left[\frac{3.91}{V}\left(\frac{550}{\lambda}\right)^{\delta} z\right]} \text{ where } \delta = 0.585V^{\frac{1}{3}} \quad (5.3)$$

This gives a very rough approximation for the transmittance of light through the atmosphere, and cannot be used to determine the intensity of light that would actually reach a satellite. It does, however, give an indication of which wavelengths can pass most easily based upon their Mie scattering. The result is that the higher the wavelength, the higher the transmittance value, as can be seen in Figure 5.4, below.

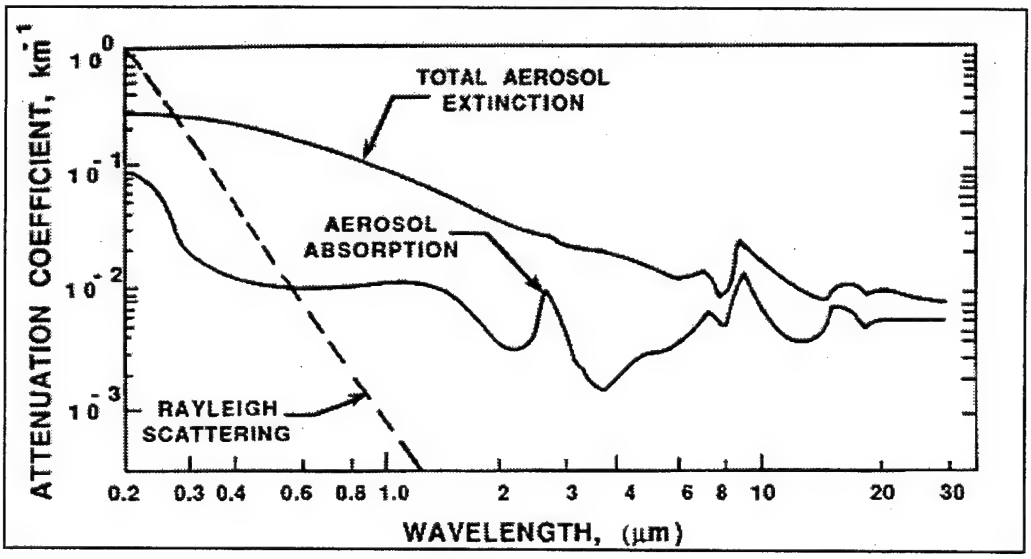

Figure 5. 4 Atmospheric Attenuation Coefficients for Rayleigh Scattering and Aerosol Scattering by the Atmosphere at Sea Level. [Ref. 22:p. 39]

Finally, geometric scattering, or nonselective scattering, becomes significant when the particle size is much larger than wavelength of the incident light. The scattering coefficient for particles, which are much larger than the photon wavelength, is almost

independent of the wavelength within this range, and hence, termed "nonselective". The geometric scattering mechanism has the effect of forward scattering most of the incident photons, especially when encountering very large particles. Thus, the attenuation is not as large as that for Mie scattering, however, it this does occur at slightly off angles. As a result, the intensity of the incident beam is somewhat dispersed. An important caveat to this is fog, which has a radius on the order of 5-15 micrometers, and is therefore close to the range for Mie scattering. As a result, they retain a large attenuation factor characteristic of Mie scattering (K=2). Rain drops, on the other hand, are on the order of a few tenths of millimeters or larger and are significantly larger than the wavelengths of visible light. Their losses are somewhat reduced owing to a strict geometric scattering mechanism. An equation for the geometric scattering coefficient for rain is given below. A dependence on the particle radius, r, is readily apparent in the geometric scattering coefficient, in addition to the rainfall rate, $\Delta x/\Delta t$ (cm/sec). [Ref. 22:p. 41]

$$\beta_{geo} = 1.25x10^{-6}\left(\frac{\Delta x}{\Delta t}\right)\frac{1}{r^3} \tag{5.4}$$

The overall loss due to geometric scattering is significantly smaller than that due to Mie scattering for the visible wavelengths considered. In general, however, this scattering process could be completely avoided by ensuring laser operation during rain free, cloudless days.

3. Thermal Blooming

Another characteristic of the Earth's atmosphere that directly affects transmission of certain wavelengths of light is the phenomenon known as thermal blooming. Thermal blooming occurs when there exists a high rate of energy absorption from the light by the molecules and is thus unique to high power optical systems such as high energy lasers. [Ref. 23:p. 63] The effect of energy addition is a rapid increase in temperature and decrease in density, which decreases the index of refraction of the path. The index of refraction is more significantly reduced in the center of the beam and less on the outer fringes of the beam. Since light bends toward the higher indices of refraction, light in the center will be bent outward, spreading the beam and reducing the beam's overall

intensity. The tendency of the light to be affected by thermal blooming correlates directly with the absorption of specific atmospheric components, and the duration of the heating caused by the light. Thermal blooming can be considered negligible if the pulse length (of a pulsed laser) is very short (less than 10^{-5} sec), or if the beam does not dwell on the same column of air for an extended period. Additionally, thermal blooming will be insignificant if the laser energy is not readily absorbed by the medium. [Ref. 24:p. 7-8] The application investigated here utilizes a continuous wave (CW) laser beam applied to the solar array for a period of several minutes. The heating is therefore considered continuous for the annealing time period. The slewing rate of the laser beam during this period ranges from tens of degrees per minute, for LEO satellites, to an almost negligible rate, for high altitude satellites. A certain amount of mixing due to wind can be expected perpendicular to the beam, which would allow for cooling of the gases and a reduction in thermal blooming. This wind may be sufficient to produce significantly cooler temperatures on one side of the beam. In this case, the high index of refraction associated with the cooler temperature could bend the light in one direction instead of uniformly spreading it. The most important consideration is the actual absorption of the laser light by the atmosphere. In general, thermal blooming tends to dominate the transmission of longer wavelengths (5-10μm), while aerosol and turbulence effects are more significant at shorter wavelengths. As a result, thermal blooming is not a significant factor in the transmission of laser energy at the wavelengths investigated.

4. Diffraction Limited Spreading

To this point, the limitations placed on the transmission of laser energy through the atmosphere has been based upon the properties of the atmosphere. There is one optical property which exists independent of atmospherics, namely diffraction. Diffraction is the uniform spreading of a beam based on the premise that all collimated light sources, even lasers, produce beams which are less than perfectly parallel. The angle which the beam diverges is called the diffraction limit and can be defined in two ways. The diffraction can be described by the divergence of the beam measured at the 84% of peak power point. A second description assumes that the beam intensity has Gaussian distribution, and the point at which the peak intensity has dropped to 1/e defines

the cutoff point for the angles. Here the half beam diffraction angle (ϕ) is in radians, and the wavelength (λ), the path length (z), and the aperture (D) are in equivalent units of length.

$$r_{Airy} = \phi_{Airy} z = 1.22\frac{\lambda z}{D}$$

$$r_{Gaussian} = \phi_{Gaussian} z = 2\frac{\lambda z}{\pi D} = 0.637\frac{\lambda z}{D} \tag{5.5}$$

5. Turbulence

Any optical system which must operate over an extended range, experiences a degradation in quality due to a type of atmospheric turbulence. There is a multitude of factors which result in the kind of turbulence which we know as mechanical or wind turbulence. These include altitude, time of day, local terrain, and local weather. Temperature deviation is the ubiquitous factor which results in the small density changes that produces the kind of turbulence that influences optics. This specific type of turbulence is known as optical or temperature turbulence. [Ref. 23:p. 59] Temperature turbulence is primarily a low altitude phenomenon isolated to 30,000 feet or below. The type of degradation due to temperature turbulence is similar to that of thermal blooming, but random in nature. A distortion of the phase of the wavefront of the outgoing beam is first manifested by changes in the local phase velocities resulting from changes in the indices of refraction. As the wave front progresses, there are random changes in direction and intensity, which result beam spreading beyond that of the diffraction limit.

Two factors, known as the inner and outer scale sizes, determine what type of interaction will take place when turbulence is encountered by a photon. Temperature fluctuations are introduced into the atmosphere through a variety of large scale phenomena such as solar radiative heating or connective heating from the Earth's surface. This large scale uniform change to the atmospheric temperature is referred to as the outer scale size, L_o. Typical sizes of the outer scale size (L_o) are about 100 m or 0.2 times the altitude, whichever is smaller. Since these cells of uniform density are much larger than the beam diameter, they act to uniformly distort the beam. From the value of L_o can be

determined the degree to which a laser beam will wander, or be distorted uniformly from its original path. This results in no change of beam diameter. Ultimately, the motion of large eddies causes the formation of smaller eddies within the beam path. The inner scale size, ℓ_0, is the size of these smaller turbulence eddies, typically much smaller than the diameter of the beam. Using this, the degree of turbulent spreading expected in the beam can be determined.

The most important factor in an analysis of turbulence and its effect on beam distortion is the refractive index structure coefficient, C_n. It is based upon the local pressure and the difference in temperatures between two points along the beam's path separated by a distance, r. [Ref. 22:p. 48] Here, the pressure (P) is in millibars, temperature (T) is in Kelvin, and separation distance (r) is in cm.

$$C_n = \left[7.9x10^{-6}\frac{P}{T^2}\right]C_T \quad \text{where } C_T = \sqrt{\langle (T_1 - T_2)^2 \rangle}\,\frac{1}{r^{\frac{1}{3}}} \tag{5.6}$$

A typical value for C_n in strong turbulence is $5x10^{-7}$ $m^{1/3}$, and for weak turbulence it is $8x10^{-9}$ $m^{1/3}$. Because pressure, temperature, as well as, temperature variability all depend upon altitude, there is a correlation between the refractive index structure coefficient (C_n) and altitude. The progression of decrease in this value is shown in Table 5.1, below.

Height (km)	C_n ($m^{-1/3}$)
0.001	$3.0x10^{-7}$
0.003	$2.0x10^{-7}$
0.01	$1.5x10^{-7}$
0.03	$1.0x10^{-7}$
0.1	$6.0x10^{-8}$
0.3	$4.0x10^{-8}$
1	$1.0x10^{-8}$
3	$<1x10^{-8}$

Table 5. 1 Refractive Index Structure Coefficients vs. Height. [Ref. 22:p. 49]

The effect that diffraction has upon laser beam propagation through the atmosphere is significant. Two other factors which affect beam spreading beyond the diffraction limit, as described above, are jitter and turbulence spreading. Spreading due to jitter is a function of the laser construction, and this can be overcome only through changes in the stabilization of the laser. Correction of jitter has no secondary impact upon the ultimate spreading due to turbulence or diffraction. The spreading due to diffraction and turbulence are linked by a common factor. Turbulence spreading, like spreading due to diffraction, can be changed through the selection of laser transmission wavelengths. The turbulence spreading, r_t, is defined below as the distance from the center of the beam at which the relative mean irradiance of the beam has dropped by 1/e. If there is knowledge of the path length, and the approximate value of the refractive index structure coefficient (C_n) is available, then a range of optimum wavelengths for the laser could be determined. The two equations necessary are the diffraction beam spreading equation and the equation for the turbulent beam spreading. The value of intensity of the beam in the given equation should be maximized by minimizing the sum of the squares of the diffraction and turbulence contributions to the focal spot area. [Ref. 22:p. 85]

$$I = \frac{Pe^{-\gamma z}}{\pi((\beta r_d)^2 + r_t^{\,2} + r_j^{\,2})}$$

$$r_d = \frac{\lambda z}{\pi D} \quad r_t = 2.01\left(\frac{C_n^{\frac{6}{5}} z^{\frac{8}{5}}}{\lambda^{\frac{1}{5}}}\right) \tag{5.7}$$

By utilizing these equations, it is easily shown that for a 4 meter beam diameter, and orbital altitudes over 300 km, the value of spreading due to turbulence is 2-3 orders of magnitude larger diffraction limited spreading. This is true even for very small values of the refractive index structure coefficient, $C_n = 1 \times 10^{-8}$. Reaching the required intensity of 2.5 W/cm^2, a laser with an output power of well beyond the GigaWatt range is required. With this simple calculation, it is determined that some means of reducing the large amount of spreading due to turbulence is required. The following sections will discuss these means and cite an example of its successful application.

C. LASER DIRECTING

1. Visual Acquisition

There are four major steps to adequately direct a laser from Earth to a satellite in orbit. They are visual acquisition, tracking, atmospheric compensation, and feedback. Visual acquisition of the satellite is accomplished by using a satellite orbit prediction algorithm to direct a telescope. Factors which contribute to this acquisition problem are lighting conditions on Earth, orbital angles, brightness of the satellite, and a suitable hand-off from a tracking file or radar signal. The ideal visual acquisition situation occurs when the satellite is sunlit and an earthbound telescope is in the darkness of night. For a satellite at geosynchronous altitude (36,000 km), the satellite is practically always in sunlight. Provided it is within 60 degrees longitude of the observation point, it will be visible continuously at night, barring its short eclipse times around the vernal and autumnal equinoxes. However, the satellite is normally quite dim due to the great distance and would be typically equivalent to a 15^{th} magnitude star. Polaris, the north star, in comparison is a magnitude 2.1 star. By contrast, a LEO satellite with orbit in the range of 200-2000 km has this situation occur only for a few hours before sunrise and after sunset daily. Additionally, for observation from a continental U.S. based telescope, the satellite must be in an inclined orbit and must be in the northern part of the orbit during these hours. The constraints on this LEO observation are more restrictive, but not incapacitating. Also, unlit LEO satellites could be tracked by infrared sensors for a short period after eclipse entry since the satellite would retain its high temperature for some period of time. A satellite at approximately 20,000 km is sunlit for most of its orbital period time and is capable of being seen for 6 hours/day. [Ref. 25:p. 223]

Acquisition during Earth daylight hours presents a more challenging problem due to scattering of light through the atmosphere. This acquisition has been accomplished for LEO satellites, but not yet demonstrated for GEO satellites. [Ref. 25:p. 222-231][Ref. 26:p. 375]

2. Tracking

Tracking a satellite involves following it with low enough wander and jitter that a laser beam projected through the telescope and directed through the atmosphere will

reside on the satellite continuously. This requires that the laser beam be near diffraction limited and the jitter then must be a fraction of the diffraction limit. A discussion of diffraction limiting follows.

The propagation of a laser beam through vacuum is governed by the diffraction theory. This states that, regardless of the directional quality of the beam, it will diverge and spread as the beam propagates away from its source. Most laser beams propagate with a Gaussian profile such as depicted in Figure 5.5. The beam radius w(z), also called the spot size, is defined as the transverse distance from the center of the beam, or beam axis, to the point where the intensity has fallen to 1/e of its on axis value. [Ref. 22:p. 1] It is given by the following equation where w_0 is the radius at the beam waist and λ is the wavelength.

$$w(z) = w_0 \sqrt{1 + \left(\frac{\lambda_z}{\pi w_0^{\,2}} \right)^2} \tag{5.8}$$

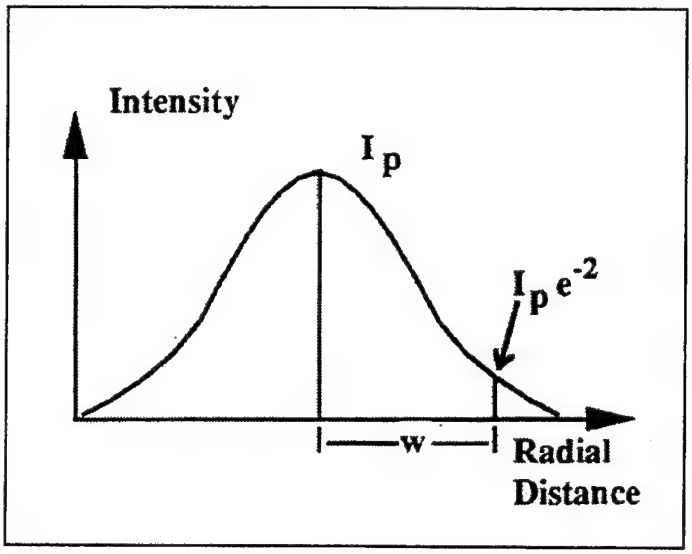

Figure 5. 5 Intensity profile of a Gaussian distribution laser beam. [Ref. 22:p. 3]

For most lasers, the beam waist or the point at which the radius of curvature of the beam is infinite, occurs a short distance from the output mirror. As the beam propagates away from the source, the spot size remains nearly constant at first, but then begins to diverge linearly with distance for significantly large distances from the waist. The smaller the spot size, the faster the beam diverges, and the sooner the beam becomes

useless for annealing satellite solar arrays. The angle indicated in the Figure 5.6 is called the beam divergence angle. This beam divergence and the beam's cross sectional area are given by the following equations.

$$\theta = \frac{w(z)}{z} \qquad A = \pi w(z)^2 = \frac{\lambda^2 z^2}{\pi w_o^2} \tag{5.9}$$

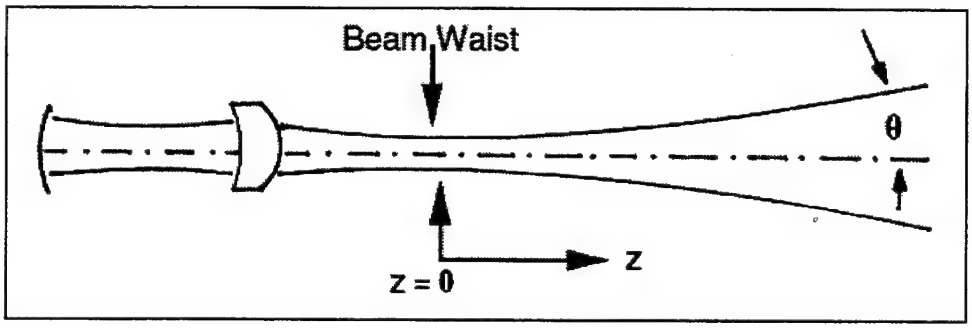

Figure 5. 6 Beam divergence angle θ of a Gaussian beam. [Ref. 22:p. 5]

It can be seen that the beam's cross sectional area can be reduced by reducing the wavelength and by increasing the beam radius at the waist. Since the wavelength is chosen to optimize the annealing process for a given solar cell material, the only option left is to increase the waist radius of the beam.

A device which accomplishes such an operation is called a beam expander, shown in Figure 5.7. The divergence angle of the output beam (θ_o) is given below where θ_i is the input divergence angle, and f1 and f2 are the focal lengths of the input and output lenses, respectively. The diameter of the expanded beam, D_o, is also given, where D_o and D_i are the output and input beam diameters. By substituting the first part of equation 5.10 into the second results in the last equation. It is, therefore, easily seen that the divergence angle is inversely proportional to the diameter of the expanding beam.

$$\theta_o = \left(\frac{f_1}{f_2}\right)\theta_i \qquad D_o = \left(\frac{f_1}{f_2}\right)D_i$$

$$\theta_o = \left(\frac{D_i}{D_o}\right)\theta_i \tag{5.10}$$

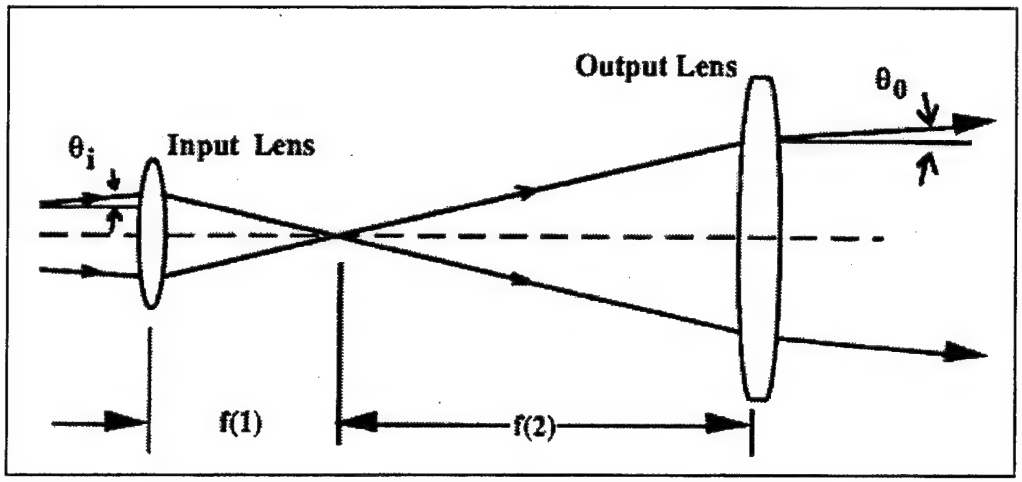

Figure 5. 7 Beam Expander with Properly Matched Lenses. [Ref. 22:p. 8]

As an example: For a beam diameter of 1 mm, which is characteristic of a He-Ne laser, the angular divergence is typically 10^{-3} radians. If this beam were aimed at the moon without a beam expander, the beam diameter at the moon would be approximately 400 km. Using a beam expander to increase the initial beam from 1 mm to 10 cm, the resulting beam at the moon would have a diameter of 4 km.

A typical number for beam divergence of a diffraction limited beam at 694 nm wavelength is 0.2 μradians. [Ref. 25:p. 223] For a satellite at GEO orbit which has a solar array of a few meters across, the pointing accuracy and jitter must be a fraction of 0.2 μradians to avoid wasting power in the beam that does not strike the panel.

3. Atmospheric Compensation and Feedback

Thus far, the discussion has not taken into account any perturbations caused by the atmosphere. Unfortunately, turbulence, the phenomenon which causes stars to twinkle, and shimmering of distant objects on a hot summer day, also causes laser beams to diverge. Here, turbulence refers to the density fluctuations arising from the atmospheric temperature fluctuatic , and not the velocity-induced turbulence encountered in fluid dynamics. [Ref. 22:p. 45] Turbulence in the atmosphere causes beam divergence to be 10 μrad or greater, regardless of telescope diameter. This is a much larger value than diffraction limited beams. Without atmospheric compensation, the beam would be so large at GEO that over 99.9% of the beam would miss the satellite array, and the resulting laser power requirements would increase 1000 times. [Ref. 25:p. 224]

Turbulence arises when air parcels of differing temperatures are mixed by wind and convection. The individual air parcels, called turbulence cells, break up into smaller cells and eventually lose their identity. This mixing produces fluctuations in the density and therefore in the index of refraction of the atmosphere. The index of refraction is given by the following equation, where P is the atmospheric pressure in millibars, T is the temperature in Kelvin, and λ is the wavelength in μmeters. Therefore, n-1 is a measure of the deviation of the refractive index from its free space value. A representative value for n-1 at sea level is $3x10^{-4}$. [Ref. 27:p. 10]

$$n-1=77.6x10^{-6}(1+\frac{7.52*10^{-3}}{\lambda^2})(\frac{P}{T}) \qquad (5.11)$$

D. ADAPTIVE OPTICS

To compensate for this atmospheric turbulence, adaptive optics must be used. Adaptive optics refers to the real time changing of the optical properties of the laser system to compensate for disturbances encountered in the atmosphere. This requires a reference beacon, or light source, which is above the atmosphere in nearly the identical direction that the beam is propagating. While a natural star of sufficient intensity may be used to correct for these disturbances, a satellite can be moving at a relatively rapid rate, and a moveable "guide star" is required. This "guide star" can be produced by focusing a relatively low power laser light source onto a reflective layer of the atmosphere along the path, but slightly ahead of, the satellite itself. This permits the light from the guide star to be sensed to correct for turbulence induced phase distortions. Additionally, this will allow for direct visual tracking of the satellite using reflected sunlight, without being outshined by the beacon. A block diagram of such a system is depicted in Figure 5.8.

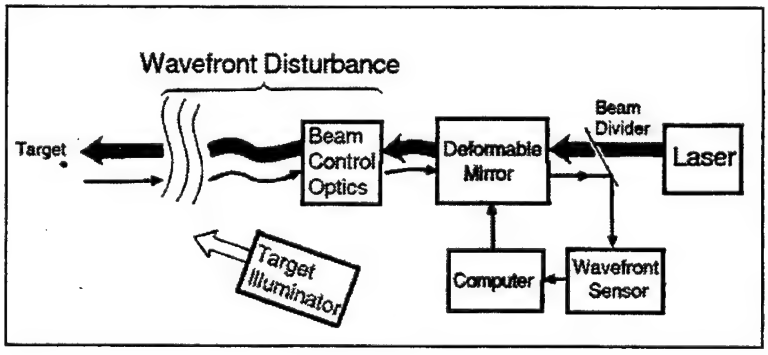

Figure 5. 8 Adaptive Optics Wavefront Compensation System. [Ref. 28:p. 216]

1. Artificial Guide Stars

There are two methods which can be used for producing this beacon. The first method is to produce a low altitude beacon (approximately 20 km), which relies on the Rayleigh backscattering of molecules of atmospheric oxygen and nitrogen when illuminated with a pulsed laser. The returned light is sensed and converted into a control input to the piezo-electric actuator controlled output mirror of a nearby power beaming laser, as seen in Figure 5.9 below. This method has been demonstrated and proven successful, however, it has two problems. The first problem, which is common to all adaptive optics and cannot be corrected, arises from the fact that light used in this technique is distorted by turbulence in its travel upward through the atmosphere and return. A tilt induced on the upward travel may be completely removed on its return trip. [Ref. 21:p. 224] Secondly, the relatively low altitude beacon induces an effect known as anisoplanatism. This results from the fact that backscattered light from a finite altitude does not follow the same path as that of the power beam to the more distant satellite. It is therefore necessary to place the guide star as close to the outer fringes of the atmosphere as possible. A second method of producing the guide star uses the illumination of the mesospheric sodium layer (95 km high) to produce a much higher altitude beacon. Incident light from a relatively low power continuous wave Nd:YAG pumped dye laser is used to illuminate this sodium layer at its resonance line of 589 nm. [Ref. 29:p. 364] The sodium layer is only about 10 km thick at this point. Using a 2.5 W dye laser, a focused column width at this height of 0.25 meters, or 0.5 arcseconds has been demonstrated. The result is a high intensity beacon (equal to a magnitude 9 star), at a much higher altitude than that used in the first technique. [Ref. 30:p. 342]

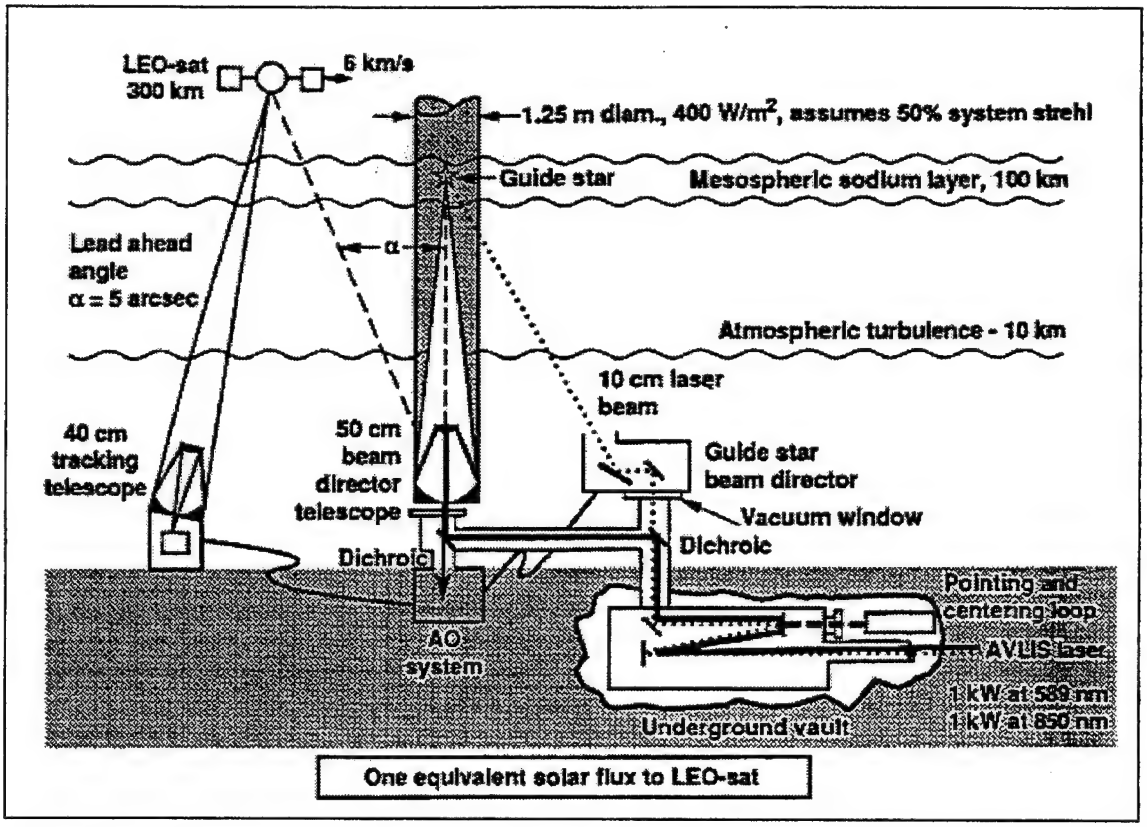

Figure 5. 9 Laser Guide Star for Adaptive Optics Compensation of the Wavefront of a High Power Laser Beam. [Ref. 40:p. 241]

2. Wavefront Sensors and Segmented Mirrors

To correct in real time for aberration induced by the turbulence, sensors are placed behind the laser beam projection telescope to instantaneously measure the reference beacon's wavefront and determine what corrections are necessary. The main component of the sensor system is the Hartmann array, which is a simple system of lenslets which breakup the returning wavefront into discrete areas or pixels, shown in Figure 5.10. These are responsible for determining the slope of the wavefront, or the phase shifting, at each individual pixel and passing it on to the mirror controller. Typically, the Hartmann array controls a series of flat segmented mirrors in the laser power beaming train.

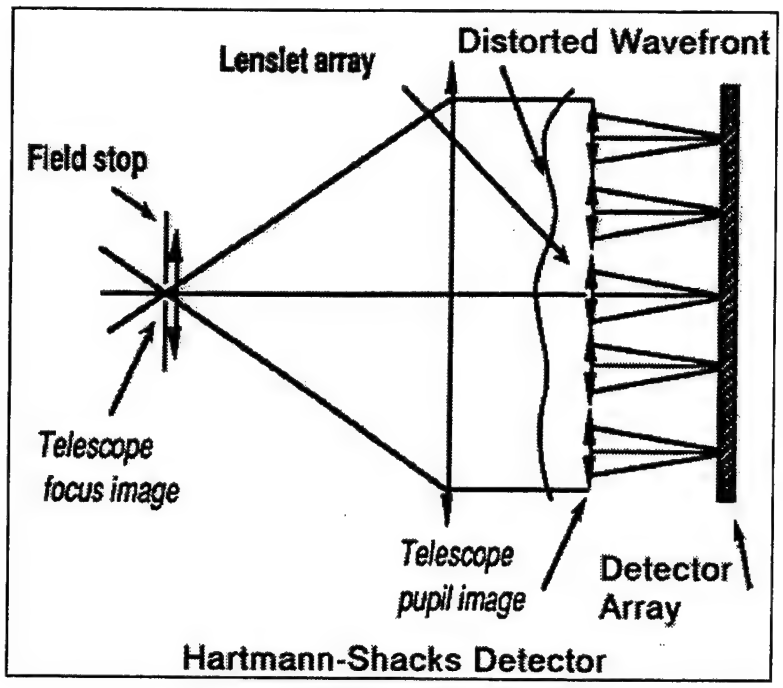

Figure 5. 10 Principle of Hartmann Wavefront Sensor. [Ref. 31:p. 22]

The phase information is used to produce command signals for correction of the output mirror of the laser train. These signals change the relative positions and orientations of each segment of the deformable mirror so the outgoing coherent laser wavefront is now distorted. The distortion is such that the aberrations introduced by the atmosphere return it to its original form. [Ref. 25:p. 224] This mirror has a multitude of thin surfaces which rest upon many closely spaced actuators, as indicated in Figure 5.11 below. [Ref. 37:p. 19] Since the atmosphere is not static, the elements of the mirror must be corrected at a rate of greater than about 200 Hz for visible wavelengths. The outgoing laser pulses used for the annealing, therefore, have an aberration applied which is consequently "undone" as the beam travels through the atmosphere toward the satellite. The resulting beam seen by the array at the satellite is spatially coherent and near diffraction limited quality. [Ref. 25:p. 224]

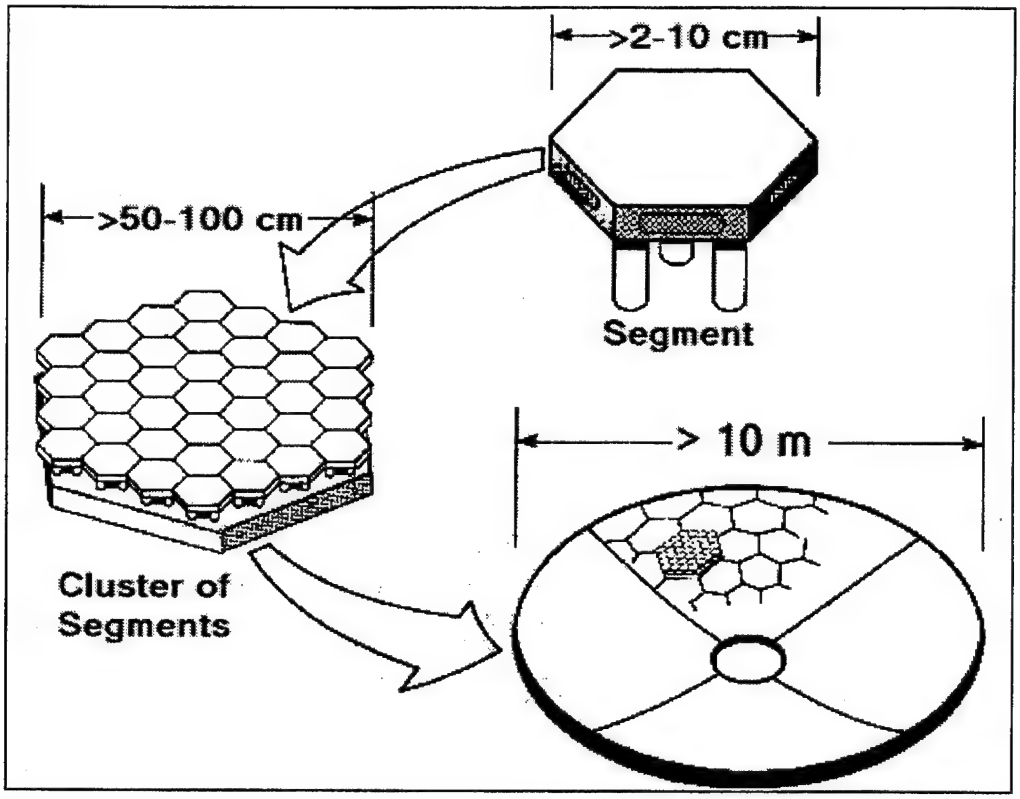

Figure 5. 11 Large Segmented Adaptive Mirror Composed of Thousands of Smart Segments. [Ref. 37:p. 19]

The area of adaptive optics was the focus of several DOD programs in the 1970's and 1980's, with limited success. Progress in the area of adaptive optics came about after 1991, when NASA undertook a dedicated research effort to produce both large low cost adaptive optics telescopes, and reliable lasers with high continuous power. The ongoing result of the focus is the program called PAMELA (Phased Array Mirror, Extendible Large Aperture). These telescopes are large segmented mirror adaptive optic driven telescopes with near diffraction-limited quality. The mirrors in development are to be on the order of 10 meters in diameter with mass-parallel-processor algorithms that can control the segmented mirrors at kilohertz rates. [Ref. 37:p. 14] A successful demonstration of the capability was completed by NASA Marshal Space Flight Center in 1994 with a 36 element 0.5 meter telescope. This telescope and compensation system proved their capability to produce near diffraction limited quality images while correcting at a rate of 300 Hz. [Ref. 37:p. 20]

3. Laser Safety

The laser safety procedures for a power beaming system such as this can be colossal. The obvious problem is having an extremely high power laser not merely pass through airspace, but rapidly sweep across it. Self-imposed limitations on the sweep rate and the minimum permitted angle are necessary, but not sufficient to provide adequate control of such a high energy beam. A procedure developed for Lawrence Livermore National Laboratory (LLNL) incorporates a narrow angle radar boresighted to the laser beam to detect high altitude aircraft which might stray near its path. This limits the potential of the laser striking a large radar observable aircraft, but some light civilian aircraft do not have a significant radar cross section. A program developed at the University of Chicago's Chicago Adaptive Optics System (ChAOS), utilizes a wide field of view low light camera which is aligned with the laser beacon. The camera is designed to receive light from low magnitude stars and output a signal when it is not able to do so. If it is not able to detect these stars down to a set magnitude, such as when a light civilian aircraft with a flashing strobe washes out the screen of the camera, it will inhibit lazing.

4. Laser Power Beaming

The Air Force Phillips Lab (AFPL) Starfire Optical Range had attempted to demonstrate this adaptive optics capability with a 1.5 meter aperture system. Using a 6 ms pulse at 694.3 nm, from a pulsed ruby laser with a peak output of 50 kW, they attempted to prove the concept of laser power beaming to geosynchronous altitudes. The beaming of power through the atmosphere requires that the intensity of the beam be virtually maintained throughout the travel and limited only by diffraction. The Strehl number (I_{rel}) is the ratio of actual peak on-axis intensity to the theoretical limit based on spreading due to diffraction only. A Strehl number of 0.64 corresponds to a beam divergence of 1.25 times the diffraction limit. To achieve sufficient transfer of energy, a Strehl number of 0.5, which is a typical value during good seeing conditions at night, is required.

5. Required Intensity

A formula for intensity, similar to the formula used previously, is used to determine the on axis beam irradiance at distance r, which is listed below. Here the value

for the sum of the squares of r_d, r_t, and r_j is assumed to be a direct function of the diffraction limited value of r_d.

$$I = \left(\frac{f_a f_o \cos(\theta) P_l I_{rel}}{\pi r_b^{\,2}} \right) e^{\left(\frac{-r^2}{r_b^2}\right)} \quad \text{where } r_b = \frac{2\lambda r \beta}{\pi D} \tag{5.12}$$

In this equation, f_o is the fraction of beam energy transmitted through the beam-director optics; f_a is the fraction of beam energy transmitted through the atmosphere vertically; θ is the beaming angle away from zenith, and P_L is the total laser power. The factor, β, is the actual laser beam divergence relative to diffraction limited divergence, I_{rel} is the Strehl ratio due to atmospheric turbulence, tracking noise, etc., r_b is the beam radius at 1/e times the on-axis intensity, and D is the beam director aperture. A few examples of the expected power required to receive 2.5W/cm^2 of laser power on the beam axis are listed in Table 5.2 below. The first column is the expected result of a laser power beaming demonstration of a joint Department of Energy sponsored project between Air Force Phillips Labs, COMSAT Labs, and Sandia National Labs. Their goal was to demonstrate a low power proof of concept that would be followed by a demonstration of high power beaming. The proof of concept demonstration utilized 50 kW of laser output with the following results. The ultimate goal was to supply a satellite's array with laser light equal in intensity to that of the sun. Note that, with atmospheric compensation, the required laser power for sunlight replacement in the GEO power beaming column is 300 kW and the beam radius is 5.9 meters. Without the compensation, the numbers grow to 300 MW and 185 meters. The last three columns have calculated values of laser power output required for annealing assuming two different values for an adaptive optic driven telescope beam diameter of 4 and 12 meters. The values for power required for the larger 12 meter mirror is placed in parentheses. This 12 meter diameter mirror is the same as the proposed PAMELA (Phased Array Mirror, Extendible Large Aperture) project.

	Parameter	GEO Demo	GEO Beaming (1 Sun)	GEO Annealing	1/2 GEO Annealing	LEO 750 km Annealing
P	Power (kW)	50	300	10,900 (1200)	3,700 (389)	7.94 (0.882)
λ	Wavelength (nm)	694	840	840	840	840
β	Laser Diffraction	1.3	1.2	1.2	1.2	1.2
D	Beam Director Aperture (m)	1.5	4	4 (12)	4 (12)	4 (12)
f_o	Beam Director Transmission	0.4	0.9	0.9	0.9	0.9
f_a	Vertical Atmospheric Transmission	0.7	0.8	0.8	0.8	0.8
θ	Beaming Angle (°)	45	45	45	45	45
I_{rel}	Atmospheric Turbulence Strehl Number	0.3	0.5	0.5	0.5	0.5
z	Slant Range $m*10^6$	37	37	37	21.7	1
r_b	Beam Radius with Compensation	14.2	5.9	5.9	3.48	0.16
	Beam Radius no Compensation (m)	185.0	185.0	185.0	185.0	185.0
I	On-axis Beam Irradiance (W/m^2)	4.71	690	25000	25000	25000

Table 5. 2 Power Requirements for Various Beaming Scenarios Using a Ground Based Laser. Adapted from [Ref. 24:p. 27]

E. LASER TECHNOLOGY

1. Falcon RPL (Reactor Pumped Laser)

The types of lasers which are capable of annealing orbiting solar cells from Earth require vast amounts of energy and are still in the developmental stages. Nuclear power pumping has been investigated as one possible method of generating the large amount of energy required to fire such a laser. One reactor-pumped laser (RPL) program administered by the Department of Energy (DOE) is called the FALCON (Fission-Activated Laser CONcept). It has many strengths including continuous high power operation, modular construction, self-contained power, compact size (excellent for shipboard operations), and a variety of wavelengths (from visible to infrared).

A reactor pumped laser (RPL) works on the principle of using the energy of fission products to excite a laser medium. This occurs when highly energetic fission products produce secondary electrons through a variety of means which have the effect of ionizing electrons and exciting a laser medium composed typically of a mixture of noble gases. If the medium is contained within a cavity, and the spontaneous emissions are reflected at the ends by mirrored surfaces, a stimulated emission with an associated gain can result. Thus, except for the excitation process the RPL is identical to a common gas laser.

The FALCON RPL has demonstrated firings of limited power (about 300 W) at numerous wavelengths including three wavelengths in the visible. These three visible wavelengths correspond with the range of required wavelengths for InP, or GaAs and silicon solar cell's peak response. The laser output efficiencies of the three wavelengths, 725, 703, and 585 nm, are 0.10%, 0.05%, and, 0.10% respectively. [Ref. 32:p. 3] The wavelength selection depends on the lasing medium, with a variety of different wavelengths being demonstrated every year.

Two designs for RPL's include a laser facility with a self-critical reactor core, and a facility composed of a water cooled reactor used to drive lasers adjacent to it. [Ref. 32:p. 3] One of the largest obstacles is related to the cooling of the reactor. If the system is limited in lasing time to a few minutes then the thermal inertia of the core and pool could maintain the system within limits. An alternative would be to use the vast cooling water available if the system were utilized as a ship-borne asset. The preliminary analysis indicates that a multi-megawatt laser would easily fit on a ship about the size of a Navy guided missile cruiser. Beam-director technology is easily able to compensate for large-scale low frequency motion of the ship due to swells. The small-scale higher frequency ship vibrations, and atmospheric anomalies, as previously discussed, can also be nullified through adaptive optics. [Ref. 32:p. 4] Shipboard operations additionally can increase the intensity of a beam aimed at a GEO satellite by operating close to the equator, which reduces the beaming angle.

The FALCON RPL is thought to have a potential peak power in the tens of megawatts range. Using 300 kW as a starting point for peak power and a 4 meter

adaptive optical dish, the required intensity of 2.5 W/cm^2 is attainable out to a range of 6150 km. If the dish is enlarged to 8m, the range will become 12,290 km. This is still short of the hoped for 21,000 km "half-GEO" slant range. To attain the needed irradiance at this range, assuming a 4 meter dish, a peak power output of the laser would need to be 3.7 MW. With an 8 meter dish, this is reduced to 932 kW. According to Dr. Ron Lipinski of Sandia National Laboratories, these power levels are well within the expected capabilities of the FALCON laser considering the current technology.

2. MIRACL Laser

Another laser which has received some attention in the realm of power beaming, is a laser which has been developed for use as a weapon, is called the Mid-Infrared Advanced Chemical Laser (MIRACL). This is a chemical laser using deuterium fluoride, DF, or hydrogen fluoride, HF, as the lasing medium. A chemical reaction involving fluorine and deuterium, or fluorine and hydrogen, is the means of supplying the energy necessary for creating the population inversion in the lasing medium. This laser has an unclassified demonstrated output power of 1 MW or more. The primary limiting factor is that the output of chemical lasers is in the near infrared, which is too long of a wavelength for direct use in this application. The MIRACL laser has output in a narrow band of 3.6 $\pm$0.2μm for the deuterium fluoride, and 2.7 $\pm$ 0.1μm for the hydrogen fluoride medium. Because of direct atmospheric absorption of the 2.7 μm line, only the longer wavelength is usable. However, if somewhat shorter wavelengths were to become available from this laser, they could be frequency doubled placing the output in the range for optimum use by this application. This frequency doubling technique, however, is not very efficient and tremendous losses could be expected.

3. Free Electron Lasers (FEL)

Another type of laser which has received the most attention for power beaming is the free-electron laser (FEL). This type of laser is capable of a wide range of visible wavelengths and theoretically has sufficient output power necessary for this application. A free-electron laser consists of a source of relativistic electrons (>1 MeV), a laser optical resonance cavity, and a series of static magnetic fields aligned with the cavity, as shown in Figure 5.12. These fields are static, but periodic along the length of the cavity, and is

referred to as the wiggler field. [Ref. 35:p. 32] A short pulse of electrons from a LINAC is introduced to the cavity along with light of an optical wavelength, usually from a laser. As the electron pulse enters the periodic magnetic field, it acquires a small oscillating transverse velocity, which is effectively an oscillating current. [Ref. 35:p. 33] This current can couple with the electric field of the light in the cavity resulting in the transfer of some of its energy to the light. In the simplest case, the electron pulse makes a single pass through the cavity and then exits, while the amplified light is reflected by mirrors at the ends of the cavity and can receive amplification by another pulse.

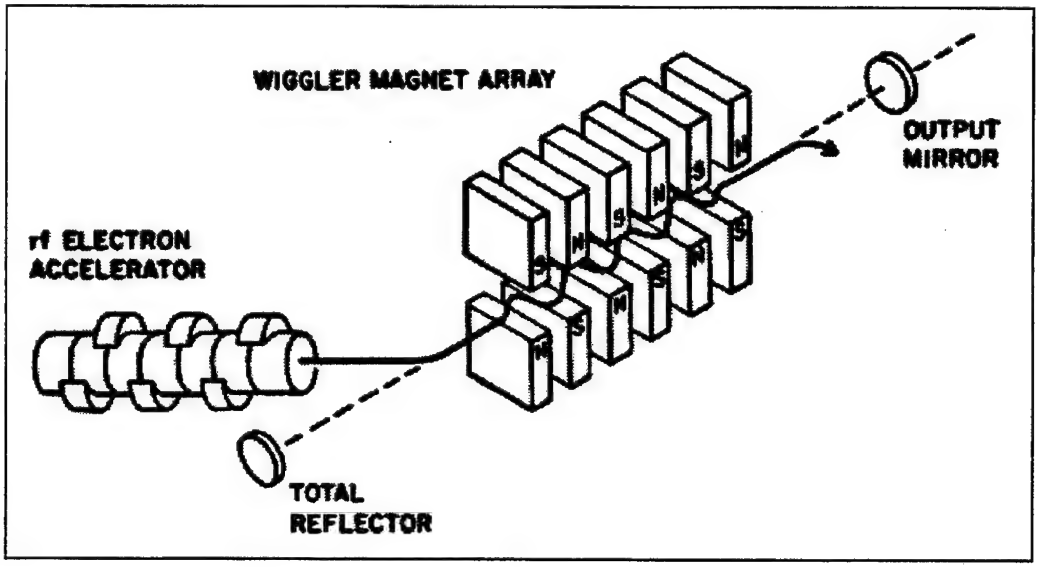

Figure 5. 12 Depiction of Operation of a Free Electron Laser (FEL). [Ref. 35:p. 43]

The greatest attributes of FEL's are their high power and tunability over a wide range of wavelengths. FEL's have outputs that range from the far IR to ultraviolet wavelength's. The production of a given wavelength of output depends on a variety of factors. These include the energy of the electrons, and the strength and the length of the wiggler field, as shown in the equation below. The electron energy required, for typical values of the FEL wiggler field period (λ_o) of 5 cm, the undulator parameter (K), which is proportional to the field strength ($K \propto B$) of $K \approx 1$, and an output wavelength (λ) of 800 nm, is only 125 MeV. This is easily in the range of output energies for linear accelerators.

$$\lambda = \frac{\lambda_o(1+K^2)}{2\gamma^2} \tag{5.13}$$

Lasers based upon this technology have been produced, but the output has been limited due to several factors. The limitations of FEL's include the loss of electrons from the system after a single pass, and a loss due to the change in the energy of electrons as they passes through the wiggler field. A variable or "tapered" wiggler field is a means by which the energy loss of electron's could be countered. It incorporates a gradually changing wiggler field intensity and/or field period to maintain a resonant condition as given in the equation above. This greatly increases the single pass gain of the laser cavity. However, the solution to the problem of low efficiencies through the loss of electrons themselves counters this increase in single pass gain. Developments in the FEL have lead to a technique which increases the efficiency of the laser by recirculating discarded electrons back into the cavity. The ability of the laser to utilize the electrons which have passed through the cavity and are recovered related to the amount of energy removed from these electrons during each pass. If a large amount of energy was removed then the recovered beam has a wide spread of electron energies and cannot be reused, by a "tapered" wiggler field. Both the sensitivity to the electron energy spread, and the peak power extracted from the beam are inversely proportional to the number of oscillations (N) in the wiggler field. For example, a FEL with only 25 oscillations in the wiggler field is relatively insensitive to recovered electron energy spread, and is capable of about 2% conversion of the electron energy to optical output (P=1/2N) for each pass. [Ref. 36:p. 48] This type of recovery system yields much higher efficiencies than a tapered wiggler field, and places the output of a FEL in the hundreds of kW range.

F. CONTINUOUS WAVE (CW) VS PULSED LASERS

Solar cells being investigated have output efficiencies in the range of 40-50% in response to continuous wave monochromatic light, but because many high power lasers are pulsed lasers, as opposed to continuous wave lasers, one must consider their response of solar cells. The time response of current output of solar cells varies significantly depending upon cell type. Data available compares only silicon solar cell to GaAs solar cell technology. In both instances a sharp drop in the output current following the laser

pulse, with a slower exponential decay afterwards. The silicon technology is shown to have a much slower initial decay, as well as, the characteristic exponential decay, and is thus better suited to illumination from a pulsed laser source. This is explained by comparing the minority carrier lifetimes of different types of cells. While GaAs cells have a minority carrier lifetime on the order of 10-100 nsec, the lifetime of silicon solar cells is about 10-100 μsec. This longer lifetime ensures the flow of current for a significantly longer period of time, and in this case, more effective annealing. A pulse repetition interval much shorter than the minority carrier lifetime would be required for a pulsed laser to be effective in annealing a given type of cell.

G. CURRENT POWER BEAMING PROJECTS

The development of FEL capabilities has lead the way for its projected use in power beaming projects. As of February 1995, there were over 24 existing operable high power FEL's with another 22 proposed projects worldwide. Currently, the focus for laser power beaming is the joint NASA/Navy program called NAOMI (National Advanced Optics Mission Initiative). NAOMI encompasses the PAMELA project described earlier, as well as, the SELENE (SpacE Laser ENErgy) project for production of a high powered FEL depicted in Figure 5.13 below. The goal of NAOMI is to create a facility for space power beaming in which FEL and Adaptive Optics research can be carried out. The proposed site is near the Naval Air Warfare Center China Lake, due to its climate, small population, access to large amounts of electrical power, and position within a restricted airspace. The program intends to have the first prototype telescope from the PAMELA project built at Birchum Mesa near China Lake by 1999. This telescope will be a 12 meter adaptive optics telescope designed for power beaming as well as astronomical observation. Another goal of the NAOMI project is the procuring of state-of-the-art FEL technology from the former Soviet Union. The Russian government is currently producing a 100 kW FEL which is far more advanced than any other in the world. The Russian owned FEL technology developed by the Budker Institute of Nuclear Physics (BNIP) will be shared with the U.S. scientists of the NAOMI project as a part of this program. [Ref. 37:p. 15]

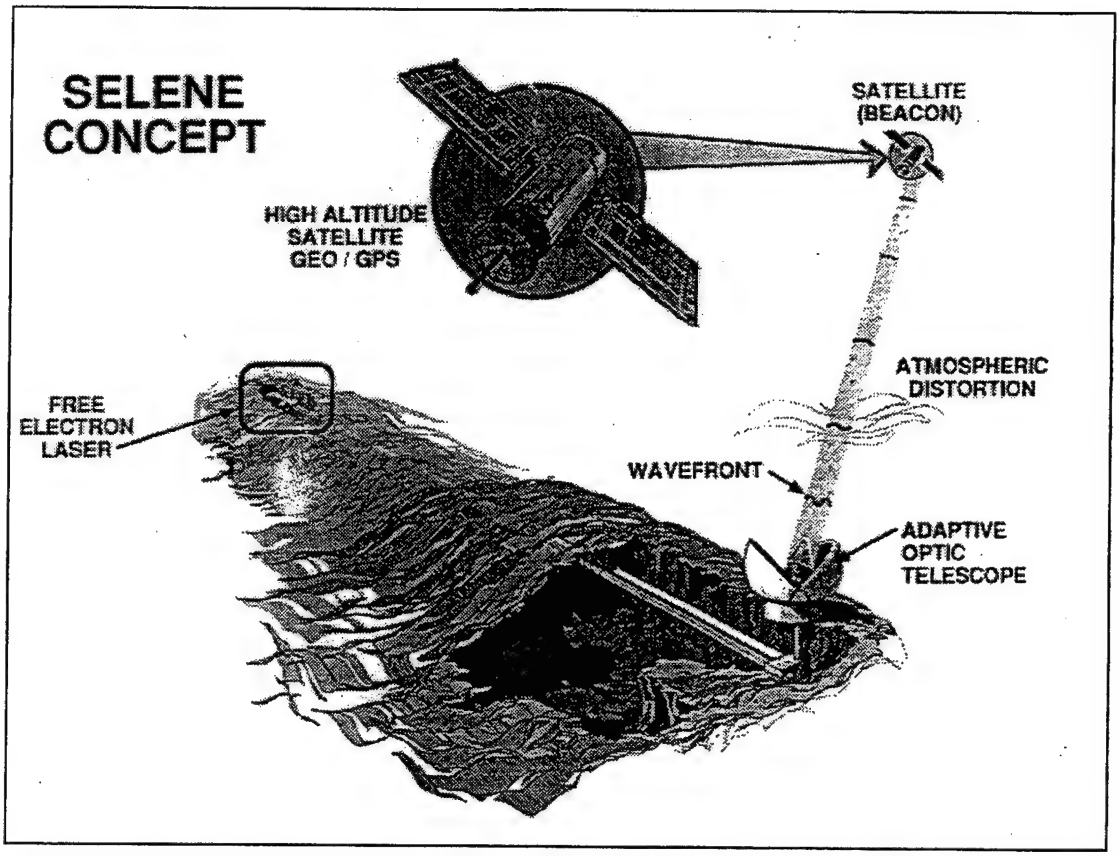

Figure 5. 13 Concept of Power Beaming Using a High Power Ground Based Free-Electron Laser FEL. [Ref. 38:p. 22]

Currently, annealing of solar arrays through photo-injection is in its research phase, but is very promising. Justification for the development of the high powered free-electron or reactor pumped lasers is easy because of their numerous applications apart from this annealing technique. A cost analysis of laser annealing is largely unknown due to the costs of developing these high powered lasers.

VI. INDIUM PHOSPHIDE SOLAR CELL ANNEALING

The primary goal of this research is to determine if diffused junction InP solar cells can be annealed effectively using moderate CW laser intensities and shortened exposure times. The intent is to prove the technique in the laboratory and to investigate its potential application. This chapter will include a description of the solar cells, the apparatus, and the laboratory testing of the cells in addition to the results of experimentation.

A. DIFFUSED JUNCTION INDIUM PHOSPHIDE SOLAR CELLS

The solar cells used in this investigation are NS-12B diffused junction indium phosphide cells produced by NIMIC Incorporated, a division of the Nippon Mining Corporation. The cells are small chips of the full-sized (1x2 cm) original cell, and have surface areas ranging from 0.43 to 0.6 cm^2. Indium phosphide solar cells are very radiation resistant and exhibit significantly lower power degradation compared to either gallium arsenide or silicon solar cells. [Ref. 33:p. 3] However, indium phosphide cells are very fragile and expensive. They, therefore, have not come into wide spread use in space applications where a high degree of durability is required. These cells have been used in a space application by the Institute of Space and Astronautical Science (ISAS) of Japan on the MUSES-A lunar orbiter.

A graph of the quantum efficiency of the InP solar cells used in this investigation is shown in Figure 6.1. This gives an indication of the cell's optimum range of wavelengths, but does not indicate the cell's overall efficiency. The overall efficiency of the cells as tested by the factory, and before cutting them into smaller sized chips, was on the order of 16.5 %. After cutting, the cell's efficiencies were on the order of 2.5 to 3% lower.

Solar cells are most often produced in one of two methods, the first is MOCVD, and the second is the diffusion method. Metal organic chemical vapor deposition (MOCVD) is the process by which a semiconductor base material is built up layer upon layer by exposure to vaporized metal-organic compounds. The result is a p-n junction with a very narrow depletion region. Diffused junction cells are created when a base of

semiconductor material is infused with dopants through its direct contact with a dopant material. The diffusion of sulfur, a group VI donor, into a base of p-type indium phosphide produces a thin layer of n-type material on top of the p-type base. This creates a much wider p-n junction which results from differing diffusion depths of the sulfur dopant into the cell's base material.

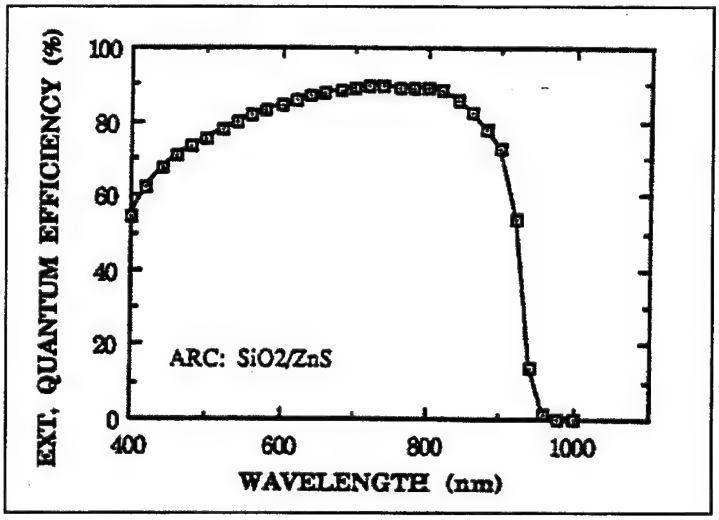

Figure 6. 1 Quantum Efficiency vs. Wavelength of Incident Light of the Nippon Mining InP Solar Cells used in this Research. [Ref. 33:p. 3]

B. TEST PLAN

The testing plan for this research entails two primary steps including the irradiation of the diffused junction InP solar cells with 27 to 30 MeV electrons, and laser annealing of the cells at one of three temperatures. The annealing was conducted under an irradiance of 2.5 W/cm^2 of light from an argon-ion laser for various periods of time. Each of these procedures was preceded, and followed by testing of the cell at 25°C under AM0 conditions. This is to determine the decrease in the output due to irradiation, and the potential recovery due to annealing.

Due to a limitation of the LINAC facility, the fluence level to which each of the cells was exposed is not known precisely. While it is very important for determining the rate at which defects are introduced in a semiconductor, knowledge of the exact fluence level is not vital to this research. The focus here is the relative degree of degradation to recovery of the cell's output vice the actual recovery of the cell. As a result, all reported values of recovery will be reported as a percent of the parameter lost due to degradation.

C. SOLAR SIMULATOR, TEST STAND, AND POWER SUPPLY SETUP

The testing of the cells was conducted at 25°C under Air Mass Zero (AM0) conditions using a solar simulator and a silicon reference cell. Both the reference cell and test cells were illuminated while on water-cooled brass test stands, and thermally regulated by a water bath to 25 ±1°C. Each of the InP test cells was too small to permanently attach leads and mount to the brass test stand. As a result, a separate water-cooled brass test stand was constructed with an attached micromanipulator electrical test probe. Before testing, the back of each cell was painted with a silver, electrically conductive paint, and with it temporarily affixed to the brass test stand surface. A fine metal probe driven by the micromanipulator was then lowered onto one of the small silver gridlines on the cell's surface, as indicated in Figure 6.2. A check of the resistance between the test probe, and the brass test stand was made until an adequate low resistance electrical contact could be ensured. A thermocouple was permanently attached to the illuminated surface of the brass test stand to ensure accurate temperature control of test cells during illumination.

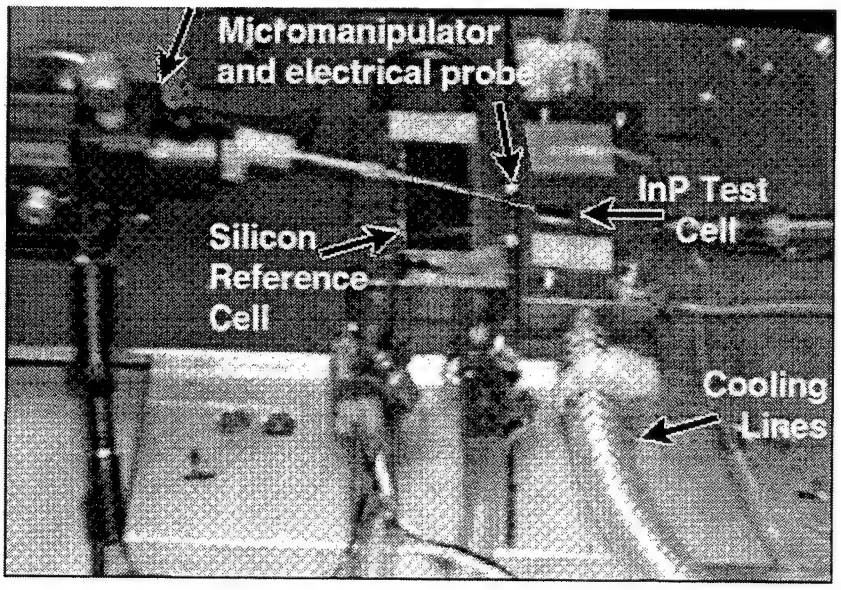

Figure 6. 2 Experimental Setup with both Reference and Test Cells affixed to Brass Test Stands. A Micromanipulator which Controls Placement of the Electrical Probe is Indicated as well as the Thermal Control Cooling Lines.

The reference cell is permanently mounted to its brass test stand, and, like the test stand for the InP cells, has an attached thermocouple probe adjacent to its illuminated

surface. The silicon reference cell has a known output under AM0 conditions, or solar radiant flux outside the Earth's atmosphere, as indicated in Table 6.1 below. [Ref. 34:p. 17] The xenon arc lamp bulb of the solar simulator, produced by Optical Radiation Corporation (ORC) SS-1000, is powered by an adjustable power supply. The output of this power supply is increased until the intensity of the light until the silicon reference cell output closely matches its known output under AM0 conditions. A silicon reference cell IV curve check was conducted both before and after testing each InP cell. This is to ensure a high degree of uniformity of test conditions because the solar simulator has some intensity variation.

Cell Size (cm^2)	I_{sc} (mA)	V_{oc} (Volts)	P_{max} (mW)
7.68	338.264	0.6063	161.411

Table 6. 1 Silicon Reference Cell Output at 25°C under AM0 Conditions.

The measurement of the IV curve for the reference test cells was conducted using a computer controlled programmable power supply. A General Purpose Information Bus (GPIB) card was added to a personal computer to drive a virtual instrument created within the LABVIEW© program. This interface allows the full control of the HP-6626A programmable power supply through the computer, and subsequent measuring and storage of data taken during a test. The virtual instrument created allows for the determination of output current over the full range of voltage output of the cell. The virtual instrument allows for step sizes as small as 0.005 volts during this measurement. As the cell is illuminated, the values of voltage supplied and current output are measured, recorded and later plotted by the computer. A depiction of the experimental setup is given in Figure 6.3 below.

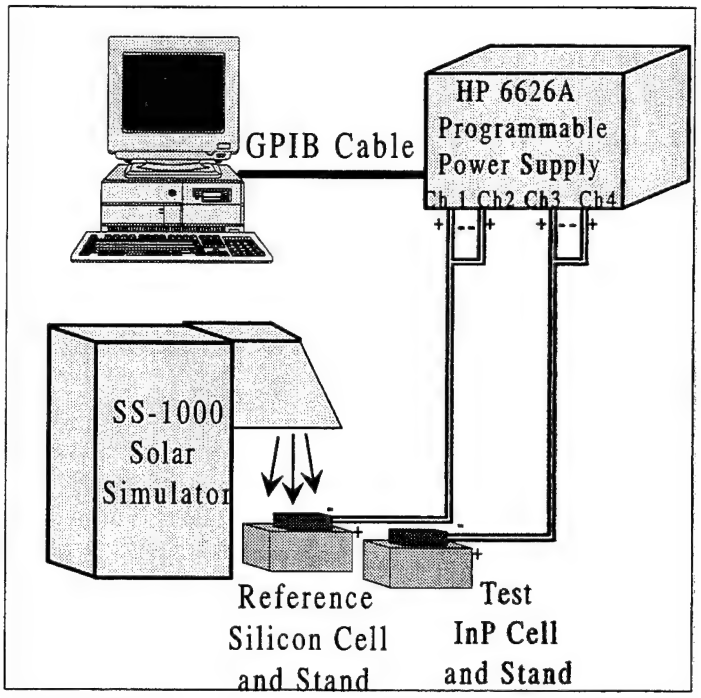

Figure 6. 3 Depiction of Solar Simulator, Solar Cell Test Stands, Power Supply, GPIB Bus, and Computer in Experimental Setup.

Due to a limitation of the HP-6626A power supply, a biasing circuit was required for the measurement of the solar cell IV curves. In order to accurately measure the cell's output for voltage inputs near zero, a minimum current must be output by the cell. Because the cell output near this zero voltage point is smaller than the tolerance, the circuit would become unregulated, so a biasing circuit was designed for the system. One channel of the power supply was set to forward bias the circuit with a constant voltage (4 volts) and current in series with the solar cell, as shown in Figure 6.4. A second channel opposes the current flow of this first channel and solar cell, and has the capability of being swept throughout the voltage range of the solar cell circuit (4 volts + V_{oc}). This same channel would also sense the voltage and current flow at each incremental change in voltage.

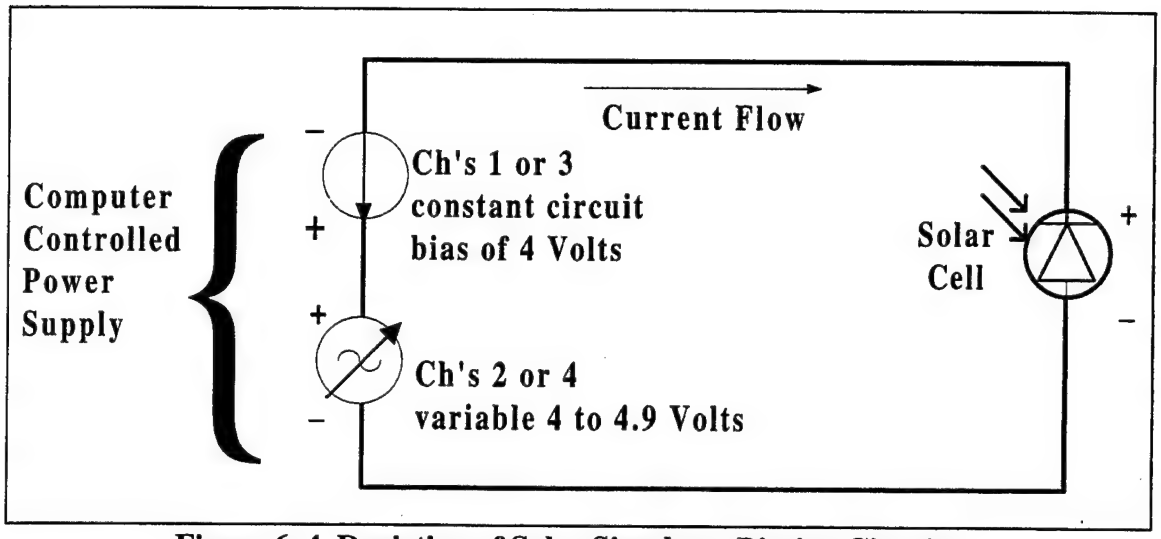

Figure 6. 4 Depiction of Solar Simulator Biasing Circuitry.

D. EXPERIMENTAL PROCEDURE

The Current-Voltage (IV) characteristic of each of the indium phosphide diffused junction solar cells was determined prior to irradiation and was used as a baseline. The surface area and output characteristics of each cell are listed in Table 6.2. Cell 5B has a poor characteristic and fill factor due to the dislodging of a conducting grid from its surface prior to initial testing.

1. AM0 IV Characteristic Testing Procedure

All IV plots were conducted under simulated AM0 (Air Mass Zero) conditions at 25°C using the solar simulator, a water thermal control bath, and a silicon reference cell for calibration. After calibration of the solar simulator using the reference cell, each test cell was mounted on a temperature controlled brass stand for testing. The parameters for each cell are listed in Table 6.2, below.

Cell #	I_{sc} (mA)	V_{oc} (V)	Fill Factor	P_{max} (mW)	η %
5B (0.43 cm^2)	12.07	0.813	0.4955	4.86	8.38
5C (0.60 cm^2)	16.86	0.821	0.8105	11.22	13.85
5D (0.458 cm^2)	13.17	0.818	0.7776	8.38	13.54

Table 6. 2 Pre-irradiation Output Characteristics of InP Test Cells.

2. Annealing Test #1

a. Electron Irradiation for Annealing Test #1

A source of 1 MeV electrons, normally used for testing the radiation degradation of solar cells, was not readily available. Electron energies available from a linear accelerator are much higher than the desired 1 MeV electrons normally used in degradation testing of solar cells. Irradiation of two of cells was conducted with 27 MeV electrons using the linear accelerator at the Naval Postgraduate School. Each of the cells was irradiated until a total fluence of $1x10^{15}$ electrons/cm^2 reached the SEM, secondary emissions monitor, of the LINAC. The cells were permitted to stand for approximately 15 minutes before handling. They were then removed from their stand and placed in a container which was cooled to 0°C. The cooling was utilized to inhibit the thermal annealing of the InP cells at room temperature. The procedure for cold storage of the cells was later eliminated due to lack of evidence of appreciable annealing at room temperature. The IV characteristic of each of the cells was produced to determine the degree of degradation.

b. Laser Annealing at 48.5°C.

The laser annealing process was conducted 48 hours after the irradiation, due to laboratory constraints. The cells were tested under AM0 conditions prior to annealing and compared to that of the IV curve immediately following irradiation. The cells were then mounted on the same brass test stand with silver conductive paint, electrically short circuited, and heated to 48.5°C. They were then exposed to the light from an 8 Watt argon ion laser, the output of which has multiple visible emission lines including the primary 488 nm, and 514 nm lines. The laser output was conducted to the test stand by means of a fiber optic cable, which provides both a uniform intensity spot and the capability for producing a divergent beam. The fiber optic cable has a maximum divergence angle of 23°. The size of the incident beam was adjusted, by varying the height of the cable above the test stand. A beam approximately 1 cm in diameter was directed onto the stand and allowed to strike an individual InP cell. The power density of the beam covering the cell was estimated to be approximately 2.5 W/cm^2. This was estimated by assuming the 8 Watts of power output of the laser was reduced by 10%, due

to losses in the fiber optic cable. Additionally, the incident beam had an area of 3.14 cm^2 (1 cm diameter). The short circuit current of the first cell, Cell 5B, ranged from 262 to 279 mA, and periodic tests showed an open circuit voltage of 0.761 V. The size of this first cell is 0.43 cm^2, which makes the current density through the cell 0.61 mA/cm^2. Since the degraded output of this first cell was 10.5 mA under AM0, this output is equivalent to an exposure of the cell to light intensity 25 times that of AM0. This cell was annealed for one hour, and then allowed to cool to room temperature. The second cell, Cell 5C, was illuminated with the same laser, however due to technical problems, the I_{sc} output of this cell was only 72 to 75 mA, and V_{oc} was 0.77. The second cell has an area of 0.60 cm^2, which means that the current density for annealing this cell was only 0.12 mA/cm^2. This was much lower than the anticipated 0.5 mA/cm^2. The annealing of this cell was maintained for only 15 minutes, and allowed to cool to room temperature.

c. Results of 48.5°C Annealing

The two cells were tested again for electrical properties under AM0 at 25°C, with the resulting IV characteristics. Figures 6.5 and 6.6, below, depict the IV characteristics of Cell 5B and 5C for the pre-radiation, post-radiation, and post-annealing phases. The annealing process returned 17% of the lost power to Cell 5B and 18.7% to Cell 5C. While this is a measurable recovery, this limited recovery drove the following annealing trials to higher temperatures.

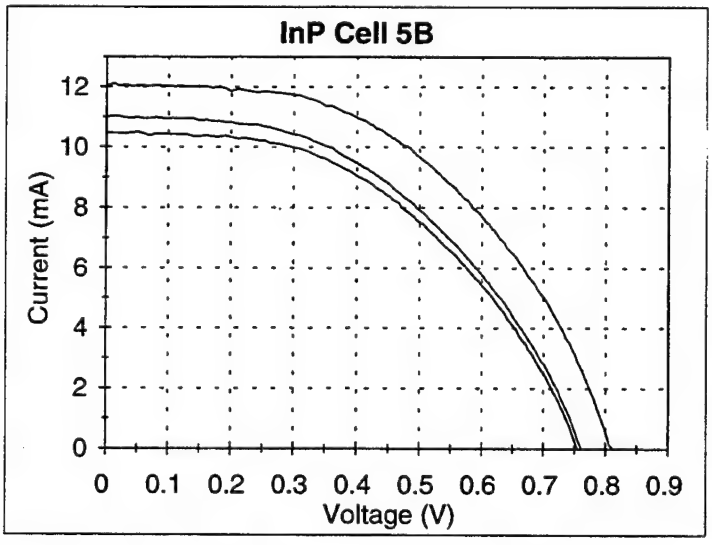

Figure 6. 5 IV Curve for Cell 5B Before and After Irradiation, and After Laser Annealing at 48.5°C for 60 minutes.

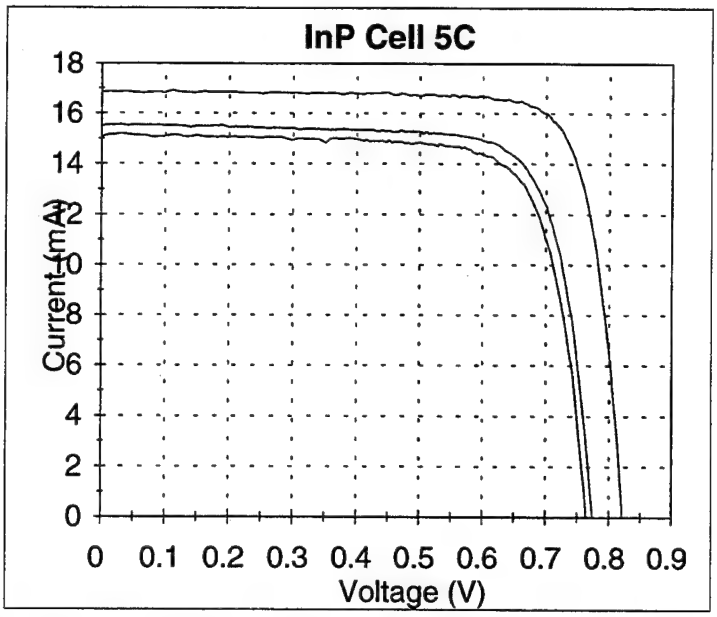

Figure 6. 6 Curve for Cell 5C Before and After Irradiation, and After Laser Annealing at 48.5°C for 15 minutes.

Cell #	Max Power Pre-Rad (mW)	Max Power Post-Rad (mW)	Max Power Annealed (mW)	% Annealed
5B	4.86	3.82	3.995	17.15
5C	11.22	8.87	9.312	18.71

Table 6. 3 % Power Recovery Due to Annealing Process at 48.5 °C.

A reduction in the total fluence was planned for the next phase of testing to determine if the degree of degradation plays a role in annealing. Cell 5B was determined to be unsuitable for additional testing, which severely limited the number of possible additional annealing experiments. As a result, Cell 5C was thermally annealed for 1 hour at 227°C to return as much of its output as possible prior to returning it to additional annealing experiments. The following test incorporated an elevated temperature and a reduced fluence level.

3. Annealing Test #2

a. Electron Irradiation for Annealing Test #2

The second annealing experiment involved only one cell, Cell 5C, and degraded by a total fluence level of $5x10^{14}$ electrons/cm^2 upon the LINAC's SEM. The cell was tested at 25°C under AM0 conditions before the irradiation. Irradiation of cells was conducted with 27 MeV electrons using the linear accelerator and the cell was allowed to stand for 15 minutes. The cell was then removed from its stand and immediately tested under AM0 conditions to determine

the degradation. The cooling process used in the first irradiation was eliminated due to lack of any appreciable annealing at room temperature. The IV characteristic of each of the cells was produced to determine the degree of degradation.

b. Laser Annealing at 60°C.

The laser annealing process was conducted 24 hours after the irradiation, and the cell was tested under AM0 conditions prior to annealing. The cell was mounted on the brass test stand with silver paint, short circuited, and heated to 60°C. It was then exposed to the light from an 8 Watt argon ion laser, with a beam approximately 1 cm in diameter directed onto the stand as before. The irradiance of the beam covering the cell was estimated to be approximately 2.5 W/cm^2. The short circuit current (I_{sc}) output of this cell held in the range of 99.8 to 105.2 mA, and V_{oc} was 0.77 Volts. This means that the current density for annealing during this procedure was 0.175 A/cm^2, or about 7 times the output of AM0 conditions. The annealing of this cell was maintained for a total of only 15 minutes, and allowed to cool to room temperature.

c. Results of 60°C Annealing

The cell was again tested for electrical output under AM0 at 25°C, with the resulting IV characteristic. Figure 6.7 shows the IV characteristic of Cell 5C for the pre-radiation, post-radiation, and post-annealing phases. The annealing process returned 48% of the lost power to the cell.

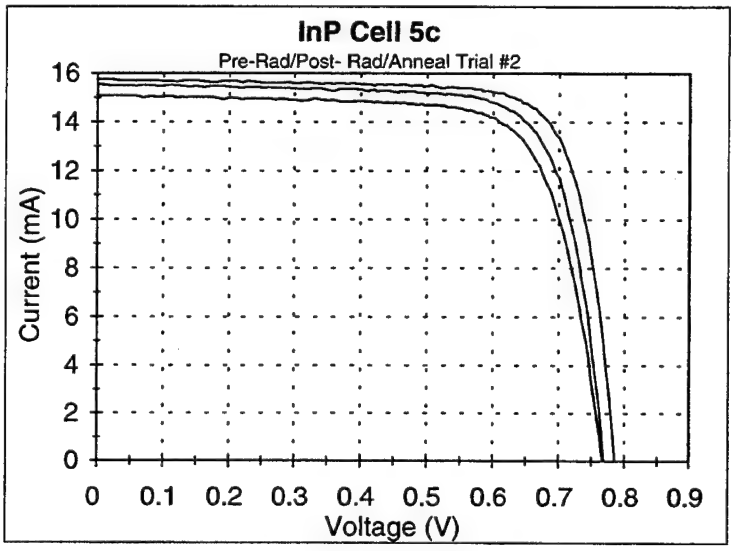

Figure 6.7 IV Curve for Cell 5C Before and After Irradiation, and After Laser Annealing at 60°C for 15 minutes.

Cell #	Max Power Pre-Rad (mW)	Max Power Post-Rad (mW)	Max Power Annealed (mW)	% Annealed
5C	9.68	8.62	9.14	48.3%

Table 6. 4 % Power Recovery Due to Annealing Process at 60 °C.

4. Annealing Test #3

a. Electron Irradiation for Annealing Test #3

The third annealing experiment involved two cells, Cell 5C and Cell 5D, and both were degraded by a total fluence level of $5x10^{14}$ electrons/cm^2 upon the LINAC's SEM. The cells were tested at 25°C under AM0 conditions before the irradiation. Irradiation of these cells was conducted with 27 MeV electrons using the linear accelerator, and the cells were allowed to stand for 15 minutes. The cells were then removed from their stand and immediately tested under AM0 conditions to determine the resultant degradation. The IV characteristic of each of the cells was produced to determine the degree of degradation. The annealing procedures for these cells were identical except for the annealing temperature.

b. Laser Annealing at 60°C (Cell 5C) and at 75°C (Cell 5D).

The cells were both tested again under AM0 conditions prior to annealing to ensure no change had occurred due to annealing at room temperature. The laser annealing process was conducted approximately 24 hours after the irradiation. The cells were each then mounted to the test stand with silver conductive paint and short circuited. The two tests were accomplished individually with the first being Cell 5C, which was heated to 60°C during the test. The second was Cell 5D, which was held at a temperature of 75°C during the testing. They were both then exposed to the light from the argon ion laser directed onto the stand as before. The irradiance of the beam covering the cell was estimated to be approximately 2.5 W/cm^2. An attempt was made to determine if a short exposure time of two minutes would appreciably anneal the cells. The cells were annealed first for this two minute time period, removed and then tested under AM0 conditions. No appreciable recovery was noted in either cell, so a second annealing period of 13 minutes was completed. Each cell was laser annealed for a total period of 15 minutes. The short circuit current (I_{sc}) output of Cell 5C was stable at 101.5 mA (or 0.169 A/cm^2), and V_{oc} was 0.76 Volts. Again, the current density indicates that the cell's output was equal to about seven times

that of AM0 conditions. The short circuit current output of Cell 5D held stable at 99.5 mA which indicates a current density of 0.221 A/cm2 for cell area of 0.45 cm^2.

c. Results of 60°C & 75°C Annealing

Each cell was again tested for electrical output under AM0 at 25°C, with the resulting IV characteristic. Figures 6.8 and 6.9 show the IV characteristic of Cell 5C and Cell 5D for the pre-radiation, post-radiation, and post annealing phases. For Cell 5C, the annealing process returned 42.95% of the power lost by the cell. Despite the higher temperature, the recovery of Cell 5D was even less dramatic with only 21.2% of the power output lost returned to the cell, as shown in Figure 6.9.

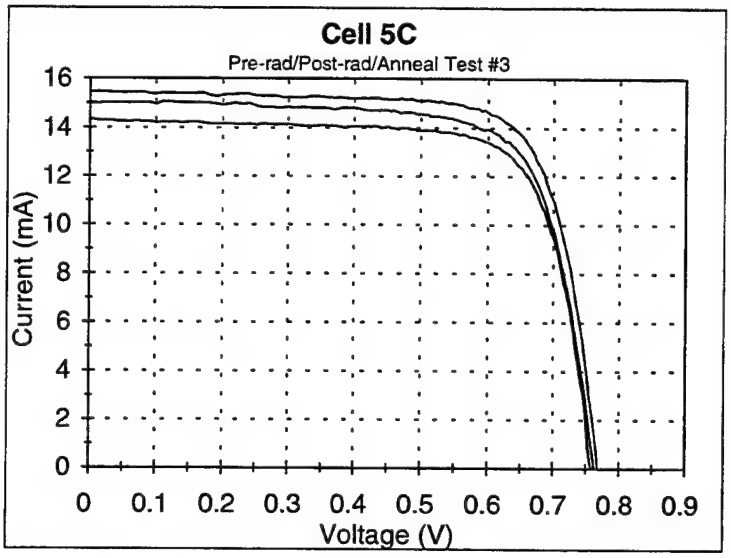

Figure 6. 8 IV Curve for Cell 5C Before and After Irradiation, and After Laser Annealing at 60°C for 15 minutes.

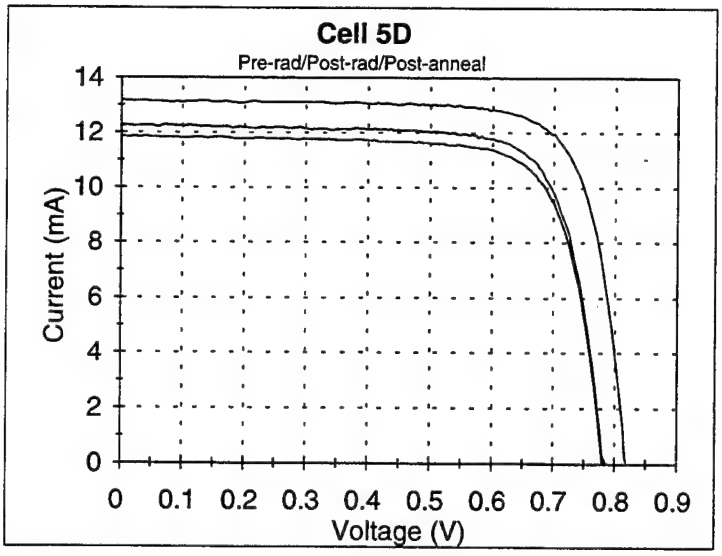

Figure 6. 9 IV Curve for Cell 5D Before and After Irradiation, and After Laser Annealing at 75°C for 15 minutes.

Cell #	Max Power Pre-Rad (mW)	Max Power Post-Rad (mW)	Max Power Annealed (mW)	% Annealed
5C	8.95	8.16	8.50	42.95
5D	8.38	7.07	7.35	21.16

Table 6. 5 % Power Recovery Due to Annealing Process for Cell 5C at 60 °C, and for Cell 5D at 75°C.

The results from the 75°C annealing test seemed to be contrary to the significant annealing attained at 60°C and thus a repeat test at this temperature was planned. No further tests of the annealing procedure were conducted due to a failure of the linear accelerator.

VII. CONCLUSIONS

The goal of this investigation was to confirm the power recovery potential of laser annealing with degraded diffused junction indium phosphide cells, and to research the potential application of this technique to satellites in orbit. Utilizing very small sized cell "chips" allowed for the illumination of the entire surface area of a test sample with an irradiance of 2.5 W/cm^2 using an 8 Watt argon laser. Several tests of the technique with varying temperatures and durations of exposure were conducted realizing the recovery of a significant portion of the power lost from irradiation with electrons.

The ability of the technique to result in some recovery was expected due to previous research using GaAs solar cells. [Ref. 21:p. 57] Although the potential results of the technique were known, the temperature and the extent to which annealing would take place were not known. Temperatures as low as 100°C have shown to be sufficient to thermally anneal these same indium phosphide cells. [Ref. 18:p. 2] Considering the additional energy which the forward biased current adds to the crystal lattice, a temperature well below that for thermal annealing was chosen as a starting point. The resulting choice of temperature range yielded excellent results. The maximum recovery occurred with at a temperature of 60°C with 48% of the lost power being recovered.

The recovery of a significant portion of the lost power was realized. However, this recovery could have been increased with the use of more appropriate energy irradiating electrons. The electron energy used, 30 MeV, was driven, not by electron energies known to exist in the space environment, but by the capability of the LINAC available. As noted earlier, the damage due to irradiation with 30 MeV electrons is significantly greater than that of 1 MeV electrons. With increasing energy comes the increased probability of displaced atoms acquiring enough energy to displace other atoms. While the amount of damage due to 30 MeV electrons is much larger, the fluence levels were reduced such that only a moderate amount of degradation occurred. More important than the degree of damage and its manifestation in the form of reduced output is the type of displacement damage that occurs. In either case, primary knock-on atoms are displaced once and result in vacancies and interstitials. The type of damage created by the 30 MeV irradiation is such that the vacancies and interstitials are much more widely

separated than if lower energy particles were used. The probability of an interstitial being energized and reuniting with its vacancy is thus reduced, denying the cell the full potential of the annealing process. The extent to which this affects the annealing process is not fully known, and requires formal investigation.

A limiting factor in the annealing technique could have been the output of the laser. The response of the indium phosphide cells to the wavelengths of output of the argon laser was adequate to produce current densities of 0.175 to 0.221 A/cm^2, or 7 to 10 times the output of the cell under AM0 conditions. This was enough to produce significant recovery at 60°C, however, previous research using forward biased current annealing at a temperature of 90°C indicated that a current density of about 0.25 A/cm^2 was required for recovery of over 60%. [Ref. 19:p. 37] The current density during this research should have been significantly higher than the 0.25 A/cm^2 to achieve comparable results. The output of the laser was on the order of 20 times the intensity under AM0 conditions, and since this light is monochromatic it should have produced a much higher current density output. This may indicate a flaw in the experimental setup such as an overestimation of the intensity of the laser light. Alternatively, an overestimation of the output of the solar cell under high intensity light, and high temperatures may be have been made. The end result in either case is that only a portion of the required current actually flowed through the semiconductor, and a much higher intensity laser is believed to be required to fully anneal the cell.

Further investigation of this annealing process should include the measurement of concentration and type of defect sites introduced and subsequently annealed by the process. Determining the types of defects introduced and the degree which they are annealed could give great insight into optimizing this technique. The intent of this research was to utilize the expertise of Robert Walters of the Naval Research Lab to conduct DLTS measurements to reach this goal. This process was begun just as the LINAC being used failed and stopped the investigation.

The results of the testing indicate that there is a great potential for annealing, however, optimization of the technique is necessary. The intensity of the laser light source and the temperature for maximum annealing potential are just two of the parameters to optimize. The application of this technique to satellites on orbit could produce significant savings over the

lifetime of a given satellite. Significant problems of power beaming through the atmosphere without excessive loss, and the thermal control of the satellite solar array and satellite itself are two factors to consider. Application of this procedure to orbiting satellites is certainly appealing, but significant technological leaps must be made before such a venture could be realized.

APPENDIX SPECIFICATIONS FOR THE REFERENCE AND TEST CELLS

SILICON
K6700A
SOLAR CELLS

SPECTRODATA

TYPICAL ELECTRICAL PARAMETERS*

Jsc = 42.5 Milliamperes/cm²
Jmp = 39.6 Milliamperes/cm²
Vmp = 0.500 Volts
Pmp = 19.8 Milliwatts/cm²
Voc = 0.605 Volts
CH = 0.77
Efficiency 14.6% Minimum Average
*AMO Sunlight (135.3 mw/cm²), 28°C

RADIATION DEGRADATION*

PARAMETER	1x10¹³	1x10¹⁴	1x10¹⁵	1x10¹⁶
Isc/Isc₀	0.97	0.95	0.86	0.75
Imp/Imp₀	0.96	0.94	0.84	0.72
Vmp/Vmp₀	0.94	0.92	0.83	0.74
Voc/Voc₀	0.94	0.92	0.84	0.76
Pmp/Pmp₀	0.90	0.86	0.71	0.53

*Fluence e/cm² 1 MeV Electrons

THERMAL PROPERTIES

Solar Absorptance = 0.79 (CMX)
Solar Absorptance = 0.77 (Fused Silica)
Emittance (Normal) = 0.85 (CMX)
Emittance (Normal) = 0.81 (Fused Silica)

WEIGHT

55 Milligrams/cm² (Bare)

TEMPERATURE COEFFICIENTS

Isc = +22.0 Microamperes/cm²
Vmp = -2.15 Millivolts/°C
Voc = -1.98 Millivolts/°C

APPLICATION NOTES

TYPICAL I-V CHARACTERISTIC CURVE*

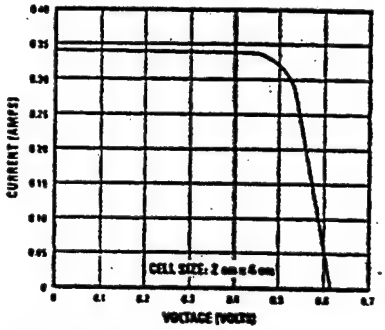

*AMO Sunlight (135.3 mw/cm²), 28°C

SPECTRAL RESPONSE

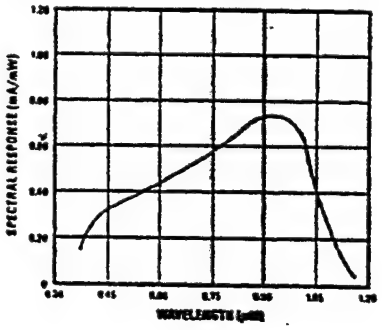

SPECTROLAB, INC.
12500 Gladstone Avenue
Sylmar, California 91342-5373
TELEPHONE: (818) 365-4811
TWX: 910-496-1758
TELECOPIER: (818) 361-5102
TLX: 182881 SPECTRUM SYLM

May 16, 1991

LIST OF CONTENT

PRODUCT : INDIUM PHOSPHIDE SOLAR CELLS
TYPE : NS12B
QTY : 5 PCS
USER : NAVAL POSTGRADUATE SCHOOL
P/O NO. : N62271-91-M-1904

Cell Type : NS12A

Dimentions : 1 cm x 2 cm x 400 μm
AR Coating : SiO2/ZnS
Shadow Loss : Appr. 5 %

Measured I-V Data (AM0, Ta=25 °C)

CELL ID NO.	Voc (V)	Isc (mA)	FF (%)	Eff. (%)
A400-1	0.823	64.4	83.1	16.3
A400-2	0.823	64.2	82.9	16.2
A400-3	0.822	64.3	83.1	16.2
A400-4	0.823	64.2	83.2	16.2
A400-5	0.823	64.2	82.8	16.1

* Efficienctes mesured at Nippon Mining with AM0 solar simulator named SPECTROLAB X-25 MK-II.

Spectral Response

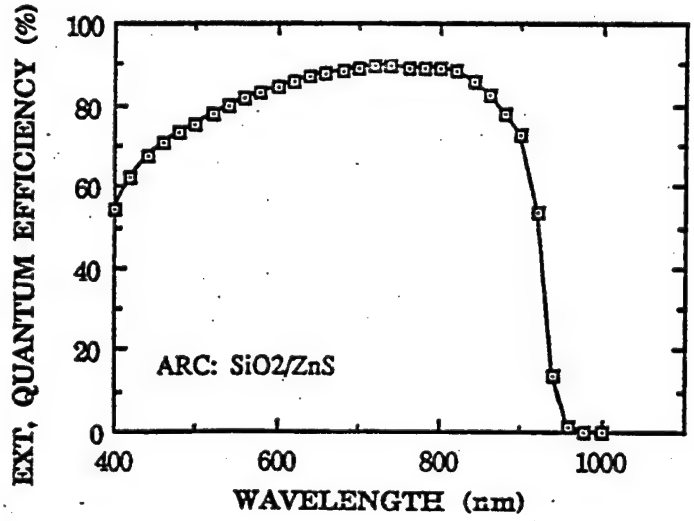

NIMIC INC.
A SUBSIDIARY OF NIPPON MINING CO., LTD.

REFERENCES

1. Larson, W. J., Wertz, J. R., Space Mission Analysis and Design, Microcosm & Kluwer Academic Publishers, 1992.

2. Messenger, G. C., TREE_ Radiation Transient Effects on Electronics, IEEE Nuclear and Space Radiation Effects Conference Short Course, July 11, 1988.

3. Green, M. A., Solar Cells: Operating Principles, Technology, and System Applications, Prentice Hall, 1982.

4. Messenger, G. C., Ash, M. S., The Effects of Radiation on Electronic Systems, Van Nostrand Reinhold, 2nd Ed., 1992.

5. Walters R. J., DLTS Study of Electron Irradiation Induced Defects in MOCVD Grown n+p InP, Master's Thesis, University of Maryland, Baltimore County, June 1990.

6. Jet Propulsion Laboratory Publication 82-69, Solar Cell Radiation Handbook, Third Ed, by H. Y. Tada, J. R.Carter, Jr., B. E. Anspaugh, R. G. Downing, November 1, 1982.

7. Jet Propulsion Laboratory Publication 43-38, Solar Cell Array Design Handbook Vol 1, by H.S. Rauschenbach, 1976.

8. Heinz, O., Olsen, R. C., Introduction to the Space Environment Naval Postgraduate School Class Notes for PH 2514, November 1993.

9. Stassinopoulos, E. G., Raymond, J.P., The Space Radiation Environment for Electronics, Proceedings of the IEEE, Vol. 76, No. 11, November 1988.

10. Summers, G. P., Measurement and Analysis of Radiation Effects in Devices and IC's, IEEE Nuclear and Space Radiation Effects Conference Short Course, July, 13 1992.

11. Phillips, C. S. G., Williams, R. J. P., Inorganic Chemistry: Principles and Non-Metals, Oxford University Press, New York, 1965.

12. Schwank, J. R., Basic Mechanisms of Radiation Effects in the Natural Space Radiation Environment, IEEE Nuclear and Space Radiation Effects Conference Short Course, July 18, 1994.

13. Summers, G.P., et al., Damage Correlations in Semiconductors Exposed to Gamma, Electron, and Proton Radiation, IEEE transactions on Nuclear Science, Vol 40 No 6, December 1993.

14. Attix, F. H., Introduction to Radiological Physics and Radiation Dosimetry, John Wiley & Sons, New York, 1986.

15. Turner, J. E., Atoms, Radiation and Radiation Protection, 2nd Ed., John Wiley & Sons, New York, 1995.

16. Walters R. J., A Study of the Annealing of Radiation-Induced Defects in InP Solar Cells, Doctoral Dissertation, University of Maryland, Baltimore County, 1994.

17. Pinzon, D., Analysis of Radiation Damaged and Annealed Gallium Arsenide and Indium Phosphide Solar Cells Using Deep Level Transient Spectroscopy Techniques, Master's Thesis, Naval Postgraduate School, Monterey, CA, March 1991.

18. Walters R. J., Messenger, S. R. Summers, G. P., Thermal Annealing of Radiation-Induced Defect Centers During Recovery of Diffused Junction and Epitaxial InP Solar Cells, First World Conference on Photovoltaic Energy Conversion, December 1994.

19. Cypranowski, C., Power Recovery of Radiation-Damaged Gallium Arsenide and Indium Phosphide Solar Cells, Master's Thesis, Naval Postgraduate School, Monterey, CA, December 1989.

20. Landis, G. A., Photovoltaic Receivers for Laser Beamed Power in Space, Twenty Second IEEE Photovoltaic Specialists Conference, 1991, pp. 1494-1502.

21. Kramer, R. D., Annealing of Radiation Damaged Gallium Arsenide Solar Cells by Laser Illumination, Master's Thesis, Naval Postgraduate School, Monterey, CA, September 1994.

22. Weichel, H., Laser Beam Propagation in the Atmosphere, SPIE Optical Engineering Press, Bellingham WA, 1990.

23. Jacobs, S. F., et al, Adaptive Optics and Short Wavelength Sources, Vol. 6, Addison Wesley Publishing, Reading MA, 1978.

24. Gerry, E. T. A Comprehensive Guide to High Energy Lasers, General Enterprise, Concord, MA, 1978.

25. Lipinski, R. J., Meister, D. C., Tucker, S., et al., Laser Beaming Demonstrations to High-Orbit Satellites, SPIE, Laser Power Beaming, Vol. 2121, 1994.

26. LeFebvre, M., Cuellar, E., et al., Point Ahead Compensated Illumination Tests Using the 500-Channel Innovative Science and Technology Experimental Facility Adaptive Optics System, SPIE , Vol. 2201, Adaptive Optics in Astronomy, 1994.

27. Strohbehn, J. W., Laser Beam Propagation in the Atmosphere, Topics in Applied Physics, Vol 25, Springer-Verlag, 1978, pp. 1-39.

28. Hardy, J., Adaptive Optics-Problems and Prospects, SPIE, Vol 293, Wavefront Distortions in Power Optics, 1981.

29. Lloyd-Hart, M. Et al. Preliminary Closed-Loop Results from an Adaptive Optics System using a Sodium Resonance Guide Star, SPIE-The International Society for Optical Engineering, Vol. 2201, Adaptive Optics in Astronomy, 1994.

30. Jacobsen, B., Martinez, T., et al., Field Evaluation of Two New Continuous Wave Dye Laser Systems Optimized for Sodium Beacon Excitation, SPIE Vol. 2201, Adaptive Optics in Astronomy, 1994.

31. Kern, P.Lena, P., et al., COME-ON: An Adaptive Optics Prototype Dedicated to Infrared Astronomy, ECO Proceedings, New Technologies for Astronomy, Vol. 1130, 1989.

32. Felty, J. R., Lipinski, R. J., et al, DOE Reactor Pumped Laser Program, Department of Energy, Defense Programs, DP-241, pp. 1-13. Or DOE Reactor Pumped Laser Program, SPIE Vol. 2121, Laser Power Beaming, 1994, pp. 1-9.

33. InP Solar Cells Manufacturer's Specification Sheet, NIMIC Inc. of Nippon Mining Corp., May 16, 1991.

34. Morris, T., Ranaweera, T., Sakoda, D., PANSAT Solar Panel Test Plan, Naval Postgraduate School Space Systems Academic Group, April 14, 1994.

35. Goldstein, J., High Power Free-Electron Laser Concepts, SPIE , Vol. 2376, Laser Power Beaming II, 1995, pp. 32-44.

36. Colson, W. B., Status of High Power Free Electron Lasers, SPIE , Vol. 2376, Laser Power Beaming II, 1995,pp. 45-52.

37. Rather, J., NASA's Daughters: SELENE, PAMELA, and NAOMI, SPIE, Vol. 2376, Laser Power Beaming II, 1995, pp. 11-20.

38. Bennett, H., DOD and Navy Applications for Laser Power Beaming, SPIE, Vol. 2376, Laser Power Beaming II, 1995, pp. 21-30.

39. Jain, R., "Calculated Performance of Indium Phosphide Solar Cells Under Monochromatic Illumination," IEEE Trans Electron Devices, Vol 40, 1993, p. 1893-1895.

40. Friedman, H. W., Near-term Feasibility Demonstration of Laser Power Beaming, SPIE Vol. 2121, Laser Power Beaming, 1994, p. 232-242.

INITIAL DISTRIBUTION LIST

		No. Copies
1.	Defense Technical Information Center 8725 John J. Kingman Rd., STE 0944 Ft. Belvoir, VA 22060-6218	2
2.	Library, Code 13 Naval Postgraduate School Monterey, CA 93943-5101	2
3.	Chairman, Code AA Department of Aeronautical and Astronautical Engineering Naval Postgraduate School Monterey, CA 93943-5106	1
4.	Professor S. Michael, Code EC/Mi Department of Electrical and Computer Engineering Naval Postgraduate School Monterey, CA 93943-5121	4
5.	Professor O. Biblarz, Code AA/Bi Department of Aeronautical and Astronautical Engineering Naval Postgraduate School Monterey, CA 93943-5106	1
6.	Dr. Robert J. Walters Naval Research Labs Code 6615 4555 Overlook Ave SW Washington D.C. 20375	1
7.	Dr. Ronald J Lipinski Department 06514 Sandia National Laboratories P.O. Box 5800 Mail Stop 1145 Albuquerque, NM 87185-1145	1
8.	LT Charles T. Chase RFD #1 Box 1465 Richmond, ME 04357	1